

MINERALOGY, SPATIAL DISTRIBUTION, AND ISOTOPE GEOCHEMISTRY OF  
SULFIDE MINERALS IN THE BIWABIK IRON FORMATION

A THESIS  
SUBMITTED TO THE FACULTY OF THE GRADUATE SCHOOL  
OF THE UNIVERSITY OF MINNESOTA  
BY

Stephanie Ann Theriault

IN PARTIAL FULFILLMENT OF THE REQUIREMENTS  
FOR THE DEGREE OF  
MASTER OF SCIENCE

Dr. James Miller and Dr. Michael Berndt

October 2011

© Stephanie A. Theriault, 2011

## **Acknowledgements**

A heartfelt thanks to my hardworking, patient, and dedicated co-advisors, Dr. Jim Miller & Dr. Mike Berndt. Special thanks also to the other members of my thesis committee, Dr. Josef Werne & Dr. Nate Johnson. Isotope analysis was conducted with the help of Dr. Ed Ripley and his students Valentina Taranovic, Kelli Donoghue, and Eric Stifter at Indiana University Bloomington – Department of Geological Sciences. The opportunity to work and learn at their laboratory was an invaluable experience. I was very fortunate to learn from Mark Severson at the Natural Resources Research Institute (NRRI) and Dr. Peter McSwiggen on the intricacies of the Biwabik Iron Formation. Bryan Bandli at the University of Minnesota Duluth helped navigate me through the world of the scanning electron microscope. Financial support was provided by both the University of Minnesota Duluth – Department of Geological Sciences and the Minnesota Department of Natural Resources – Division of Lands and Minerals. Additional help and support from Kim Lapakko, Dave Antonson, Travis Bavin, Jean Matthews, the UMD Geology faculty, support staff, fellow graduate students, as well as my family and friends kept me sane through the process. And a final, but important, thank you to my undergraduate professors at the University of St. Thomas for inspiring my love and curiosity for geology and encouraging me to continue my education and maintain ethics in my research. I am forever indebted to each and every one of you. Thank you all for helping me make this thesis possible.

## Abstract

The Biwabik Iron Formation (BIF), which is located along the Mesabi Range in NE Minnesota, was deposited in the near shore environment of the Paleoproterozoic Animikie Basin. Although mined for natural ore and taconite, it does contain measurable amounts of sulfide minerals, as pyrite and pyrrhotite. This study is part of a larger study to evaluate whether sulfur from waste rock piles and tailings basins along the Mesabi Range are contributing to sulfate in the St. Louis River Watershed (SLRW).

The primary objective of this study is to characterize the mineralogic and lithologic occurrence, spatial distribution, and sulfur isotope geochemistry of both primary and secondary sulfide minerals in the BIF in order to better establish their variation and understand their origin. Previous isotopic studies conducted on sulfides in Animikie Basin sediments have focused largely on primary (syn-depositional) sulfides in order to determine the chemistry of ocean water at the time of deposition. These studies concluded that primary sulfides were the result of bacterial reduction of Paleoproterozoic seawater sulfate. Consistent with previous studies, primary sulfides appear as small anhedral “blebs” with  $\delta^{34}\text{S}$  values of -5.4‰ to +12.4‰. Secondary sulfides display a wide range of morphologies (cubes, framboids, veins, and anhedral masses), geographic and stratigraphic distribution, and  $\delta^{34}\text{S}$  values (+80.37‰ to -36.11‰). These secondary occurrences are largely attributed to metamorphic effects of the mafic Duluth Complex or to oxidation and desilicification processes attending the formation of natural iron ores.

A secondary objective of this study is to evaluate the source of sulfur to the SLRW. Sulfur isotope values from sulfates collected in the SLRW near mining operations yielded  $\delta^{34}\text{S}$  results of +4‰ to +9‰. This range is similar to the  $\delta^{34}\text{S}$  of primary sulfides in the BIF. However, it was determined that the average  $\delta^{34}\text{S}$  value of all 72 sulfide occurrences analyzed in this study is 8‰. Therefore, it is more probable that the entire range of primary and secondary sulfide are contributing to sulfate in the SLRW, rather than one specific occurrence of sulfide.

# Table of Contents

<b>ACKNOWLEDGEMENTS</b> .....	<b>I</b>
<b>ABSTRACT</b> .....	<b>II</b>
<b>CHAPTER 1: INTRODUCTION</b> .....	<b>1</b>
<b>CHAPTER 2: GEOLOGIC SETTING OF THE BIWABIK IRON FORMATION</b> .....	<b>5</b>
2.1 LITHOSTRATIGRAPHY OF THE ANIMIKIE GROUP .....	7
2.2 DEPOSITIONAL SETTING OF THE ANIMIKIE GROUP .....	11
2.2.1 <i>Transgressive and Regressive Sequences</i> .....	12
2.2.2 <i>Disconformity</i> .....	15
2.2.3 <i>Sediment Sources and Shifting Ocean Chemistry</i> .....	15
2.3 TECTONIC EVOLUTION OF THE ANIMIKIE BASIN .....	16
2.3.1 <i>Penokean Orogeny</i> .....	16
2.3.2 <i>Duluth Complex</i> .....	19
2.4 ORE FORMATION .....	22
<b>CHAPTER 3: SULFUR GEOCHEMISTRY</b> .....	<b>24</b>
3.1 SULFUR ISOTOPES .....	24
3.1.1 <i>Sulfur Isotope Analysis</i> .....	25
3.1.2 <i>Secular Variations of <math>\delta^{34}S</math></i> .....	26
3.2 SULFUR ISOTOPE GEOCHEMISTRY OF PALEOPROTERZOIC IRON FORMATIONS .....	27
3.2.1 <i>Sulfur Isotope Studies of the Biwabik and Gunflint Iron Formations</i> .....	28
3.2.2 <i>Sulfide Mineral Paragenesis in the Gunflint Iron Formation</i> .....	35
<b>CHAPTER 4: METHODS</b> .....	<b>37</b>
4.1 SAMPLING STRATEGY .....	37
4.2 SULFUR ISOTOPE ANALYSES .....	40
4.3 SULFIDE MINERAL IDENTIFICATION AND PETROGRAPHIC ANALYSIS .....	41
<b>CHAPTER 5: RESULTS</b> .....	<b>44</b>
5.1 SULFIDE PETROGRAPHY AND MINERALIZATION .....	44
5.2 SULFUR ISOTOPE RESULTS .....	45
5.2.1 <i>Geographic Trends</i> .....	52
5.2.2 <i>Sub-Unit Stratigraphy Trends</i> .....	55
5.2.3 <i>Mineral Occurrence Trends</i> .....	58
<b>CHAPTER 6: DISCUSSION</b> .....	<b>61</b>
6.1 IDENTIFICATION OF PRIMARY AND SECONDARY SULFIDES .....	62
6.2 PRIMARY SULFIDE MINERALIZATION .....	64
6.3.1 <i>Metamorphic Sulfides</i> .....	69
6.3.2 <i>Anhedral Sulfides</i> .....	72
6.3.3 <i>Euhedral Sulfides</i> .....	73
6.3.4 <i>Vein Sulfides</i> .....	76
6.3.5 <i>Other Sulfides</i> .....	79
6.4 SOURCES OF SULFUR IN THE BIWABIK IRON FORMATION .....	80
6.5 SULFIDE MINERAL PARAGENESIS IN THE BIWABIK IRON FORMATION .....	83
6.6 SOURCES OF SULFUR IN THE ST. LOUIS RIVER WATERSHED.....	84
<b>CHAPTER 7: CONCLUSION</b> .....	<b>86</b>

<b>REFERENCES .....</b>	<b>90</b>
<b>APPENDICES .....</b>	<b>95</b>

## List of Tables

Table 1: Sulfide geographic location, lithology, morphology, and mineralogy for SEM samples.....	45
Table 2: Corrected $\delta^{34}\text{S}$ values for samples collected from the Virginia and Biwabik Iron Formations .....	47
Table 3: The $\delta^{34}\text{S}$ values reported from Poulton et al. (2010) using the $\text{SF}_6$ -gas method and $\text{SO}_2$ -gas method corrected values for the Virginia and Biwabik Iron Formations....	49
Table 4: The $\delta^{34}\text{S}$ values reported from sulfate values collected by the MnDNR.....	51
Table 5: Summary criteria for primary and secondary sulfide minerals .....	64

## List of Figures

Figure 1: The St. Louis River Watershed in Northeastern Minnesota.....	3
Figure 2: Distribution of Paleoproterozoic iron formations in Lake Superior region. ....	6
Figure 3: Stratigraphic comparison of the Lake Superior region Ranges.....	6
Figure 4: Stratigraphic correlations between the Mesabi and Gunflint Ranges . ....	8
Figure 5: Simplified cross section of the Biwabik Iron Formation. ....	10
Figure 6: Simplified cross-section of the Gunflint Iron Formation.....	10
Figure 7: Schematic model for the environment of deposition for the Mesabi Range....	12
Figure 8: Evolution of the Penokean Orogeny. ....	18
Figure 9: The relationship between mineral occurrences in the Biwabik Iron Formation and the distance from the contact with the Duluth Complex.....	21
Figure 10: The spatial relationship between taconite ore, natural ores, and faults in the Mesabi Range.....	23
Figure 11: Range of $\delta^{34}\text{S}$ values for various sulfur-bearing materials. ....	25
Figure 12: Distribution of samples and corresponding $\delta^{34}\text{S}$ values collected from the Gunflint Range, at Kakabeka Falls, Ontario, Canada. ....	31
Figure 13: Distribution of primary sulfide samples from Animikie Group sediments.....	33
Figure 14: Directional fluxes of organic carbon and hydrothermal Fe (II) in the Animikie Basin. ....	34
Figure 15: Ocean chemistry model for the sedimentary sequences along the Mesabi and Gunflint Ranges. ....	34
Figure 16: Carbonate and sulfide mineral paragenesis in the Gunflint Iron Formation ...	36
Figure 17: Locations of drill core along the Mesabi Range selected for this study.....	38
Figure 18: Location of sulfur isotope and thin section samples collected for this study..	43
Figure 19: Range and average of $\delta^{34}\text{S}$ values relative to geographic location. ....	53
Figure 20: Geographic distribution of $\delta^{34}\text{S}$ values in terms of mineral occurrence. ....	54
Figure 21: Geographic distribution of $\delta^{34}\text{S}$ values in terms of stratigraphic sub-unit. ....	54
Figure 22: Geographic distribution of $\delta^{34}\text{S}$ values, comparing values from this study and the Poulton et al. (2010) study. ....	55
Figure 23: Range and average of $\delta^{34}\text{S}$ values relative to sub-unit stratigraphy. ....	56
Figure 24: Stratigraphic distribution of $\delta^{34}\text{S}$ values, in terms of mineral occurrence. ....	56
Figure 25: Stratigraphic distribution of $\delta^{34}\text{S}$ values, in terms of geographic location.....	57
Figure 26: Stratigraphic distribution of $\delta^{34}\text{S}$ values, comparing values from this study and the Poulton et al. (2010) study. ....	57
Figure 27: Average and range of $\delta^{34}\text{S}$ values relative to mineral occurrences. ....	58
Figure 28: Distribution of the $\delta^{34}\text{S}$ values associated with the various mineral occurrences present in the Mesabi Range, in terms of geographic location. ....	59
Figure 29: Distribution of the $\delta^{34}\text{S}$ values associated with the various mineral occurrences present in the Mesabi Range, in terms of stratigraphic sub-unit.....	60
Figure 30: Geographic distribution of primary, secondary, & metamorphic sulfides. ....	61
Figure 31: Geographic distribution of primary sulfide minerals in the Biwabik Iron Formation.....	67

Figure 32: Geographic distribution of secondary sulfides in terms of their mineral occurrence.....	68
Figure 33: Different types of sulfide occurrences. A. anhedral mass; B. euhedral cubes; C. framboidal; D. vein. ....	68
Figure 34: The univariant curve for Pyrite-Pyrrhotite.....	70
Figure 35: Layered concentrations of pyrrhotite and magnetite in a metamorphosed section of the Biwabik Iron Formation.....	71
Figure 36: Massive, strata-bound, secondary sulfide masses/aggregates.....	73
Figure 37: Euhedral cubes of pyrite in the Biwabik Iron Formation.....	74
Figure 38: Framboidal pyrite located along dissolution surfaces.....	76
Figure 39: Secondary sulfide minerals located in veins.....	78
Figure 40: Natural Ore from the Fayal Mine.....	79
Figure 41: Geographic and depth distribution of sulfur isotopes in the Biwabik Iron Formation.....	82
Figure 42: Estimated mineral paragenesis for the sulfide minerals observed in the Biwabik Iron Formation.....	84

## **Chapter 1: Introduction**

The Biwabik Iron Formation, a Paleoproterozoic iron formation located in northeast Minnesota, has been mined extensively for taconite over the past century. As not all of the formation was of economic value, a significant portion of the Biwabik and overlying Virginia Formation were placed in waste rock piles and tailings basins, many of which are in the northern part of the St. Louis River watershed (SLRW). Although the iron formation has not been mined for sulfide minerals, it does contain measurable amounts and has long been recognized as a source of sulfate in the SLRW (Berndt and Bavin, 2011b). The SLRW is the largest tributary to Lake Superior and covers a 9412 km<sup>2</sup> area in northeastern Minnesota, emptying into Lake Superior at Duluth (Fig. 1).

An additional concern about sulfur in northeastern Minnesota is its role in the natural production and concentration of methylmercury in the watersheds. Methylmercury is the type of mercury that accumulates in fish tissue and is thought that biological sulfate reduction in wetlands can drive the formation of methylmercury (Berndt and Bavin, 2011a). As a result, there is concern that sulfate loading from mining sources can stimulate methylmercury formation in the watersheds of northern Minnesota.

There has been limited information available regarding mineralogy, geochemistry, and distribution of sulfides in the Biwabik Iron Formation. Consequently, it has not been possible to properly assess the sulfur budget of the SLRW or to determine the best

management practices for mitigating sulfate release into the basin. The Minnesota Department of Natural Resources (MnDNR) put together a three-phase, two-year, sulfur cycling project in the SLRW, beginning July 1, 2010 and concluding June 30, 2012. Each part of the project is to determine the sulfur status of a given part of the SLRW: sulfide distribution in the Biwabik Iron Formation, sulfate and methylmercury distribution in the SLRW, and the effect of sulfate reduction and methylmercury formation, downstream, on St. Louis River Harbor sediments. During the summer of 2010, water samples were collected from sites located directly downstream from a number of active and inactive mine sites. Rock samples containing visible sulfide minerals in drill core from the Biwabik Iron Formation were also collected at that time. St. Louis River Harbor sediments were assessed during the fall of 2010 and again in the summer of 2011.

With all this information, the MnDNR hopes to evaluate the extent of sulfur cycling in the basin, and what, if any, mitigation measures need to be taken to reduce sulfate input to the SLRW. By documenting the source and distribution of the sulfur in the Biwabik Iron Formation (as well as in the SLRW), the primary benefits of this project are twofold. In addition to providing important geochemical and mineralogical data for the study and cooperating mining industries to use in making decisions on mitigating potential sulfate loading into the SLRW, the data generated will also have important implications for understanding the genesis and post-depositional history of the Biwabik Iron Formation. Therefore, the role of this thesis, in the context of the larger MnDNR study, is to assess the lateral and stratigraphic distribution of sulfide minerals in the Biwabik Iron

Formation in terms of sulfur isotope ( $\delta^{34}\text{S}$ ) geochemistry, mineralogy, and paragenesis. Isotopic measurements provide a useful tool for determining source and fate relationships for chemical species in relatively complex geochemical systems.

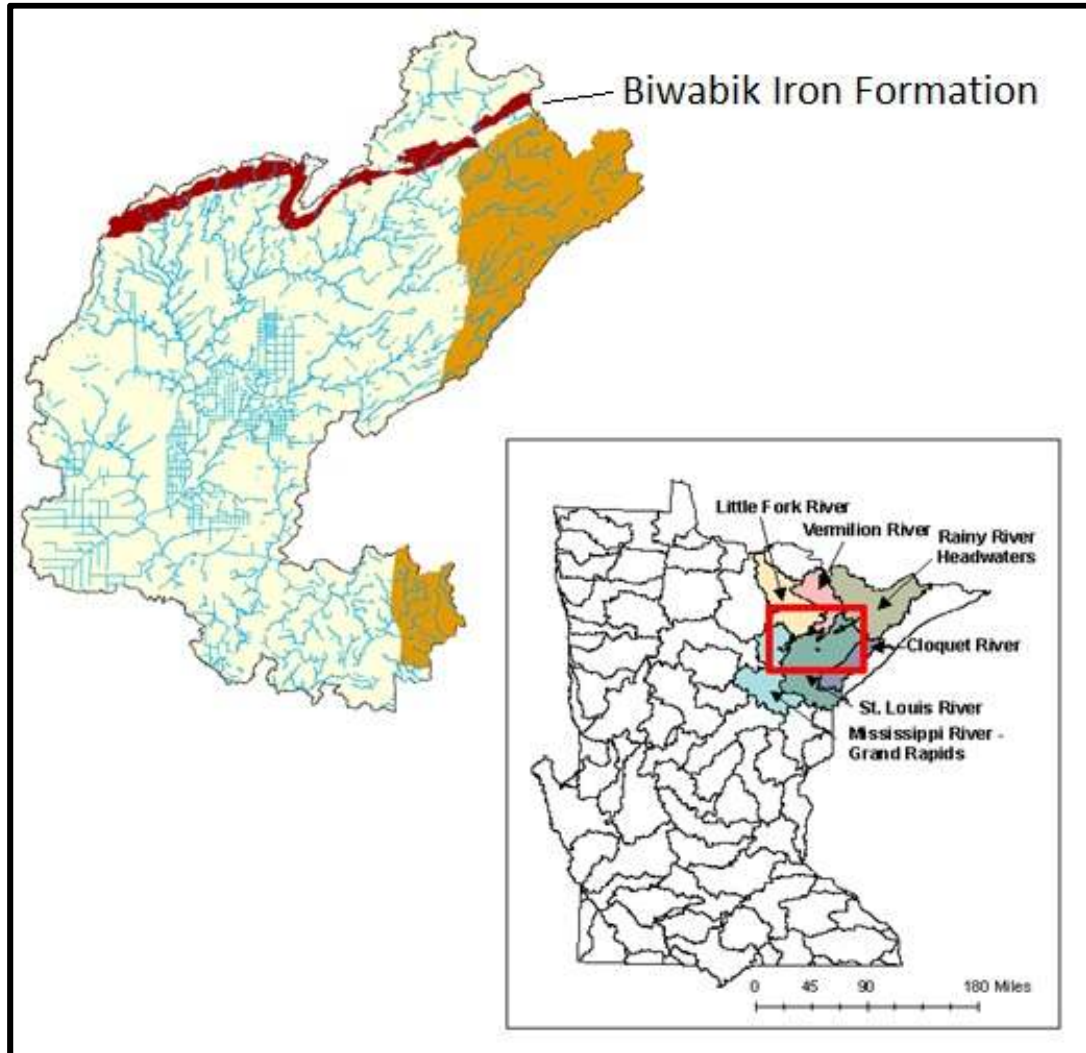


Figure 1: The St. Louis River Watershed in Northeastern Minnesota. Biwabik Iron Formation is located along the northern boundary, as seen in red (Berndt and Bavin, in process).

Scientifically, the main objectives of the thesis are to determine the origin, relative timing, and distribution of sulfide mineralization in the Biwabik and Virginia Formations. Sulfur isotope data analyzed from samples within the Biwabik Iron Formation along with

mineral paragenesis are used to assess whether the sulfides are sedimentary, diagenetic, biogenetic, and/or hydrothermal in origin. This in turn helps constrain the processes by which the Biwabik Iron Formation was deposited and subsequently deformed. Because samples were acquired across the strike length of the Mesabi Iron Range, the effects of thermal metamorphism caused by the intrusion of the overlying Duluth Complex are evaluated as an ancillary benefit.

## **Chapter 2: Geologic Setting of the Biwabik Iron Formation**

The Mesabi Range, which includes the Biwabik Iron Formation, is a part of a larger group of Paleoproterozoic iron formations in the Lake Superior region (Figs. 2 and 3) deposited in a foreland basin during the Penokean Orogeny. The other ranges, located in northeastern Minnesota, northern Wisconsin, and in the Upper Peninsula of Michigan, include: Cuyuna Range, Gunflint Range, Gogebic Range, Marquette Range, and Menominee Range (Schulz and Cannon, 2007; Waggoner, 2010). Iron formation deposition in these ranges ceased around 1.85 Ga, before the close of the Penokean Orogeny at 1.83 Ga. This orogenic event also deformed the region, with the Mesabi and Gunflint Ranges affected the least. However, the Mesabi and Gunflint Ranges, which were possibly continuous at deposition, were separated and thermally metamorphosed by the intrusion of the 1.1 Ga Duluth Complex. The Mesabi Range was much more affected than the Gunflint Range by this metamorphic event. Natural ore, or direct-shipping ore, was subsequently generated along faults and fractures via fluid flow through the Biwabik Iron Formation at some point after the emplacement of the Duluth Complex. The Mesabi Range is of primary focus for this thesis, with special attention also paid to the Gunflint Range, as studies relating to this project were conducted in that range.

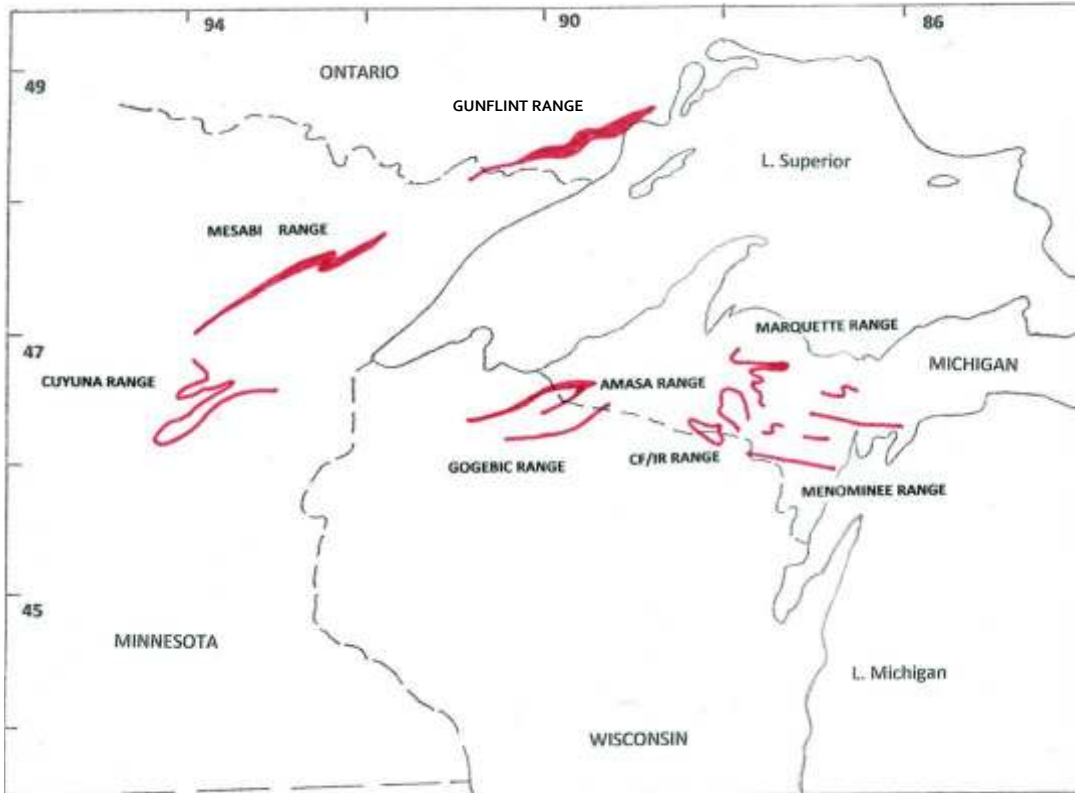


Figure 2: Distribution of Paleoproterozoic iron formation-bearing ranges in the Lake Superior region (Waggoner, 2010).

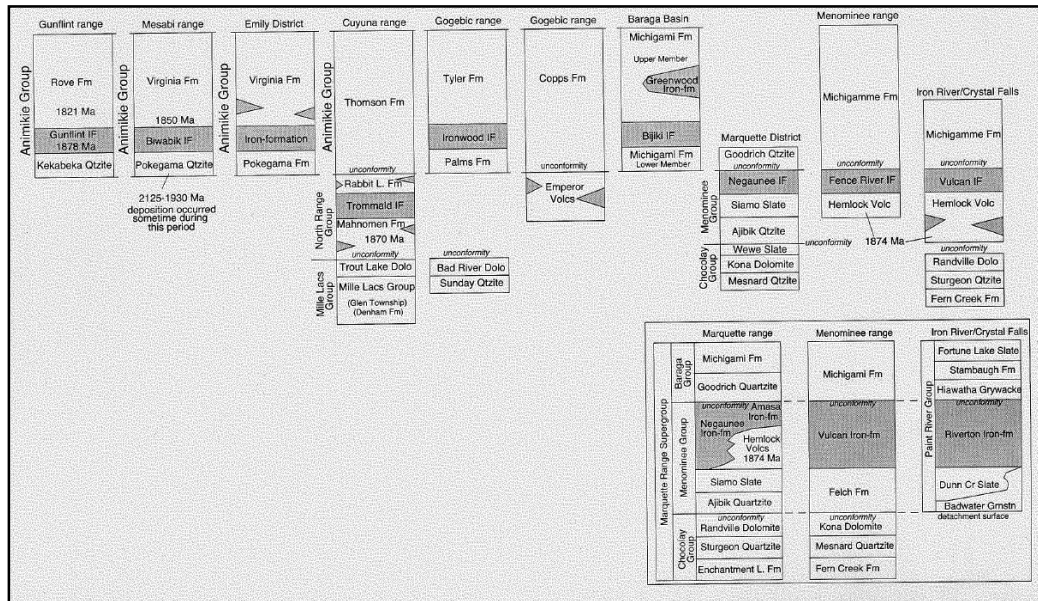


Figure 3: Stratigraphic comparison of the Lake Superior region Ranges (in Ojakangas et al., 2005 after Morey and Southwick, 1995).

## 2.1 Lithostratigraphy of the Animikie Group

The Animikie Group sediments include the Mesabi Range, the Gunflint Range, and the Cuyuna Range (Fig. 4). The lithostratigraphic package comprising each range is quite similar, consisting of a basal arenite, an iron formation with an intermediate black slate, and an upper greywacke slate. They all strike east northeast and have a dip of 5-15° SE. The stratigraphic similarities in the Animikie Group sediments are suggestive that they were deposited contemporaneously (Morey, 1970; 1972; Ojakangas et al., 2005; Jirsa et al, 2008).

The Mesabi Range has three units: Pokegema Quartzite, Biwabik Iron Formation, and Virginia Formation. They rest unconformably on the Mille Lacs and North Range Groups in the south and Archean basement rocks in the north. The Gunflint Range has three correlative stratigraphic units: the Kakabeka Quartzite, Gunflint Iron Formation, and Rove Formation (Morey, 1970; 1972).

The Pokegema Quartzite is the lowermost unit of the Animikie Group along the Mesabi Range, with a maximum thickness on the western edge of about 800m and an average thickness of about 90m (Morey, 1972; Ojakangas et al., 2005). The Pokegema lies unconformably on Archean rocks and is composed mainly of a well-indurated, fine-grained quartz arenite, but also contains significant amounts of feldspathic quartz arenite, feldspathic greywacke, and micaceous quartzose argillite. A maximum age of  $2125 \pm 45$  Ma and a minimum age of  $1930 \pm 25$  Ma have been determined from radiometric dating of



The Biwabik Iron Formation of the Mesabi Range has been described by Morey (1972) as a “ferruginous chert that contains 25-30% iron”. It ranges in thickness from 100m to 250m and has been subdivided into four lithological units, from oldest to youngest: Lower Cherty, Lower Slaty, Upper Cherty, and Upper Slaty (Fig. 5). The slaty portions are fine-grained, finely laminated, and primarily comprised of iron silicates and iron carbonates. The cherty portions are massive, granular, and rich in quartz (Severson et al., 2010). The main minerals in this iron formation are chert, magnetite, siderite, ankerite, and minnesotaite with minor amounts of greenalite, stilpnomalane, and hematite (Severson et al., 2010). Trace amounts of sulfides are also present and they include pyrite, pyrrhotite, covellite, chalcopyrite, and molybdenite (Gundersen and Schwartz, 1962). Minor, but notable, units within the iron formation are an intermediate slate layer between the Lower Cherty and Lower Slaty, two algal- (or stromatolitic-) bearing beds, and a limestone cap at the top of the Upper Cherty (Morey, 1970; 1972; Ojakangas et al., 2005; Jirsa et al, 2008).

The correlative unit to the Biwabik Iron Formation is the Gunflint Iron Formation in the Gunflint Range. The Gunflint Iron Formation is 90-120 meter thick and is split into six major facies: a basal conglomerate, an uppermost limestone, and four cyclic units of Upper and Lower Gunflint (Goodwin, 1956). Minor facies include an algal/stromatolitic chert, tuffaceous shale, and a limestone cap, all of which are comparable to minor units seen in the Mesabi (Fig. 6). The Gunflint also contains basaltic lava flows (Morey, 1970;

Morey, 1972). Radiometric dating on a tuffaceous shale layer near the top of the Gunflint yielded an age of  $1878 \pm 2$  Ma (Fralick et al., 2002).

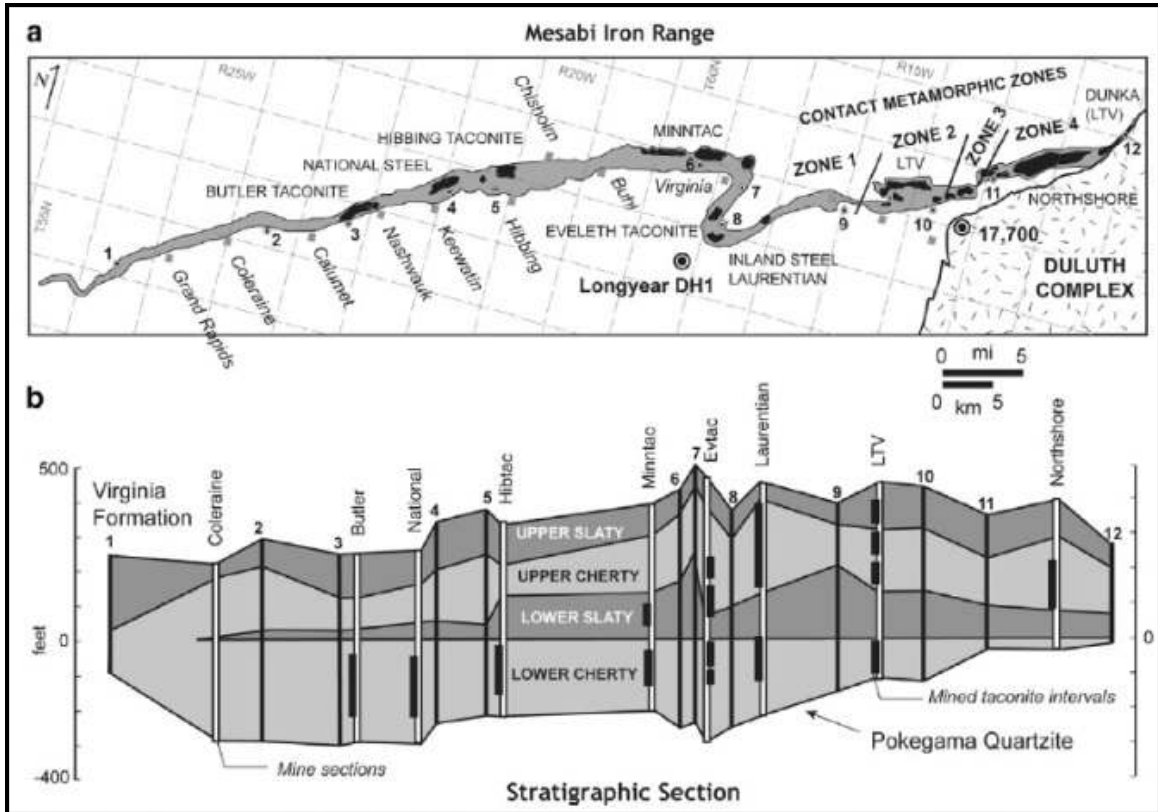


Figure 5: Simplified cross section of the Biwabik Iron Formation (in McSwiggen and Morey, 2008 after Jirsa et al., 2008).

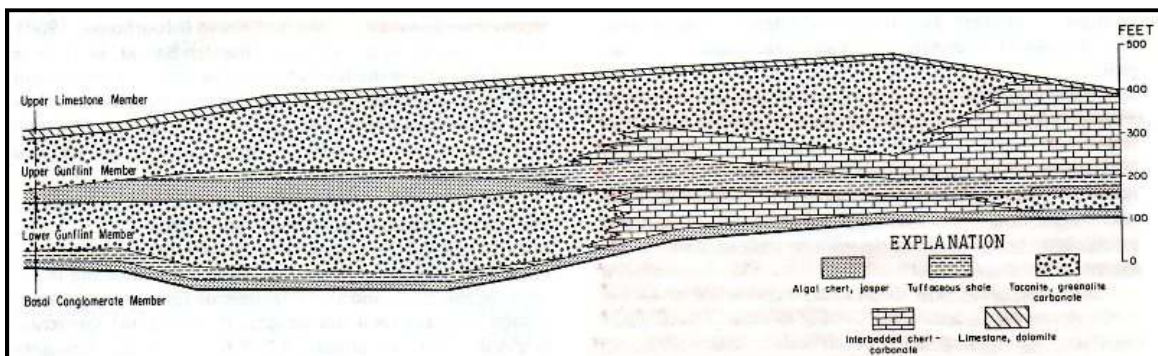


Figure 6: Simplified cross-section of the Gunflint Iron Formation (Morey, 1972).

The Virginia Formation is the uppermost Animikie Group unit along the Mesabi Range. It consists of argillite, argillaceous siltstone, very fine-grained greywacke, and minor amounts of carbonates, chert, and cherty sideritic iron formation. Argillite makes up nearly 80% of the lowermost 120-150 meters with alternating units of argillite, siltstone, and very fine greywacke in the upper portions. Morey (1970, 1972) concluded that most of the clastic sediments found in the Virginia Formation are derived from Archean rocks in the north and Paleoproterozoic rocks in the south (Morey, 1970; 1972). Radiometric dating of a zircon from an ash layer at the base of the Virginia Formation gave a date of about 1850 Ma (Hemming et al., 1996).

The stratigraphy of the Rove Formation, in the Gunflint Range, is almost exactly the same as the Virginia, where argillite makes up nearly 90% of the lower most 150 meters. This unit also contains alternating units of argillite, siltstone, and greywacke (with minor occurrences of quartzite) making up the rest (Morey, 1972). Radiometric dating on an ash layer near the base of the Rove Formation gave ages of  $1836 \pm 5$  Ma and  $1821 \pm 16$  Ma and zircons found 400 meters above the base of the Rove gave ages of 1780 Ma (Fralick et al., 2002).

## 2.2 Depositional Setting of the Animikie Group

Deposition of the Animikie Group sediments occurred in a shallow sea, which spread across what is now the Lake Superior region. It is thought that the Animikie Basin began with the deposition of clastic material on a stable shelf environment and morphed into

fine-grained sand and mud deposition in a deeper basin with low energy (Fig. 7). Many of the changes seen in lithology throughout the Animikie Basin were suggested to be the result of tectonic instability and volcanism during deposition. However, recent advances suggest a different depositional history, as will be described in more detail. (Morey, 1970; 1972; Ojakangas, 1983; Pufahl et al., 2000; Fralick et al., 2002; Ojakangas et al., 2005; Schulz and Cannon, 2007; Severson, 2010; and Poulton et al., 2010).

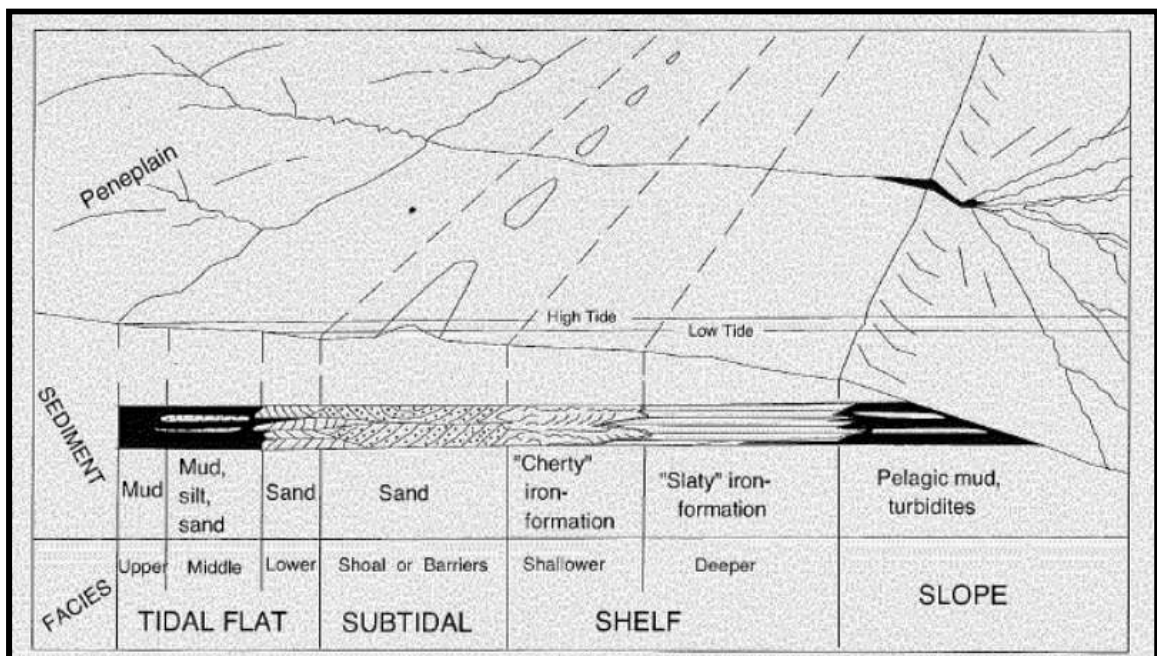


Figure 7: Schematic model for the environment of deposition for the Mesabi Range. The tidal flat and subtidal facies represents the Pokegema Formation, the Biwabik Iron Formation is represented by the shelf facies and the slope facies represents the Virginia Formation (Ojakangas, 1983).

### 2.2.1 Transgressive and Regressive Sequences

Morey (1970, 1972) presented one of the first depositional models for the Animikie Group sediments, suggesting that the transgressive and regressive sequences were the result of changes in relative baseline. He posited that the Pokegema and Kakabeka

Formations were formed in a high energy, tidally influenced, shoreline environment characterized by the deposition of sand and pebbles. The transition into the Biwabik and Gunflint Iron Formations represents the transition from a clastic depositional environment to an off shore environment characterized by chemical precipitation (Morey, 1972; Ojakangas et al., 2005).

To support his depositional model, Morey (1972) used mineral relationships in the Biwabik, observing the following vertical sequence: “hematite; hematite + magnetite; magnetite; magnetite + silicate; silicate; silicate + carbonate. The cycle then reverses itself, leading to hematite in the algal unit in the middle part of the upper cherty member. The water depth again deepened, resulting ultimately in the deposition of carbonate facies at the top of the iron formation” (Morey, 1972). Again, he found that deposition during the Biwabik is characterized by alternating phases of shallow and deep-water deposition (or transgressive and regressive cycling). Oxide-rich, granular facies were deposited in the shallow water and primary iron sulfides were deposited in the deep, reducing waters (Morey, 1972). He also suggested that the iron and silica were sourced to the Animikie Basin sea through “direct emanation or by reactions of water with the hot volcanic materials” (Morey, 1970; 1972), not terrigenous material.

Following the deposition of the Biwabik Iron Formation and without time markers or any obvious unconformities, Morey (1970, 1972) then interpreted the Rove and Virginia Formations were deposited almost contemporaneously in a deep, quiet water environment

with reducing conditions, allowing for the deposition of the argillite (plus some carbonates and pyrite). As this occurred, the basin began to subside at a rate faster than deposition allowing for the formation of a slope which accumulated very fine-grained silt material. Multiple turbidity currents along the slope deposited sand and silt derived from the surrounding plutonic material (Morey, 1972).

Ojakangas (1983, 2005), Schulz and Cannon (2005), and Severson et al. (2010) also generally agreed with Morey (1970, 1972) on the conditions that formed the Pokegama and Biwabik Formations. In short, the Pokegama Quartzite was deposited near the shoreline in a shallow, tidally influenced environment with a terrigenous sediment input. The Biwabik Iron Formation was then deposited seaward in a shelf environment, characterized by mineral precipitation stimulated by deep-ocean, iron-rich waters (Ojakangas, 1983; Ojakangas et al., 2005; Severson et al. (2010). It was suggested that the cherty members of the Biwabik were precipitated in a shallow, high-energy environment whereas the slaty members were more indicative of calm, deep-water settings (Fig. 7) (Ojakangas et al., 2005). Pufahl et al. (2000), while studying the correlative Gunflint Formation, also attribute the lateral facies changes to alterations in relative baseline. The Gunflint began with a transgressive sequence at the base (including conglomerate seen in the Kakabeka), shifted into a regressive sequence in the middle, and back to a transgressive sequence at the top of the formation, possibly including the Rove Formation (Pufahl et al., 2000).

### *2.2.2 Disconformity*

In the past decade, new geochronologic data from ash layers in the Rove Formation (Fralick et al., 2002) indicate a +40 Ma disconformity between the Biwabik/Gunflint and Rove/Virginia formations. This suggests an interruption in depositional conditions between the iron formation and overlying argillites; the interval coincidentally brackets the time during which the Sudbury meteorite impact occurred (1850 Ma; Schulz and Cannon, 2007). The Sudbury Igneous Complex, which filled the meteorite impact crater, is located about 980 km from Duluth near Sudbury, Ontario. Addison et al. (2005) also noted some ejecta between the Gunflint and Rove Formations that appeared to have been deposited sub-aerially, further implying a major shift in depositional environment, including the possibility of emergence.

### *2.2.3 Sediment Sources and Shifting Ocean Chemistry*

Although the timing of the the cessation of iron formation deposition coincides with the Sudbury Impact, geologists, such as Poulton et al. (2010), do not believe the meteorite impact is the driving mechanism. Rather, Poulton et al. (2010) hypothesize a shift from aqueous mineral precipitation to terrigenous sediment input disrupted the ocean chemistry. They posit that the terrigenous input stimulated increased sulfate reduction which in turn depleted the dissolved iron (as the flux of sulfate was greater than the flux of reactive iron), allowing for the ocean to shift from a primarily ferruginous environment to a sulfidic environment, effectively ceasing all iron formation precipitation (Poulton et al., 2010).

## 2.3 Tectonic Evolution of the Animikie Basin

The Animikie Group sedimentary rocks along the Mesabi Range were affected by at least two tectonic events. The first was moderate faulting and folding occurring during and following deposition due to compressional effects of the 1.85 Ga Penokean Orogeny (Morey and Southwick, 1995; Schulz and Cannon, 2007). At 1.1 Ga, the Animikie Group was then thermally metamorphosed by the emplacement of the Duluth Complex during the formation of the Midcontinent Rift (French, 1968; McSwiggen and Morey, 2008; Jirsa et al., 2008). Morey (1970) pointed out that the Biwabik Iron Formation contains several other structural features that may or may not be explained by these deformational events, including the Virginia Horn, the Siphon Structure, the Biwabik Fault, numerous cross faults, and the Sugar Lake Anticline, to name a few. Gruner (1964) and White (1954) each concluded the southward dip found in some of the structures in the Mesabi Range, such as those seen in the Biwabik Fault and Sugar Lake Anticline, may be attributed to the formation of the Lake Superior anticline during the Midcontinent Rift event (Morey, 1970).

### 2.3.1 *Penokean Orogeny*

Several tectonic models have been proposed for the evolution of the Penokean Orogeny. Some scientists, like Morey and Southwick (1995), found that prior to iron formation deposition, the Animikie Basin was experiencing extension. Then, during iron formation deposition the basin began to compress. Alternatively, Pufahl et al. (2000) suggested the evolution of the Animikie Basin is “consistent with ... beginning as a passive margin

with a back arc basin, and ending as a telescoped back arc basin that closed as a result of a change in relative plate convergence direction” (Pufahl et al., 2000). Schulz and Cannon (2007) agree.

The most complete and presently accepted summary of current ideas on the tectonic progression of the Penokean Orogeny (Fig. 8) was presented by Schulz and Cannon (2007). The oldest portion of Penokean is the Chocolay Group, a basal quartzite in the Menominee Range, which was deposited between 2.3 and 2.2 Ga in a rift basin with an extensive ocean. The Penokean Orogeny evolved in the Becker Embayment, which possibly formed as a result of rifting in the Penokean Margin around 2150 Ma. Deposition of the Chocolay Group was followed by a 300 Ma hiatus. By about 1890 Ma the ocean began to close and the Pembine-Wausau Terrane was formed in the east, while the Chocolay Group and equivalent sediments continued to form in the west. Deposition of the Animikie Group on top of Archean basement began at about 1880 Ma. By 1875 Ma the Pembine-Wausau Terrane was accreted against the Superior Craton in the east and subduction flipped, bringing the newly formed Marshfield Terrane towards the west. A marginal arc and tholeiitic magmas formed as a result. Near or at the time of the Sudbury impact event (1850 Ma), subduction ceased with the closure of the ocean and collision of the Marshfield and Pembine-Wausau Terranes, allowing for significant terrigenous input into the foreland basin. A fold and thrust belt was created around 1840 Ma along the southern margin of the Animikie Basin. Most of the rocks affected by the Penokean were subjected to upper amphibolite metamorphic facies and the orogeny

ceased around 1830 Ma. It has been posited that the Rove Formation continued to be deposited post-Penokean (Schulz and Cannon, 2007).

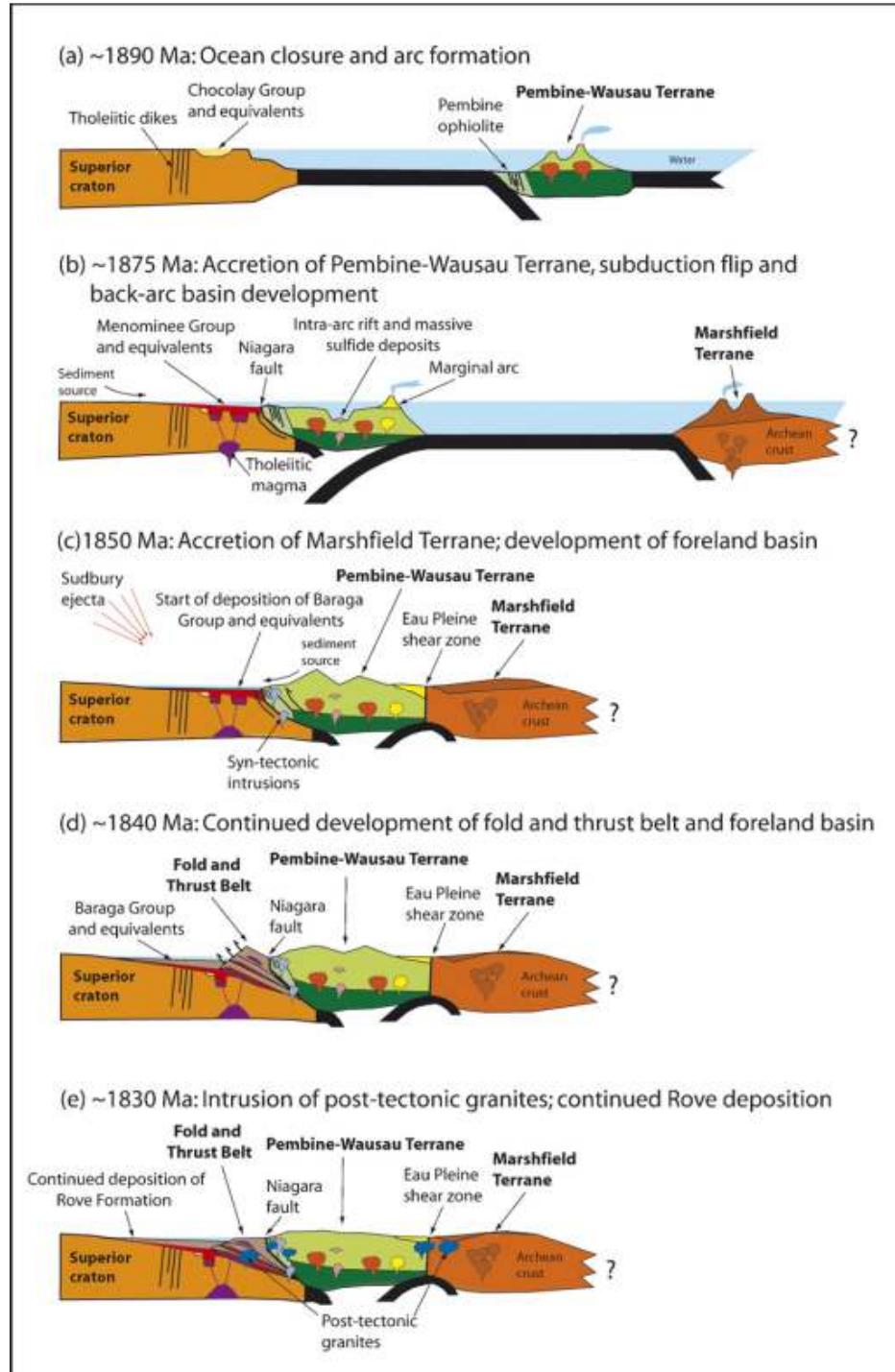


Figure 8: Evolution of the Penokean Orogeny (Schulz and Cannon, 2007).

### *2.3.2 Duluth Complex*

The Duluth Complex, a multiply emplaced intrusive complex formed during the 1.1 Ga Midcontinent Rift, had a minor deformational effect, but a very strong metamorphic influence on adjacent portions of the Biwabik and Gunflint Iron Formations. The thermal effects are constrained to an aureole in the eastern Mesabi District and the Minnesota portion of the Gunflint Range (French, 1968; Bonnicksen, 1969; Morey, 1970; Jirsa et al., 2008; McSwiggen and Morey, 2008). Initially thought to be isochemical, the Duluth Complex has since been considered to be, in part, a metasomatic intrusion. Not only were volatiles, such as water and carbon dioxide, released during metamorphism, but the Re-Os isotope values seen in the support the notion of hydrothermal fluid flow component to the intrusion (Bonnicksen, 1968, Williams et al., 2010). Both prograde and retrograde metamorphic minerals are present in the iron formation as a result of contact metamorphism by the intrusion (McSwiggen and Morey, 2008). Peak metamorphic grades were defined by the presence of grunerite and cummingtonite (garnet grade) and pyroxene-bearing rocks (sillimanite grade) (Bonnicksen, 1968). It is posited that the Duluth Complex magmas were emplaced at temperatures of about 1200°C (Jirsa et al., 2008). A maximum temperature range for the metamorphism of the Biwabik is 700-750°C, determined from  $O^{18}/O^{16}$  ratios in iron formation rocks near the contact with the Duluth Complex (French, 1968). This was later refined by Bonnicksen (1969), who found metamorphic pigeonite at the boundary yielding a minimum peak temperature in the Biwabik of roughly 825°C. Hyslop et al. (2008) concluded from Bonnicksen's peak

temperature estimate, that the Biwabik Iron Formation cooled at a rate of about 5.6°C/kyr, reaching a temperature of 400°C in about 75 kyr.

In a classic study on the metamorphism of the Biwabik Iron Formation by French (1968), he defined four metamorphic zones in the Biwabik Iron Formation and three zones in the Gunflint Iron Formation based on metamorphic mineral assemblages (Fig. 9). The four zones defined by French (1968) for the Biwabik Iron Formation are:

1. Unaltered Taconite: farthest from the Duluth Complex; characterized by fine-grained taconite, plus quartz, iron oxides, iron carbonates, and iron silicates.
2. Transitional Zone: No visible mineralogical changes; characterized by secondary replacement of the original minerals by quartz and ankerite.
3. Moderately Metamorphosed Taconite: 3.25-5 km from the contact with the Duluth Complex; attaining a temperature of about 300-400°C; characterized by the loss of layered silicates and carbonates and the appearance of grunerite.
4. Highly Metamorphosed Taconite: adjacent to the contact with the Duluth Complex; characterized by an increase in hardness and grain size; appearance of iron bearing pyroxenes.

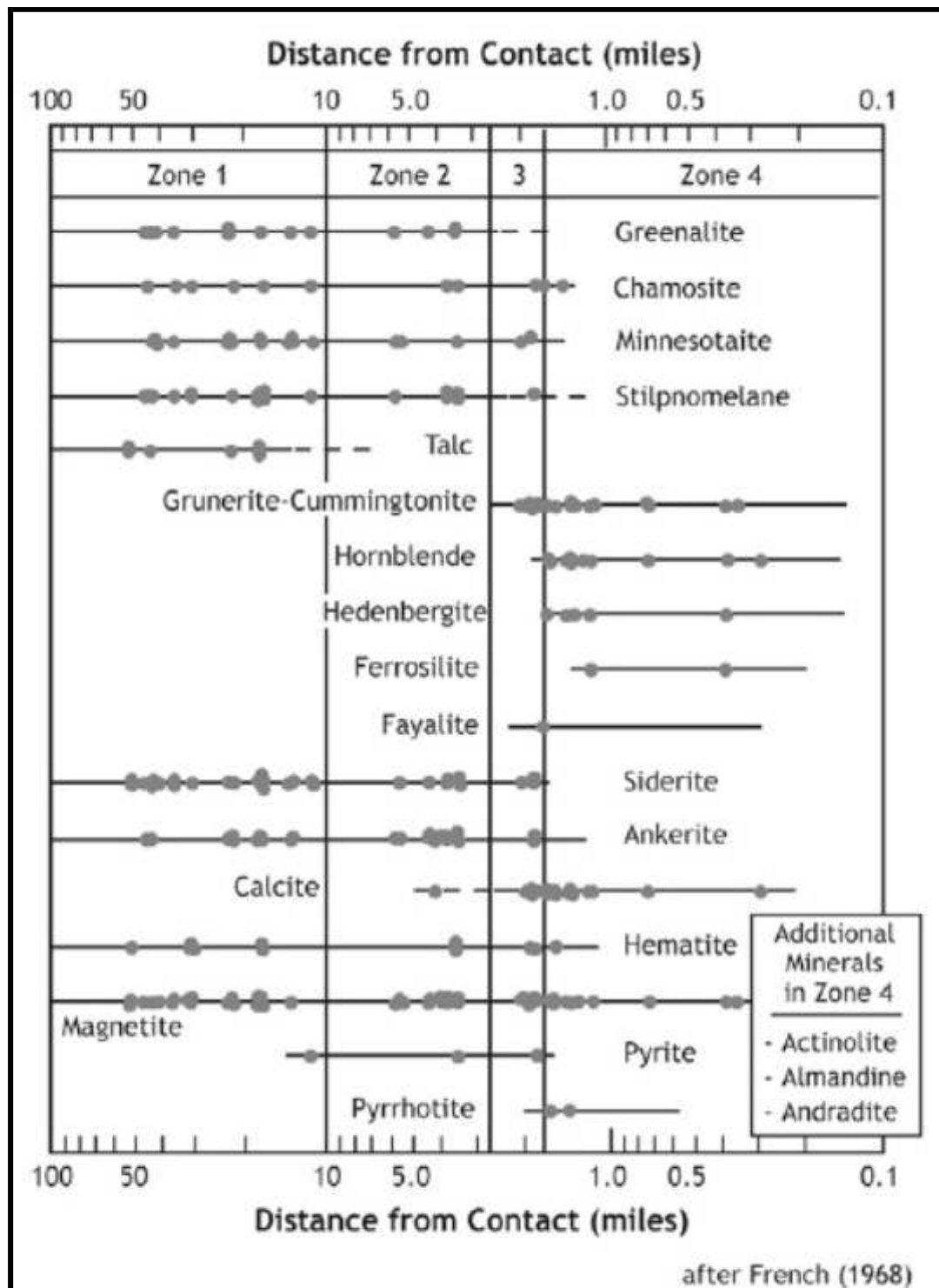


Figure 9: The relationship between mineral occurrences in the Biwabik Iron Formation and the distance from the contact with the Duluth Complex. Special attention should be paid to pyrite and pyrrhotite arrivals and departures (In McSwiggen and Morey, 2008 after French, 1968).

## 2.4 Ore Formation

Two different types of minable ore are found in the Biwabik Iron Formation: magnetic taconite ore (taconite) and direct shipping ore (natural ore). Production of natural ore ceased in the 1970s, but taconite is still actively mined. Taconite is considered the primary product of iron formation deposition with metamorphic overprinting whereas the natural ore is resultant of post-depositional fluid flow along faults and fissures (Morey, 1999; Jirsa et al., 2008; Severson et al., 2010).

Taconite occurs as three texturally different occurrences: disseminated, aggregated, and layered clusters (Morey, 1970; 1972). Magnetite, when fine-grained, is assumed to be the product of primary processes. However, coarser grained, euhedral crystals are also present near the contact within the iron formation resultant of metamorphic recrystallization caused by the emplacement of the Duluth Complex (LaBerge, 1964; LaBerge et al., 1987; Zanko et al., 2003; Severson et al., 2010). Bleifuss (1964) found that hematite and goethite appear to be the product of weathering primary magnetite and siderite (Severson et al., 2010). Most of the taconite is found in the cherty beds as tabular, stratified bodies and has primarily been extracted from the Lower Cherty, with lesser amounts from the Upper Cherty and Upper Slaty (Jirsa et al, 2008; Severson et al., 2010).

The natural ores are only found on the Mesabi and Cuyuna Ranges (Morey, 1970; 1972; Jirsa et al, 2008), located along faults, fractures, fissures, and bedding planes (Fig. 10). Morey (1999) notes that almost 80% of the natural ore in the Mesabi Range is in close

proximity to a fault. Much debate surrounds the origin of natural ore formation. The two main theories are either the natural ore was formed from descending meteoric fluid or ascending hydrothermal fluid (Morey, 1999; Severson et al., 2010). However, the formation of natural ores is not resultant of a singular process, but rather a complex interaction of multiple events (Severson et al., 2010).

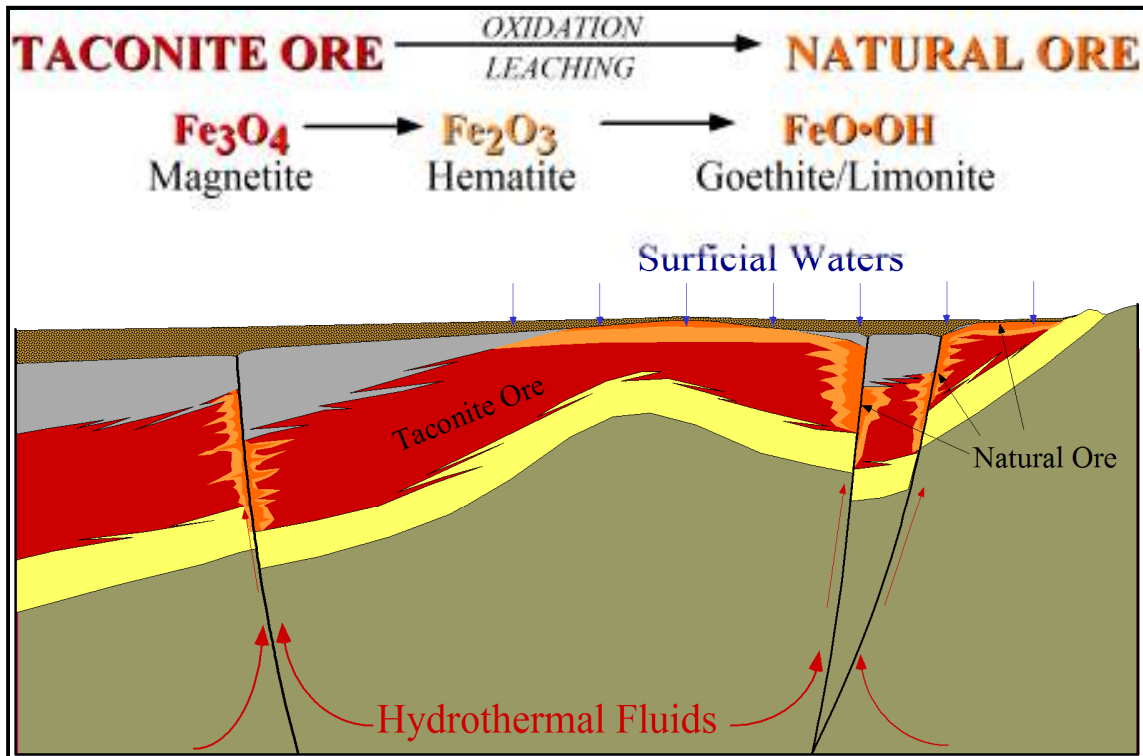


Figure 10: The spatial relationship between taconite ore, natural ores, and faults in the Mesabi Range. Distribution of natural ores are suggested to be caused either by the downward migration of surficial waters or the upward flow of hydrothermal fluids (Miller, unpublished).

## Chapter 3: Sulfur Geochemistry

The primary objective of this thesis is to delineate the distribution of sulfide minerals in the Biwabik Iron Formation in terms of sulfur isotope signature. Sulfur geochemistry in Paleoproterozoic aqueous-sedimentary systems is inherently complex, due to a combination of biological processes and nearly two billion years time. Thus, in order to properly understand the distribution of sulfur isotope values in the Biwabik Iron Formation, it is important to delineate the possible sources of variation, both natural and analytical. A review of studies regarding sulfur isotope distribution in various Paleoproterozoic iron-formations, which address the possible sources of sulfur, is useful to compare with the data collected for this study in the Biwabik Iron Formation.

### 3.1 Sulfur Isotopes

Sulfur has four stable isotopes:  $^{32}\text{S}$ ,  $^{33}\text{S}$ ,  $^{34}\text{S}$ , and  $^{36}\text{S}$ . The sulfur isotope value, or  $\delta^{34}\text{S}$ , is a measure of the ratio of the two most abundant isotopes,  $^{34}\text{S}$  and  $^{32}\text{S}$  (as  $^{34}\text{S}/^{32}\text{S}$ ), relative to that of a reference standard and is determined with the following equation:

$$\delta^{34}\text{S} = \left( \frac{(^{34}\text{S}/^{32}\text{S})_{\text{sample}} - (^{34}\text{S}/^{32}\text{S})_{\text{reference}}}{(^{34}\text{S}/^{32}\text{S})_{\text{reference}}} \right) \times 1000,$$

where  $\delta^{34}\text{S}$  is expressed in terms of per mil (or parts per thousand, ‰). The values derived from this can be used to constrain a possible origin of the sulfur in question. Figure 11 (from Coplen, 2002) shows the range of  $\delta^{34}\text{S}$  values for different sulfur sources and their related environments of origin. The reference, or standard, used for comparison

and calibration is the Cañon Diablo troilite (CDT) which has a  $\delta^{34}\text{S}$  value of 0‰, which is considered to be that of the bulk Earth signature (Gunter, 1986; Sharp, 2007).

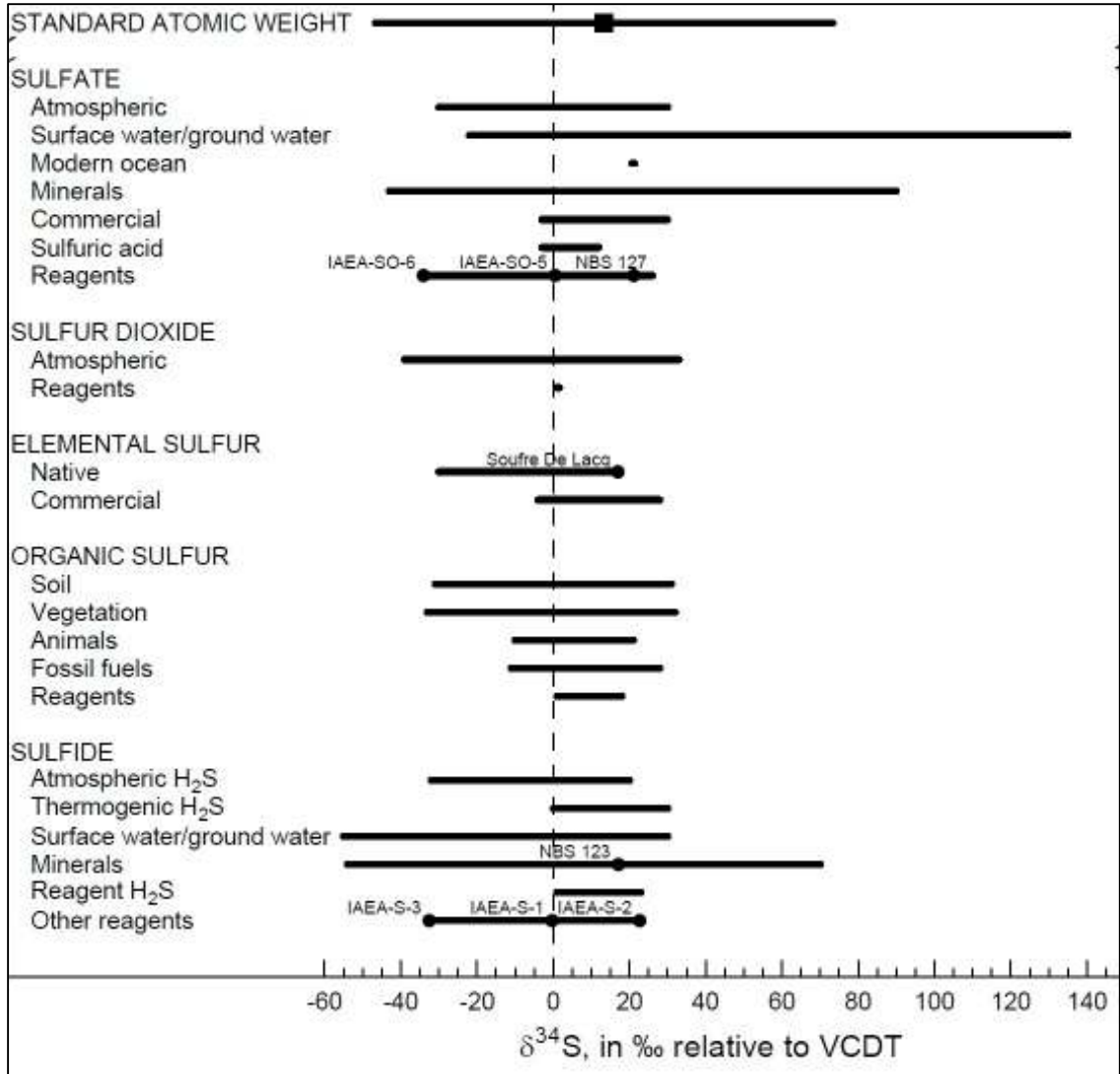


Figure 11: Range of  $\delta^{34}\text{S}$  values for various sulfur-bearing materials (From Coplen, 2002).

### 3.1.1 Sulfur Isotope Analysis

Mass spectrometric analysis methods for sulfur isotope ratios typically involve one of two gases,  $\text{SO}_2$  or  $\text{SF}_6$ . Both methods are used widely, and although small variations

between the values obtained by each exist, correction methods can be applied to compare data (Coplen et al., 2002; Vienna, 2000). In 2000, The International Atomic Energy Agency (IAEA) (Vienna, 2000) mathematically defined the relationship between the two methods as follows:

$$\delta^{34}\text{S}_{\text{SF}_6} = 1.0339\delta^{34}\text{S}_{\text{SO}_2} - 0.34$$

This is of note, as this study analyzed samples using the SO<sub>2</sub> method, but, as will be discussed later, comparison will be made with other values derived from the SF<sub>6</sub> method.

A more detailed discussion of the methods used in this study is given in Chapter 4.

### *3.1.2 Secular Variations of $\delta^{34}\text{S}$*

A variety of natural effects can account for variations in sulfur isotope values. As depicted in Figure 11, different reservoirs yield different isotopic signatures, but variations within each reservoir exist as well. Most  $\delta^{34}\text{S}$  values measured in this study range from +30‰ to -30‰, but naturally occurring values for sulfides have been recorded from -55‰ to nearly +80‰ (Raiswell, 1982; Coplen et al., 2002). Many natural processes lead to changes in  $\delta^{34}\text{S}$ , one of the most important being fractionation associated with sulfate reduction. The degree of fractionation can be affected by the specific mechanism (i.e., rate limiting step) associated with the process, temperature, relative concentration of available sulfur/sulfate during the reduction process, the source of sulfur, and the degree and type of recycling (i.e., closed vs. open systems) (Gunter, 1986; Sharp, 2007).

Most data from Precambrian sediment studies suggest that bacterial reduction of sulfate to sulfide followed by reaction with reduced iron is the most important primary mechanism leading to sulfide precipitation. The reduction of sulfate and subsequent precipitation of sulfides will occur “as long as (1) organic material is available for sulfate-reducing bacteria, (2) reactive iron is present to react with H<sub>2</sub>S, and (3) sulfate is available as a reactant” (Sharp, 2007). Once this begins, the amount of sulfur isotopic fractionation is inversely proportional to the sulfate reduction rate (Gunter, 1986). That is, rapid reduction rates, indicative of productive reducing environments, produce small degrees of fractionation, thus yielding sulfur isotope values in the sulfide close to that of the original sulfate source. Alternatively, if the conditions do not promote rapid reduction and the process is slow, conditions would then allow for greater degrees of fractionation, yielding sulfur isotopic values in the sulfide that are much lighter than the sulfate source. It is possible to estimate the  $\delta^{34}\text{S}$  value of the source sulfate values via Rayleigh distillation in some systems (Sharp, 2007).

### 3.2 Sulfur Isotope Geochemistry of Paleoproterozoic Iron Formations

Research related to sulfur isotopes and sulfide paragenesis has been sparse for the Biwabik Iron Formation. However, several notable studies were conducted in various other Precambrian iron formations that use sulfur isotopes to help understand atmospheric and ocean chemical evolution and iron formation deposition during the Paleoproterozoic. Isotopic evidence for bacterial sulfate reduction occurs in rocks as old as 3.2 to 2.8 Ga but, by 1.8 Ga the deep ocean during formation of the Animikie Basin is

believed to have been transitioning from a ferruginous ocean to sulfidic ocean environment (Johnston et al, 2006; Canfield, 2004). Therefore, it has been posited by Canfield and Raiswell (1999) and Gunter (1986) that bacterial sulfate reduction could have been a major source of sulfur during the deposition of the Animikie Group.

### *3.2.1 Sulfur Isotope Studies of the Biwabik and Gunflint Iron Formations*

As previously mentioned, it is generally accepted that the Biwabik Iron Formation and the Gunflint Iron Formation are correlative units that have been separated by the emplacement of the 1.1 Ga Duluth Complex. However, Carrigan and Cameron (1991) described the Gunflint Iron Formation as a “virtually unmetamorphosed Precambrian iron-formation” that has preserved its primary textures. The only notable effects of metamorphism were caused by diabase sills, creating localized effects (Carrigan and Cameron, 1991). That being said, the effects of the emplacement of the Duluth Complex on the Gunflint Iron Formation are minimal and therefore sulfur isotope analysis on the Gunflint Range may yield a pre-Duluth Complex geochemical signature, similar to the unmetamorphosed portions of the Biwabik Iron Formation located in the western-most portions of the Mesabi Range.

Three notable studies have been conducted on the sulfur isotope composition of the Biwabik and Gunflint Iron Formations. Carrigan (1990) and Carrigan and Cameron (1991) were the first to report sulfur isotope compositions of the Gunflint Iron Formation. Next, Johnston et al. (2006) studied the isotopic geochemistry of various Paleoproterozoic

iron formations in the Lake Superior region, including the Biwabik and the Gunflint Iron Formations. Most recently, Poulton et al. (2010) conducted a comprehensive geochemical study of sedimentary sequences along the Mesabi and Gunflint Ranges in an attempt to determine the ocean chemistry during iron formation deposition.

Carrigan (1990) and Carrigan and Cameron (1991) sampled and analyzed three type of pyrite in the Gunflint Iron Formation. The types were delineated based on their mineral textures: fine-grained, disseminated (Type 1); coarse-grained, euhedral (Type 2); and ellipsoidal concretions (Type 3). Figure 12 shows the stratigraphic distribution of samples and their corresponding  $\delta^{34}\text{S}$  values. Their study found that  $\delta^{34}\text{S}$  values were not related to a specific lithology or the result of metamorphism. Rather, variations resulted from the sulfide minerals stratigraphic position. More specifically, throughout the majority of the Gunflint Iron Formation pyrite had a narrow range of values from +4‰ to +12‰. However, in the Kakabeka Falls area in Ontario, values ranged from -18.2‰ to +22‰ (Fig. 12). They suggested that the narrow range of slightly  $\delta^{34}\text{S}$ -enriched values was due to bacterial reduction of low concentrations of dissolved sulfate whereas the wide range of values observed in the Kakabeka Falls area was resultant of sulfur derived from fluid, possibly hydrothermal, circulating through the basin via syn-depositional faults.

In a more general study of Paleoproterozoic iron formations in the Lake Superior area, Johnston et al. (2006) analyzed samples from the Gunflint, Biwabik, Trommald, Mahnomen, and Rove Formations to examine the transition from a ferruginous to a

sulfidic ocean, corresponding to the cessation of iron formation precipitation around 1.84 Ga. Their study noted an average range of  $\delta^{34}\text{S}$  values in the iron formation to be  $8.4 \pm 4.6\%$ . These values were interpreted to be the signature of sedimentary (or primary) sulfides formed via rapid sulfate reduction on a continental shelf and intracratonic basin. The combination of depositional setting and incomplete reduction resulted in  $\delta^{34}\text{S}$  values less than that of seawater sulfate.

This was followed up by a more recent, detailed study conducted by Poulton et al. (2010), which aimed to constrain the mechanisms behind the same shift in ocean chemistry. Poulton et al. (2010) used a variety of geochemical analyses, such as iron speciation, aluminum content, organic carbon content, and sulfur isotope values, to constrain the environments of sulfide deposition. For the Mesabi and Gunflint Ranges, they relied specifically on the sulfur isotope chemistry of samples interpreted to contain primary sulfides (i.e., those formed at the time of iron formation deposition). Figure 13 shows the stratigraphic distribution of  $\delta^{34}\text{S}$  values at various locations along the Mesabi and Gunflint Ranges reported in their study.

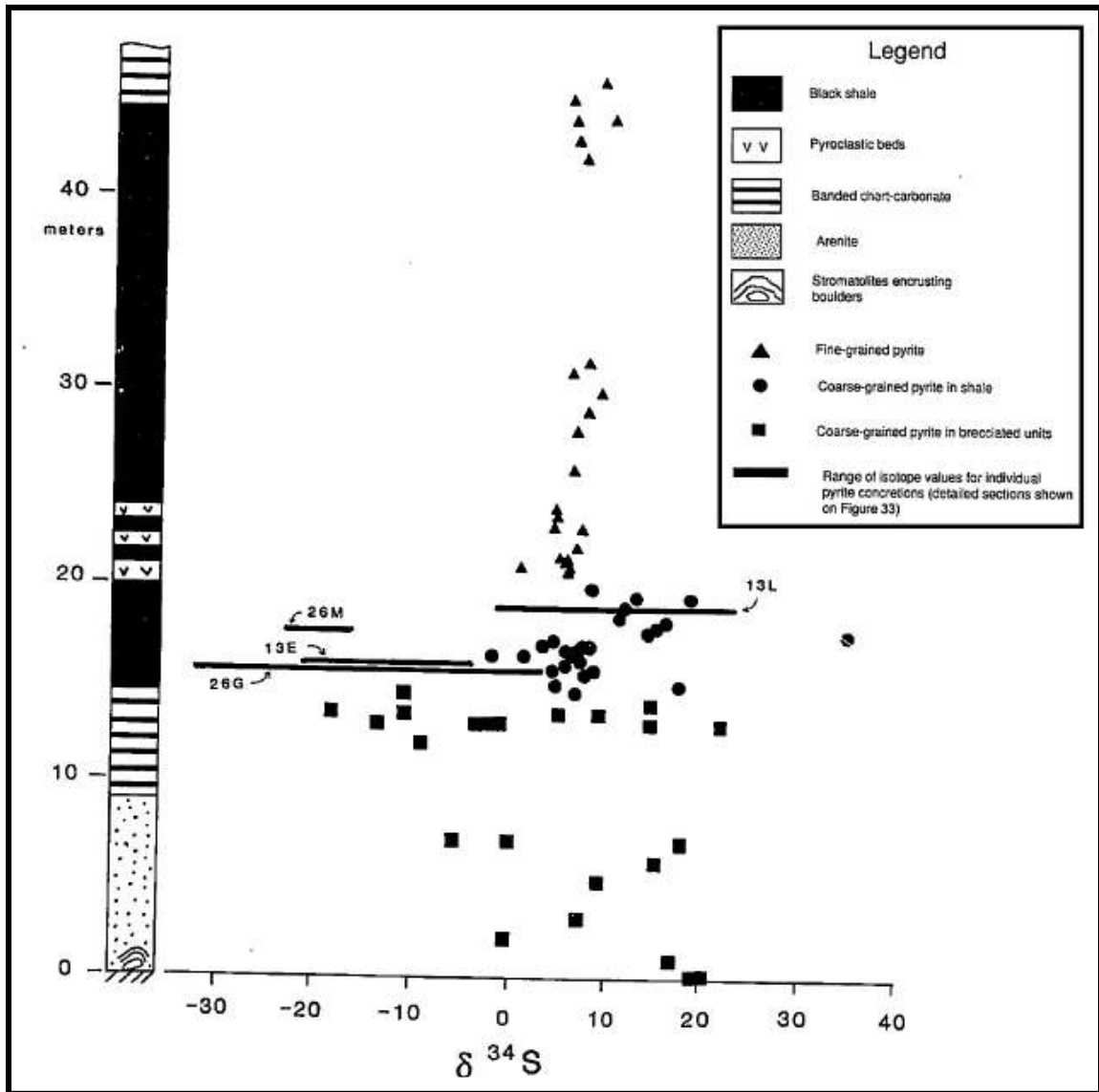


Figure 12: Distribution of samples and corresponding  $\delta^{34}\text{S}$  values (in parts per mil) collected from the Gunflint Range, at Kakabeka Falls, Ontario, Canada (From Carrigan, 1990).

Poulton et al. (2010) concluded that the sulfur isotope geochemistry reflects two distinct zones of ocean chemistry: euxinic and ferruginous. The euxinic zone, located near-shore, yielded heavier  $\delta^{34}\text{S}$  values nearing that of late Paleoproterozoic seawater sulfate (~17‰). The average  $\delta^{34}\text{S}$  values for sulfide formed in the deep water, ferruginous zone

were slightly lighter, around  $5.5 \pm 3.6\%$ . They suggested that a combination of organic carbon and sulfate fluxes shaped the two zones. More specifically, a decreased supply of organic material to the deep water limited the rate of sulfate reduction, thus explaining the lighter sulfur isotope values seen in the ferruginous zone. In contrast, the euxinic zone, which was more readily supplied with organic matter from continental weathering, saw almost all of the sulfate in the water reduced into sulfides and subsequently precipitated. In terms of iron fluxes, Poulton et al. (2010) posit that the primary source of Fe (II) is hydrothermal vents, and therefore iron is readily supplied to the deep-water ferruginous zone and decreases systematically, due to precipitation, as it travels towards the euxinic zone (Figure 14). For primary sulfide minerals, the  $\delta^{34}\text{S}$  values progressively deplete as they move from shoreline to deep-water; this distribution is supported by studies conducted by Johnston et al. (2006) and Canfield (2004), as mentioned above. As seen in Figure 15, taken from the Poulton et al. (2010) report, the euxinic zone corresponds to Rove Formation in the Gunflint Range and a small portion of the lower Virginia Formation in the eastern part of Mesabi Range. The ferruginous zone corresponds to almost the entire stratigraphic sequence along the Mesabi Range and the Gunflint Iron Formation along the Gunflint Range.

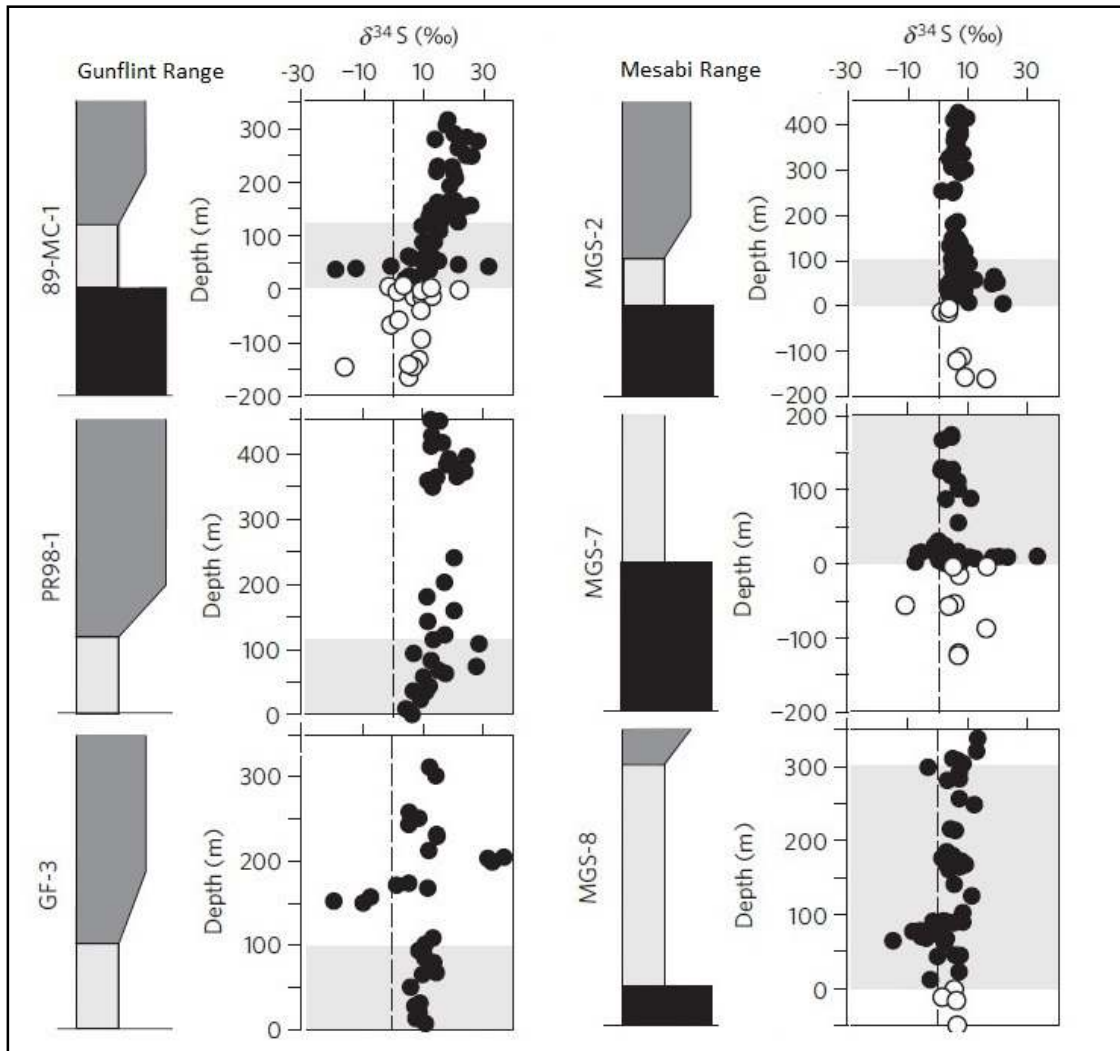


Figure 13: Distribution of primary sulfide mineral samples from Animikie Group sediments and their corresponding  $\delta^{34}\text{S}$  values. Darkened circles represent values obtained from samples located in the Rove and Virginia Formations, open circles are for samples from Gunflint and Biwabik Iron Formations (From Poulton et al., 2010).

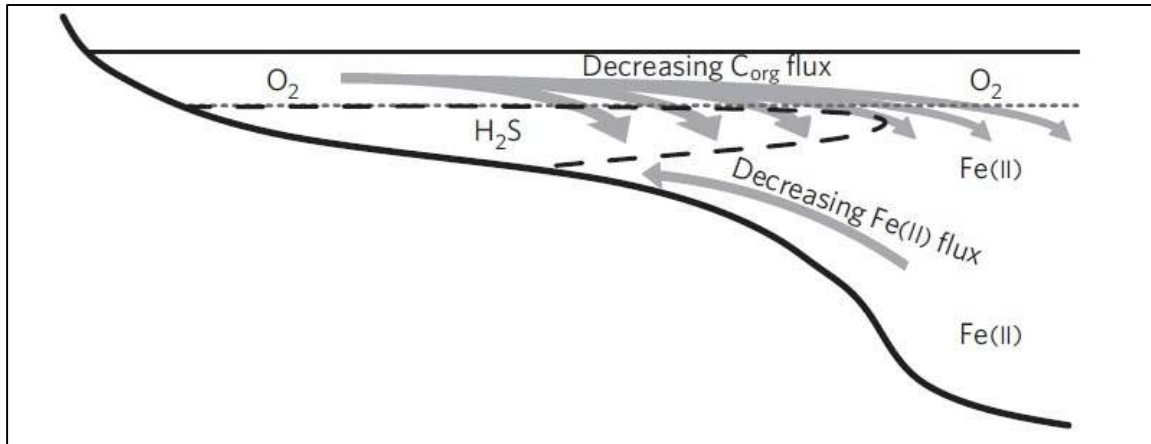


Figure 14: Directional fluxes of organic carbons and hydrothermal Fe (II), limiting factors in sulfate reduction (From Poulton et al., 2010).

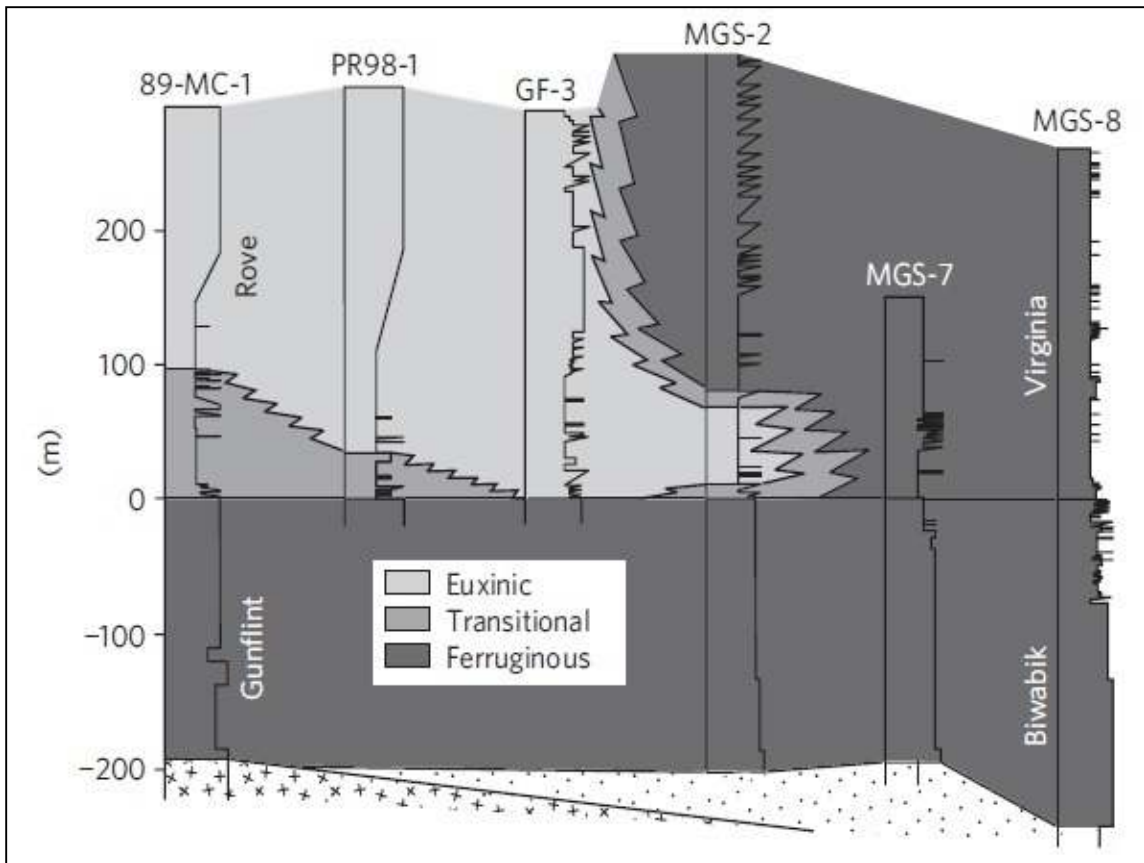


Figure 15: Ocean chemistry model for the sedimentary sequences along the Mesabi and Gunflint Ranges (From Poulton et al., 2010).

The average  $\delta^{34}\text{S}$  values measured from samples located in the iron formations from both Carrigan and Cameron (1991) and Poulton et al. (2010) studies agree with the range of values found by Johnston et al. (2006) in other Lake Superior-type iron formations. This suggests an overall similar mechanism of primary sulfide precipitation during the deposition of the Animikie Group sediments. That is, the primary sulfide minerals formed as a result of bacterial reduction of late Paleoproterozoic seawater sulfate. The degree to which the seawater sulfate was reduced, however, is a function of the localized conditions, including the supply of organic material.

### *3.2.2 Sulfide Mineral Paragenesis in the Gunflint Iron Formation*

Carrigan and Cameron's (1991) study of the Gunflint Iron Formation reported detailed descriptions of the sulfide mineralogy and textural occurrences of sulfides from which they interpreted the sulfide mineral paragenesis. The main sulfide minerals found in the Gunflint Formation are pyrite and pyrrhotite, with pyrite occurring in distinctly fine-grained or coarse-grained habits (Carrigan and Cameron, 1991). Fine-grained pyrite was most abundant and is interpreted as being indicative of primary sulfide precipitation. They interpret coarse-grained pyrite to have formed by recrystallization during burial. The occurrence of pyrrhotite is attributed to contact metamorphism-induced transformation from pyrite. Carrigan and Cameron's (1991) paragenetic sequence for the carbonate and sulfide minerals in the Gunflint Iron Formation is shown in Figure 16.

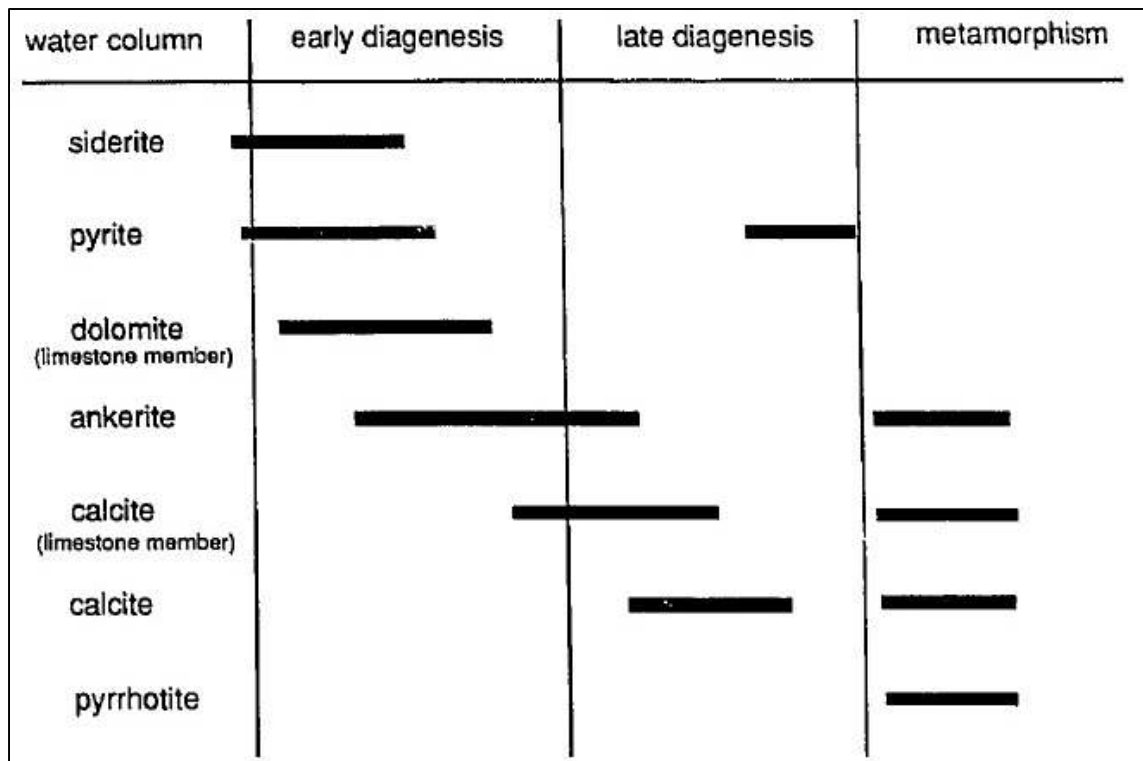


Figure 16: Carbonate and sulfide mineral paragenesis in the Gunflint Iron Formation (From Carrigan, 1990).

In studies of the overall mineral paragenesis of the Biwabik Iron Formation within the thermal aureole of the Duluth Complex, French (1968) and McSwiggen and Morey (2006) noted that pyrite gives way to pyrrhotite within 3.25 km from the intrusive contact (Fig. 9). Although the sulfide isotope studies by Johnston et al. (2006) and Poulton et al. (2010) did not describe the range of sulfide mineral occurrences in the Biwabik Iron Formation in detail, a similar paragenetic distribution of primary and secondary sulfides as observed in the Gunflint by Carrigan and Cameron (1991) would be expected for the Biwabik given the stratigraphic correlation and depositional similarities between the two iron formation units.

## **Chapter 4: Methods**

A detailed, two component sampling strategy was delineated to properly address the main objectives of this study: the lateral and stratigraphic distribution of sulfide minerals in the Biwabik Iron Formation. During sample selection, it became evident that sulfide mineral habit may also be an important factor relating to the overall sulfide paragenesis and therefore it was added as an additional objective. Once the strategy was implemented and carried out, the samples were photographed, carefully described, analyzed for their sulfur isotopic composition, and/or were cut and made into polished thin section for mineral paragenesis and identification purposes.

### **4.1 Sampling Strategy**

The first component of the sampling strategy was to select drill cores evenly spaced along the entire strike length of the Mesabi Range and that profile the entire stratigraphy of the Biwabik Iron Formation starting from the lower portion of the Virginia Formation and continuing into at least the top of the Pokegama Formation. Collecting samples along the Mesabi Range is particularly important in order to determine what, if any, lateral differences exist due to the effects of metamorphism by the Duluth Complex. The second component was to evenly profile the stratigraphy by obtaining samples from each member of the Biwabik Iron Formation (Upper Slaty, Upper Cherty, Lower Slaty, Lower Cherty, and Intermediate Shale) and the lower part of the Virginia Formation. It was estimated that this two-component sampling strategy would yield a minimum of 50-60

samples. An ancillary benefit to this overall ideal sampling strategy is it entails a careful inspection of all sections of the core for its sulfide content and lithologic setting, as well as locations where visible sulfide minerals are not present in the rock record. Biased sampling was deemed the preferred method of sample selection due to the heterogeneity of the iron formation, low sulfide concentrations, and monetary constraints.

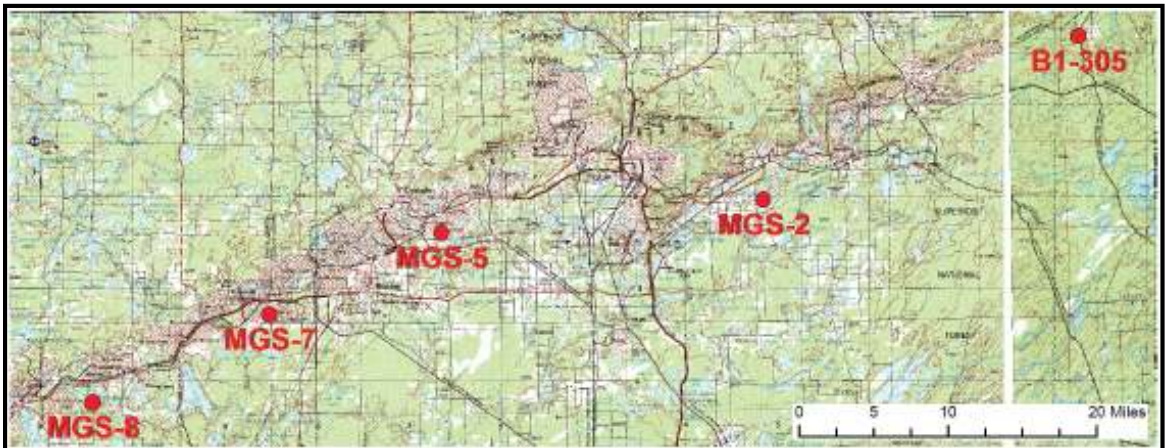


Figure 17: Locations of drill core along the Mesabi Range selected for this study.

Five drill cores were chosen across the Mesabi Range that met the criteria specified above and were well spaced across the range, covering a strike length of approximately 110 kilometers (Fig. 17). Four cores were drilled by the Minnesota Geological Survey as part of the “Mesabi Deep Drilling Project” in the late 1960’s. From southwest to northeast, MGS-8 is located near the town of Calumet, MGS-7 is located near Keewatin, MGS-5 is located southwest of Chisholm, and MGS-2 is located near Biwabik. The fifth core (B1-305) was drilled by Bear Creek (now Kennecott-Rio Tinto) as an exploratory hole for Cu-Ni sulfide mineralization associated with the base of the Duluth Complex. The mineralized gabbro of the Duluth Complex, which is part of the Mesaba deposit currently held by Teck American, is in intrusive contact with the Virginia Formation just

above its contact with the Biwabik Iron Formation. This core provides samples of the iron formation that were most intensely affected by the thermal metamorphism of the Duluth Complex. The drill cores were logged in detail by Mark Severson of the Natural Resources Research Institute (NRRI) between 1993 and 2005, which was very helpful in the focusing in on sampling particular stratigraphic units for this study. Sampling was conducted at the Minnesota Department of Natural Resources core library in Hibbing, Minnesota

During sample selection, the core was initially scanned in its entirety and any visible sulfide occurrences were noted. Each occurrence was briefly described as to its morphology, host lithology, relative size, stratigraphic distribution, and depth in the core run. Then, a half- to quarter-core samples, measuring between 5 and 20 centimeters, were collected from each stratigraphic unit in all five cores, if available. Two samples of natural ore (direct shipping ore) were collected in the field at the Fayal Mine. In total, 123 samples were collected. This is larger than the initial estimate of 50-60 samples, as the sulfide minerals present in the core were smaller than originally anticipated and thus may not have contained enough sulfides per sample to allow for both sulfur isotope analysis and to make a thin section. In addition, the sulfide mineral occurrences were more varied than anticipated. Therefore, additional samples were collected to address the distribution and geochemistry of the various morphologies of sulfide occurrences. In some instances, no samples were collected either due to lack of sulfides or lack of available core. Thus,

portions of the range were not characterized and therefore additional sampling is necessary for a more complete interpretation.

Following sample selection from the drill core, detailed macroscopic descriptions of the sulfide occurrences were tabulated, including sulfide type, habit, size, host rock, distribution, and any other distinguishing characteristics. Representative samples of each morphology were then sampled at each core location and stratigraphic unit, as possible, for isotope analysis and/or petrographic analysis. Representativeness was based on size, as there were analytical sample weight requirements. Figure 18 shows the locations of the samples used for sulfur isotope analysis and thin sections in this study.

## 4.2 Sulfur Isotope Analyses

Sulfur isotope sample preparation and analysis was conducted at the Department of Geological Sciences, Indiana University Bloomington. Sulfide minerals were drilled out of core samples with a carbide bit into a powder under a microscope. Generally, between 0.1 to 0.7 mg (depending on the amount of silicate contamination) of each sulfide sample powder was placed into 3.5 x 5 mm tin boats with an oxidizer, vanadium pentoxide ( $V_2O_5$ ). Each tin boat was sealed and run through a continuous flow CE Instruments 1110 CHN elemental analyzer connected to a Finnigan MAT-252 stable isotope ratio mass spectrometer. Both international and internal standards were used, including NBS-127, EMR-Cp, ERE- $Ag_2S$ , and PQB2 (+20.35‰, +0.9‰, -4.7‰, +41.5‰, respectively). Values were reported in parts per thousand, or “per mil” (‰), relative to the reference

sample, Cañon Diablo Troilite (V-CDT), in standard  $\delta$  notation. International and internal standards fell within  $\pm 1.1\%$  of the accepted values and average individual sample reproducibility was  $\pm 1.3\%$ , due to natural variability within each sample. All of the standards fell within the acceptable peak range of  $1000 \pm 200$  mV and therefore sample peaks within the range of 500-1500 mV were considered appropriate, as determined by the laboratory. Of the 63 sulfide samples analyzed, 17 were duplicated and eight others were thrown out, due to either insufficient sample size or analytical error, for 72 total data points (Fig. 18). Similar methods for sulfur isotope analysis at this laboratory have been cited in Ripley et al. (2010), Werne et al. (2008), and Studley et al. (2002).

#### 4.3 Sulfide Mineral Identification and Petrographic Analysis

Twenty-six polished thin sections were prepared of sulfide-bearing samples for petrographic study and mineral chemical analysis (Fig. 18). Standard-sized (24 x 46 mm), probe-grade polished thin sections were made by Quality Thin Sections of Tucson, Arizona from billets cut from the core samples. The sections were examined with a petrographic microscope under reflected and transmitted light. Petrographic analysis of the samples was conducted mainly to establish the textural relationships between the sulfide minerals relative to the surrounding silicate and oxide minerals. This information has implications for the paragenesis of the sulfide minerals, particularly in determining whether they are primary (formed during deposition of the iron formation) or secondary. If secondary, the sulfide may occur in veins or as porphyroblasts. If formed from

hydrothermal fluids, sulfides may be associated with hydrous silicates. If formed by thermal metamorphism, pyrrhotite may occur as pseudomorphs after pyrite cubes.

Some polished thin sections were also investigated with the scanning electron microscope housed in the Department of Geological Sciences at the University of Minnesota Duluth. The UMD SEM is a variable pressure JEOL JSM-6490LV equipped with an Oxford energy dispersive spectrum detector. The SEM was used mainly to assist with mineral identification when such identification was uncertain by petrographic techniques.

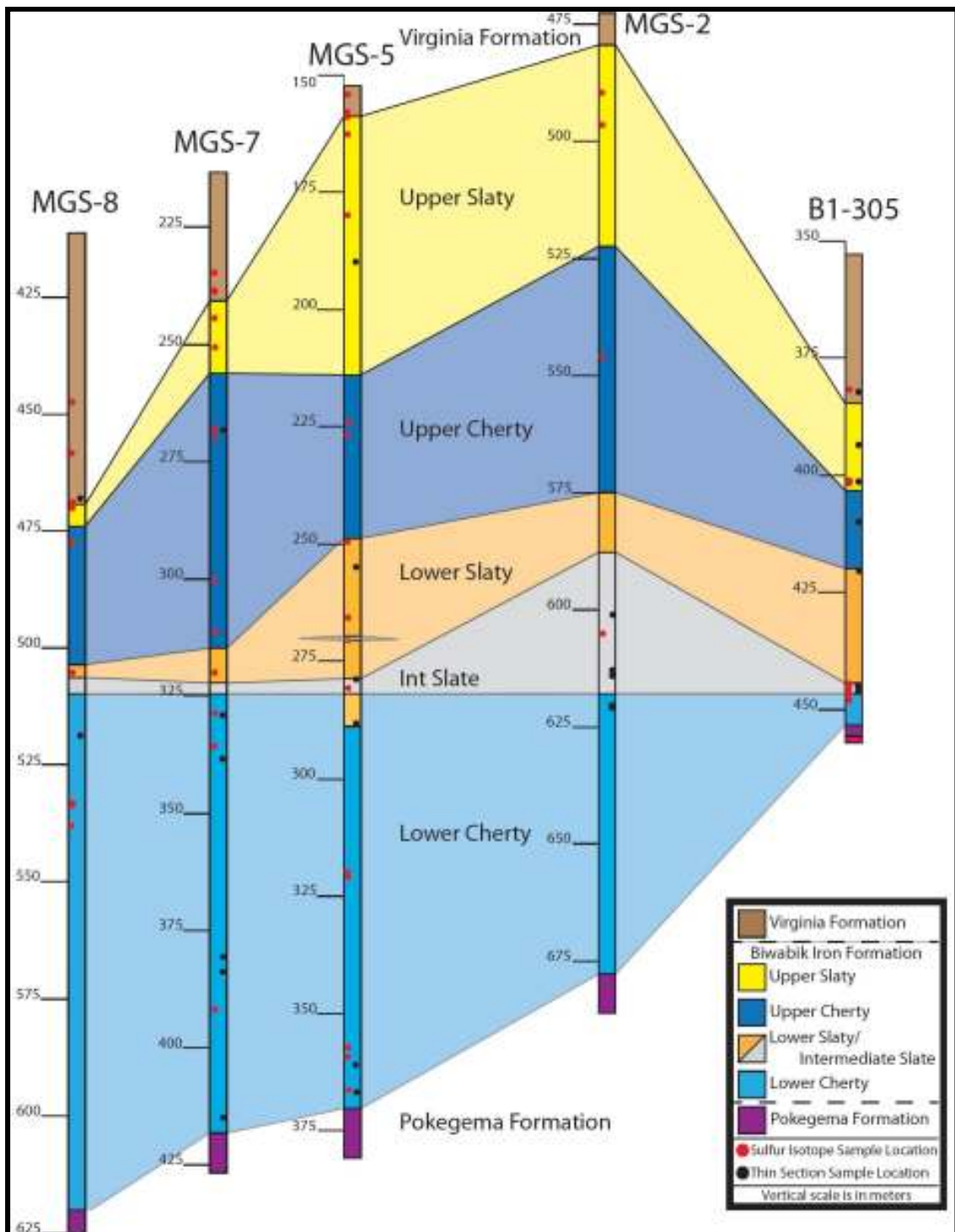


Figure 18: Location of sulfur isotope and thin section samples collected for this study

## **Chapter 5: Results**

In total, 123 sulfide-bearing mineral samples were collected for this study. Of these samples, 63 were analyzed for their sulfur isotope signature and 20 were made into polished thin sections for petrographic study and possible SEM-EDS analysis. Sulfur isotope values were analyzed based on their associated geographic location, stratigraphic sub-unit, and mineral occurrence type to determine trends.

### **5.1 Sulfide Petrography and Mineralization**

Five different visible sulfide mineral morphologies were observed in drill core and hand samples during core logging and sampling: euhedral cubes, euhedral framboids or spheroids, anhedral “blebs,” and veins. An uncommon occurrence of sulfide “needles” was also noted during logging and fine-grained, disseminated sulfides were observed during reflected-light petrographic analysis. Along with the apparent mineral occurrence type, macroscopic sample descriptions also included relative grain size, associated minerals/lithology, probable sulfide mineralogy, and/or concentration within the sample (Appendix A.1).

Both transmitted and reflected light were used during petrographic analysis to distinguish the various sulfide mineralogies present in 20 thin sections. Observations regarding sulfide mineral occurrence, concentration, habit, relative size, mineralogy, and textural relationships with adjacent phases were recorded (Appendix A.2). The scanning electron microscope aided in sulfide mineral identification. The main sulfide minerals identified

through both methods are pyrite and pyrrhotite with minor amounts of galena (PbS), cobaltite (CoAsS), arsenopyrite (FeAsS), and chalcopyrite (CuFeS<sub>2</sub>) with possible occurrences of pentlandite (Fe,Ni)<sub>9</sub>S<sub>8</sub> and cubanite (CuFe<sub>2</sub>S<sub>3</sub>). An overview of the sulfide mineralogy, as confirmed by the SEM is located in Table 1. The detailed SEM-EDS results are located in Appendix A.3.

Table 1: Sulfide geographic location, lithology, morphology, and mineralogy for SEM samples

Sample Name	Location	Lithology	Morphology	Mineralogy
B1-305-2	B1-305	Virginia Formation	bleb	pyrrhotite, chalcopyrite, pentlandite, and/or cubanite
B1-305-15	B1-305	intermediate slate	bleb	pyrrhotite
B1-305-16	B1-305	intermediate slate	bleb	pyrrhotite
MGS-2-14	MGS-2	intermediate slate	cube	pyrite
MGS-2-18	MGS-2	intermediate slate	massive bleb	pyrite
MGS-2-22	MGS-2	lower cherty	massive bleb	pyrite, arsenopyrite, cobaltite
MGS-5-13	MGS-5	lower slaty	vein	pyrite
MGS-5-18	MGS-5	lower slaty	cube	pyrite
MGS-5-20	MGS-5	lower slaty	massive bleb	pyrite
MGS-5-25	MGS-5	lower cherty	framboid	pyrite, arsenopyrite
MGS-5-27	MGS-5	lower cherty	cube	pyrite, arsenopyrite
MGS-7-9	MGS-7	upper cherty	needles	pyrite, arsenopyrite, cobaltite
MGS-7-19	MGS-7	lower cherty	cube	pyrite
MGS-7-22	MGS-7	lower cherty	massive bleb	pyrite
MGS-8-1	MGS-8	transition (virginia to upper slaty)	cube	pyrite, galena

## 5.2 Sulfur Isotope Results

Sulfur isotope analysis was conducted in four different rounds using the SO<sub>2</sub> gas method at Indiana University Bloomington. Both raw and corrected  $\delta^{34}\text{S}$  values were reported

(Appendix B.1). The correction factor for each sampling round was determined by comparing the measured  $\delta^{34}\text{S}$  values of the analytical standards to their accepted values (Appendix B.2). Corrected values of the  $\delta^{34}\text{S}$  analyses for this study are summarized in Table 2.

Due to the complexity of the stratigraphy of the Biwabik Iron Formation, isotope comparisons to sample depth was deemed inappropriate. Therefore, sulfur isotope values were instead compared to qualitative categorical descriptors: (1) geographic location (Figs. 19-21); to determine the influence of the Duluth Complex), (2) sub-unit stratigraphy (Figs. 23-25); to determine the influence of depositional environment), and (3) mineral occurrence type (Figs. 27-29); to determine the influence of morphology). Values between +2‰ and +13‰, which others (Poulton et al., 2010; Carrigan, 1990; Carrigan and Cameron, 1991) have interpreted to be the range for primary sulfides, are noted on each plot with a blue box. Implications regarding these specific compositional ranges will be addressed in Chapter 6.

Isotope data collected by Poulton et al. (2010) was included with data collected in this study in plots comparing geographic location (Fig. 22) and sub-unit stratigraphy (Fig. 26). Their samples were analyzed using  $\text{SF}_6$  gas method. Therefore, in order to compare their data to this study's  $\text{SO}_2$  analyzed data, conversion methods cited by IAEA (Vienna, 2000) were employed. The original data from the Poulton et al. (2010) study and the

newly converted data are given in Table 3, along with sample ID, depth, and associated sub-unit stratigraphy.

Sulfur isotope values for the sulfides in this study were also compared to sulfur isotope values analyzed from surface water sulfate values in the SLRW. As mentioned in Chapter 4, the sulfate samples were collected for the Minnesota Department of Natural Resources sulfur cycling study (Berndt, in progress). The values obtained for the sulfate samples can be found in Table 4.

Table 2: Corrected  $\delta^{34}\text{S}$  values for samples collected from the Virginia and Biwabik Iron Formations (B = bleb, C = cube, F = framboids, V = vein, N = needle)

Sample Number	Unit Name	Depth (meters)	Corrected $\delta^{34}\text{S}$ (‰)	Mineral Occurrence
MGS-2-B	Transition	489.81	30.55	C
MGS-2-2	Upper Slaty	496.21	-7.71	B
MGS-2-10	Upper Cherty	545.29	12.44	B
MGS-2-16	Int Slaty	604.72	9.20	B
MGS-2-16 (D)	Int Slaty	604.72	-5.35	B
MGS-5-A	Transition	154.69	-17.00	C
MGS-5-A (D)	Transition	154.69	-16.50	C
MGS-5-B	Transition	158.04	11.05	C
MGS-5-1	Transition	158.19	11.84	C
MGS-5-2	Upper Slaty	158.34	16.07	F
MGS-5-2 (D)	Upper Slaty	158.34	14.91	F
MGS-5-4	Upper Slaty	162.46	-9.81	V
MGS-5-5	Upper Slaty	179.68	11.66	C
MGS-5-10	Upper Cherty	224.18	18.65	C
MGS-5-11	Upper Cherty	226.92	-36.11	V
MGS-5-11 (D)	Upper Cherty	226.92	-34.52	V
MGS-5-12	Lower Slaty	249.33	-31.87	V
MGS-5-15	Lower Slaty	265.79	4.38	C

Sample Number	Unit Name	Depth (meters)	Corrected $\delta^{34}\text{S}$ (‰)	Mineral Occurrence
MGS-5-16	Int Slate	270.36	4.81	C
MGS-5-16 (D)	Int Slate	270.36	5.75	C
MGS-5-19	Lower Slaty	280.87	36.04	C
MGS-5-21	Lower Cherty	320.04	80.37	B
MGS-5-21 (D)	Lower Cherty	320.04	73.52	B
MGS-5-22	Lower Cherty	320.95	77.96	B
MGS-5-22 (D)	Lower Cherty	320.95	62.43	B
MGS-5-23	Lower Cherty	357.53	-27.65	V
MGS-5-24	Lower Cherty	359.36	-20.05	F
MGS-5-24 (D)	Lower Cherty	359.36	-18.69	F
MGS-5-26	Lower Cherty	366.98	23.71	C
MGS-7-A	Virginia	235.61	3.10	C
MGS-7-B	Virginia	238.35	-12.16	C
MGS-7-B (D)	Virginia	238.35	-11.93	C
MGS-7-C	Virginia	238.81	7.69	B
MGS-7-3	Upper Slaty	244.14	17.51	V
MGS-7-6	Upper Slaty	250.55	10.39	C
MGS-7-8	Upper Cherty	266.09	13.81	N (V)
MGS-7-10	Upper Cherty	267.61	22.78	C
MGS-7-11	Upper Cherty	299.62	17.96	C
MGS-7-12	Upper Cherty	311.20	10.93	B
MGS-7-13	Lower Slaty	320.04	10.05	B
MGS-7-14	Lower Cherty	328.88	13.83	C
MGS-7-14 (D)	Lower Cherty	328.88	13.56	C
MGS-7-16	Lower Cherty	335.74	10.51	C
MGS-7-17	Lower Cherty	335.74	16.20	C
MGS-7-17 (D)	Lower Cherty	335.74	12.76	C
MGS-7-21	Lower Cherty	392.13	32.49	B
MGS-8-A	Transition	445.62	3.33	C
MGS-8-B	Transition	459.64	6.68	B
MGS-8-2	Transition	468.48	-6.53	B
MGS-8-4	Upper Slaty	469.85	-16.76	B
MGS-8-6	Upper Cherty	478.23	-5.61	C
MGS-8-6 (D)	Upper Cherty	478.23	-5.20	C
MGS-8-10	Lower Slaty	504.90	37.38	V

Sample Number	Unit Name	Depth (meters)	Corrected $\delta^{34}\text{S}$ (‰)	Mineral Occurrence
MGS-8-14	Lower Cherty	533.10	-18.92	F
MGS-8-14 (D)	Lower Cherty	533.10	-16.99	F
MGS-8-16	Lower Cherty	533.25	-27.78	F
MGS-8-18	Lower Cherty	537.82	-23.56	F
MGS-8-18	Lower Cherty	537.82	-20.49	F
B1-305-1	Virginia	381.91	10.25	B
B1-305-4a,b	Upper Slaty	401.27	27.34	C
B1-305-4a,b (D)	Upper Slaty	401.27	25.99	C
B1-305-4c	Upper Slaty	401.27	7.80	V
B1-305-6	Upper Slaty	401.57	8.27	C
B1-305-14	Int Slate	444.40	6.19	B
B1-305-15	Int Slate	445.31	6.41	B
B1-305-16	Int Slate	446.23	8.85	B
B1-305-17	Int Slate	446.53	11.34	B
B1-305-18	Lower Cherty	447.60	2.39	B
B1-305-18 (D)	Lower Cherty	447.60	3.53	B
NatOre I			40.57	C
NatOre (II)			21.11	C
NatOre (II) (D)			31.21	C

Table 3: The  $\delta^{34}\text{S}$  values reported from Poulton et al. (2010) using the SF<sub>6</sub>-gas method and SO<sub>2</sub>-gas method corrected values for the Virginia and Biwabik Iron Formations.

Sample ID	Core Location	$\delta^{34}\text{S}$ (‰) SF <sub>6</sub>	$\delta^{34}\text{S}$ (‰) SO <sub>2</sub>	Depth (meters)	Unit Name
B1	MGS-2	2.91	3.14	491.62	Upper Slaty
B2	MGS-2	2.77	3.01	492.52	Upper Slaty
B4	MGS-2	3.32	3.54	498.32	Upper Slaty
B5	MGS-2	1.83	2.10	498.92	Upper Slaty
B17	MGS-2	8.01	8.08	599.22	Int Slate
B18	MGS-2	6.11	6.24	604.72	Int Slate
B19	MGS-2	8.68	8.72	640.62	Lower Cherty
B20	MGS-2	15.90	15.71	639.72	Lower Cherty
KV45	MGS-7	-0.33	0.01	225.45	Virginia

Sample ID	Core Location	$\delta^{34}\text{S}$ (‰) SF <sub>6</sub>	$\delta^{34}\text{S}$ (‰) SO <sub>2</sub>	Depth (meters)	Unit Name
V21a	MGS-7	-5.81	-5.29	227.85	Virginia
V21b	MGS-7	-6.39	-5.85	227.85	Virginia
V22	MGS-7	7.35	7.44	228.45	Virginia
V23	MGS-7	-1.00	-0.64	229.15	Virginia
V24	MGS-7	32.70	31.96	232.45	Virginia
KV46a	MGS-7	18.30	18.03	233.05	Virginia
KV46b	MGS-7	10.80	10.77	233.05	Virginia
KV46c	MGS-7	9.18	9.21	233.05	Virginia
KV47	MGS-7	23.00	22.57	233.35	Virginia
V25	MGS-7	20.30	19.96	233.65	Virginia
KV48	MGS-7	12.00	11.94	234.25	Virginia
V26	MGS-7	1.77	2.04	234.55	Virginia
KV49	MGS-7	0.83	1.13	236.45	Virginia
V27	MGS-7	7.68	7.76	236.75	Virginia
V28	MGS-7	1.08	1.37	238.25	Virginia
V29a	MGS-7	0.66	0.97	238.85	Virginia
V29b	MGS-7	-7.20	-6.64	238.85	Virginia
V30	MGS-7	1.82	2.09	239.75	Virginia
KV50	MGS-7	1.26	1.55	239.95	Virginia
B24	MGS-7	4.82	4.99	247.65	Upper Slaty
B28	MGS-7	6.98	7.08	256.25	Upper Slaty
B30	MGS-7	5.57	5.72	295.75	Upper Cherty
B33	MGS-7	-11.30	-10.60	297.35	Upper Cherty
B34	MGS-7	3.79	3.99	297.95	Upper Cherty
B35	MGS-7	16.00	15.80	328.45	Lower Cherty
B36	MGS-7	7.13	7.23	362.95	Lower Cherty
B37	MGS-7	6.68	6.79	364.45	Lower Cherty
CV28	MGS-8	-5.79	-5.27	388.48	Virginia
CV29	MGS-8	-7.60	-7.02	389.48	Virginia
CV30a	MGS-8	-2.69	-2.27	393.48	Virginia
CV30b	MGS-8	-5.04	-4.55	393.49	Virginia
CV30c	MGS-8	-0.04	0.29	393.50	Virginia
CV31	MGS-8	3.08	3.31	398.48	Virginia
CV32	MGS-8	-14.70	-13.89	400.48	Virginia
CV33	MGS-8	2.69	2.93	404.98	Virginia
CV34a	MGS-8	0.15	0.47	421.48	Virginia
CV34b	MGS-8	7.36	7.45	421.51	Virginia

Sample ID	Core Location	$\delta^{34}\text{S}$ (‰) SF <sub>6</sub>	$\delta^{34}\text{S}$ (‰) SO <sub>2</sub>	Depth (meters)	Unit Name
CV34c	MGS-8	6.16	6.29	421.52	Virginia
CV35	MGS-8	7.09	7.19	442.48	Virginia
CV36	MGS-8	-1.95	-1.56	453.98	Virginia
B40	MGS-8	5.17	5.33	465.48	Virginia
B41	MGS-8	2.08	2.34	478.28	Upper Cherty
B42	MGS-8	5.77	5.91	479.48	Upper Cherty
B43	MGS-8	6.02	6.15	481.68	Upper Cherty
B45	MGS-8	6.40	6.52	528.58	Lower Cherty

Table 4: The  $\delta^{34}\text{S}$  values reported from sulfate values collected by the Minnesota Department of Natural Resources (Berndt, in progress).

Sample ID	Date	$\delta^{34}\text{S}$ (‰) Sulfate	Sample ID	Date	$\delta^{34}\text{S}$ (‰) Sulfate
LLC-1-1	5/4/2010	8.37	ETR-2-6	7/19/2010	6.21
LLC-1-2	5/25/2010	8.89	ETR-2-7	8/11/2010	4.30
LLC-1-3	6/9/2010	8.38	ETR-2-8	9/15/2010	4.43
LLC-1-4	6/22/2010	8.62	ETR-2-9	10/20/2010	5.31
LLC-1-5	7/7/2010	8.38	ETR-3-1	5/4/2010	5.82
LLC-1-6	7/19/2010	9.17	ETR-3-2	5/25/2010	8.05
LLC-1-7	8/11/2010	9.64	ETR-3-3	6/9/2010	6.23
LLC-1-8	9/15/2010	8.27	ETR-3-4	6/22/2010	7.74
LLC-1-9	10/20/2010	7.29	ETR-3-5	7/7/2010	6.17
LLC-2-1	5/4/2010	11.20	ETR-3-6	7/19/2010	6.16
LLC-2-2	5/25/2010	13.03	ETR-3-7	8/11/2010	6.33
LLC-2-3	6/9/2010	14.60	ETR-3-8	9/15/2010	6.36
LLC-2-4	6/22/2010	14.68	ETR-3-9	10/20/2010	5.59
LLC-2-5	7/7/2010	13.43	SC-1-1	5/4/2010	7.05
LLC-2-6	7/19/2010	14.83	SC-1-2	5/25/2010	7.10
LLC-2-7	8/11/2010	11.96	SC-1-3	6/8/2010	7.37
LLC-2-8	9/15/2010	13.19	SC-1-4	6/22/2010	7.86
LLC-2-9	10/20/2010	13.40	SC-1-5	7/7/2010	6.53
SR-1-1	5/4/2010	35.28	SC-1-6	7/19/2010	7.40
SR-1-2	5/25/2010	36.03	SC-1-7	8/12/2010	7.29
SR-1-3	6/8/2010	38.51	SC-1-8	9/15/2010	7.30
SR-1-4	6/22/2010	39.60	SC-1-9	10/20/2010	6.85
SR-1-5	7/7/2010	36.15	SC-2-1	5/4/2010	10.81

Sample ID	Date	$\delta^{34}\text{S}$ (‰) Sulfate	Sample ID	Date	$\delta^{34}\text{S}$ (‰) Sulfate
SR-1-6	7/19/2010		SC-2-2	5/25/2010	13.43
SR-1-7	8/11/2010		SC-2-3	6/8/2010	16.85
SR-1-8	9/15/2010	33.73	SC-2-4	6/22/2010	16.72
SR-1-9	10/20/2010	31.06	SC-2-5	7/7/2010	14.58
SR-2-1	5/4/2010	14.88	SC-2-6	7/19/2010	17.01
SR-2-2	5/25/2010	14.27	SC-2-7	8/12/2010	18.69
SR-2-3	6/8/2010	12.50	SC-2-8	9/15/2010	16.10
SR-2-4	6/22/2010		SC-2-9	10/20/2010	13.70
SR-2-5	7/7/2010		SC-3-1	5/4/2010	9.09
SR-2-6	7/19/2010		SC-3-2	5/25/2010	10.13
SR-2-7	8/11/2010		SC-3-3	6/8/2010	10.87
SR-2-8	9/15/2010		SC-3-4	6/22/2010	11.47
SR-2-9	10/20/2010	23.36	SC-3-5	7/7/2010	15.05
ETR-1-1	5/4/2010	6.39	SC-3-6	7/19/2010	11.49
ETR-1-2	5/25/2010	6.43	SC-3-7	8/12/2010	
ETR-1-3	6/9/2010	7.26	SC-3-8	9/15/2010	
ETR-1-4	6/22/2010	7.14	SC-3-9	10/20/2010	
ETR-1-5	7/7/2010	1.92	SC-4-1	5/4/2010	6.85
ETR-1-6	7/19/2010	4.98	SC-4-2	5/25/2010	7.64
ETR-1-7	8/11/2010	4.18	SC-4-3	6/8/2010	7.43
ETR-1-8	9/15/2010	4.94	SC-4-4	6/22/2010	7.75
ETR-1-9	10/20/2010	5.10	SC-4-5	7/7/2010	7.43
ETR-2-1	5/4/2010	7.19	SC-4-6	7/19/2010	7.23
ETR-2-2	5/25/2010	7.18	SC-4-7	8/12/2010	7.18
ETR-2-3	6/9/2010	7.36	SC-4-8	9/15/2010	8.02
ETR-2-4	6/22/2010	6.62	SC-4-9	10/20/2010	7.52
ETR-2-5	7/7/2010	4.79			

### 5.2.1 Geographic Trends

Geographic location does appear to have a slight correlation with the sulfur isotope value of the sulfide minerals (Figs. 19-22). Samples collected closest to the Duluth Complex (B1-305) have the narrowest range of sulfur isotope values, 2.96‰ to 11.34‰ (one outlier sample measured at 25.99‰ and 27.34‰) with an average value of 9.9‰. The

widest range of sulfur isotope values, -35.31‰ to +76.94‰, were found in the central portion of the Mesabi Range, MGS-5, near the Virginia Horn, with an average of 8.50‰. Samples collected farthest away from the Duluth Complex, MGS-8, have the lightest sulfur isotope values, averaging about -5.45‰. Samples collected from the Natural Ore at the Fayal Mine were some of the heavier values recorded, averaging at 33.37‰.

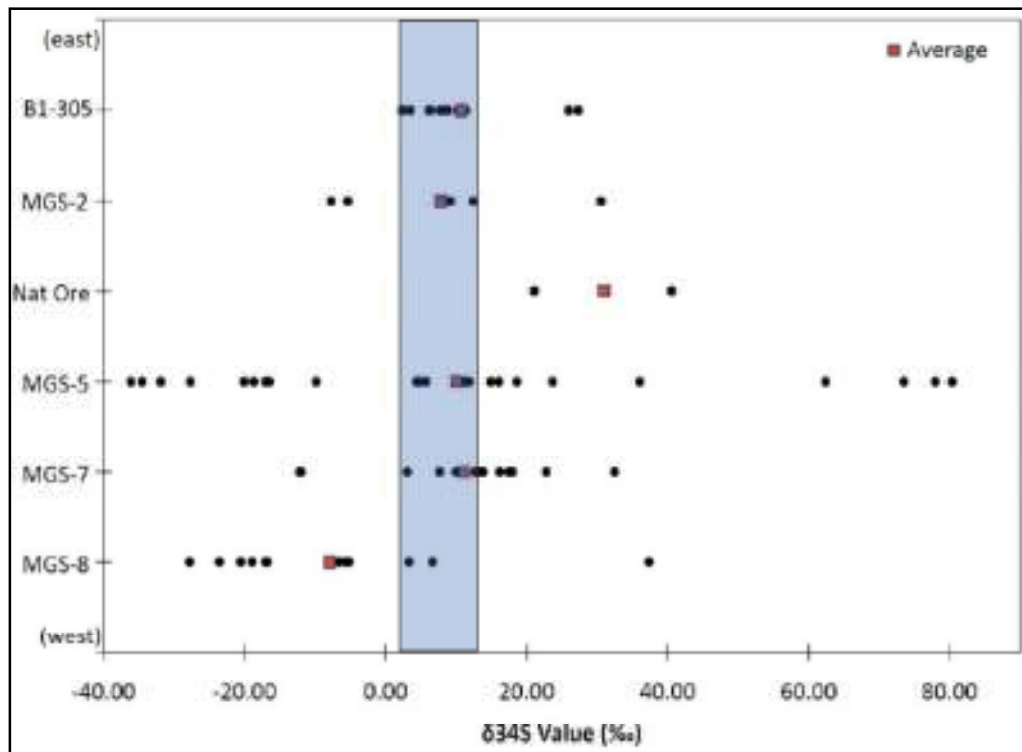


Figure 19: Range and average of  $\delta^{34}\text{S}$  values relative to geographic location.

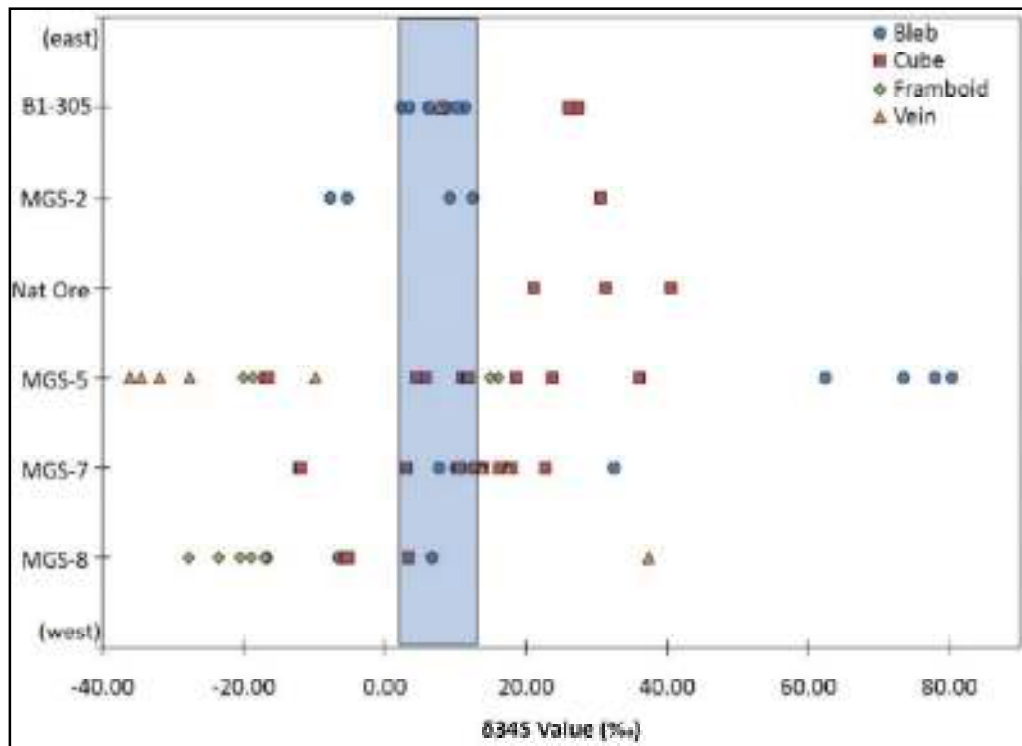


Figure 20: Geographic distribution of  $\delta^{34}\text{S}$  values in terms of mineral occurrence.

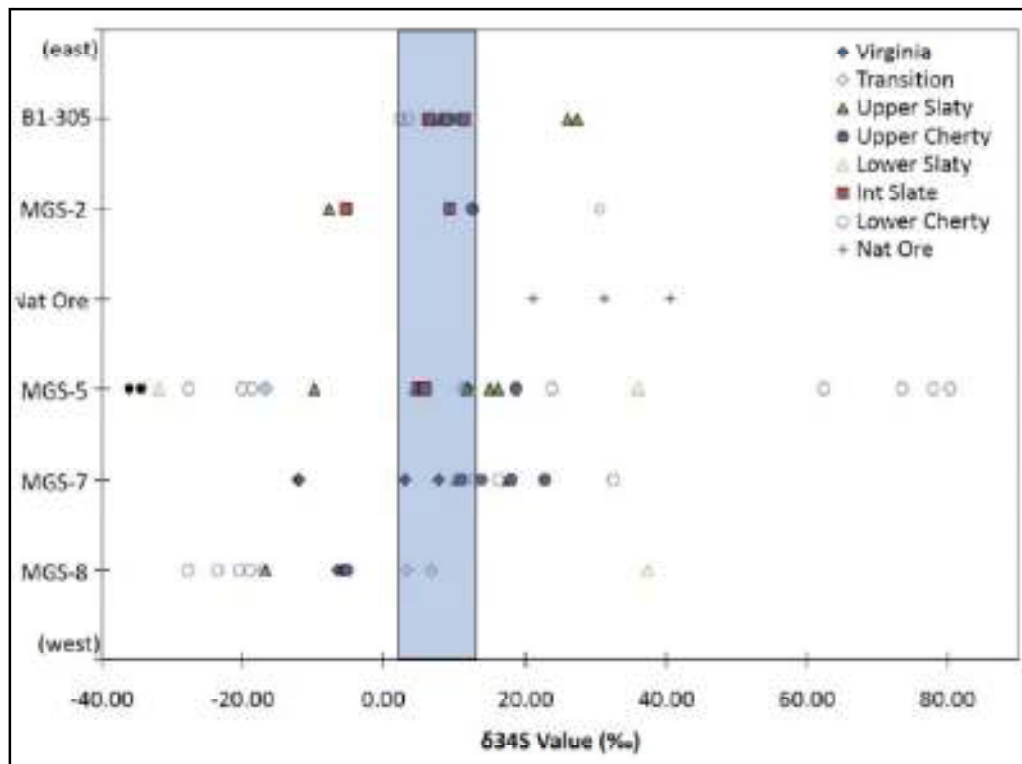


Figure 21: Geographic distribution of  $\delta^{34}\text{S}$  values in terms of stratigraphic sub-unit.

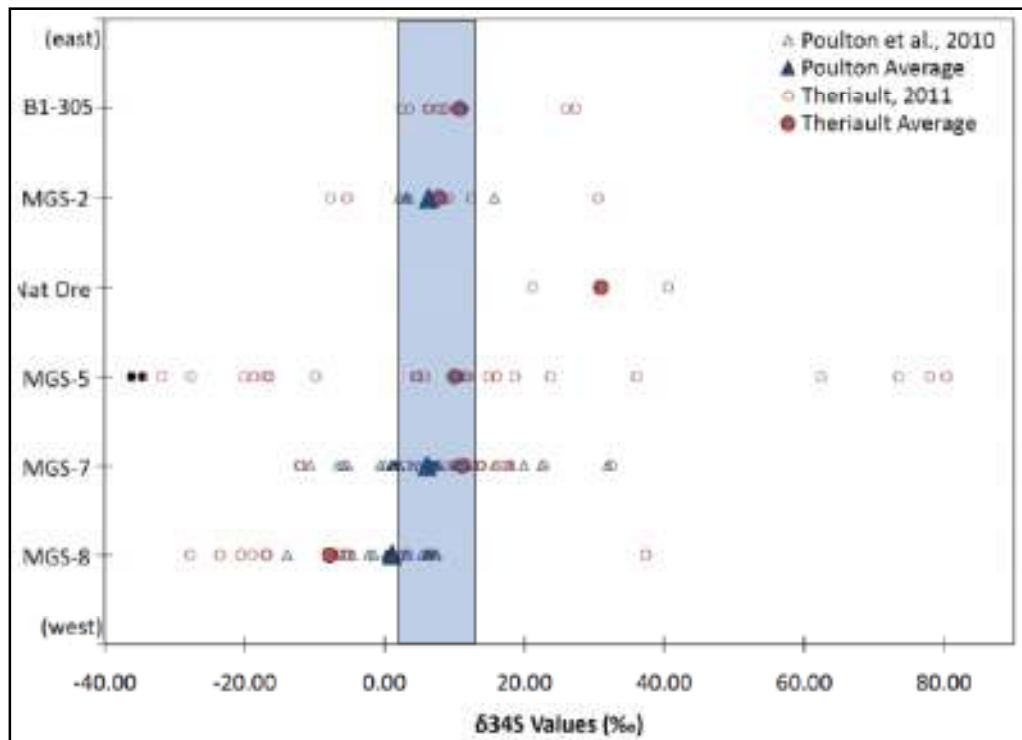


Figure 22: Geographic distribution of  $\delta^{34}\text{S}$  values, comparing values from this study and the Poulton et al. (2010) study.

### 5.2.2 Sub-Unit Stratigraphy Trends

The distribution of sulfur isotope values does not seem to be strongly tied to sub-unit stratigraphy (Figs. 23-26). This conclusion is similar to that of Carrigan (1990) and Carrigan and Cameron (1991) where they also suggested that stratigraphy played little role in the distribution of  $\delta^{34}\text{S}$  values in the Gunflint Iron Formation. The only unit that displays a narrow range of values is the Intermediate Slate layer, with an average  $\delta^{34}\text{S}$  value of 6.7%. The other stratigraphic sub-units tend to have a wide range of  $\delta^{34}\text{S}$  values.

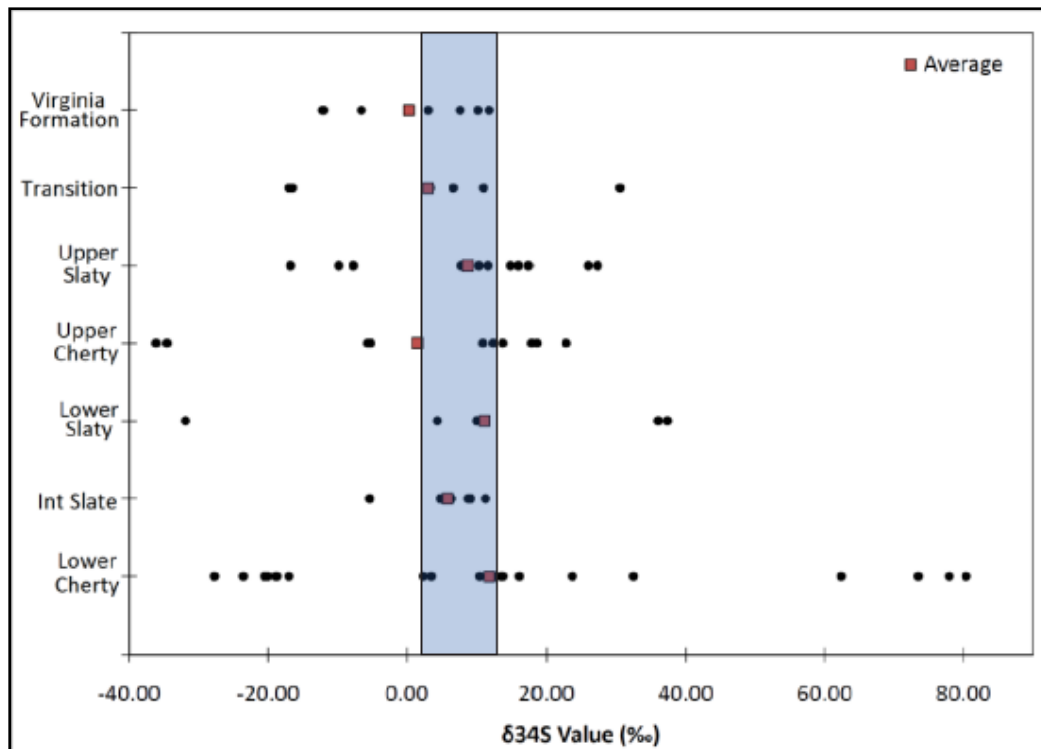


Figure 23: Range and average of  $\delta^{34}\text{S}$  values relative to sub-unit stratigraphy.

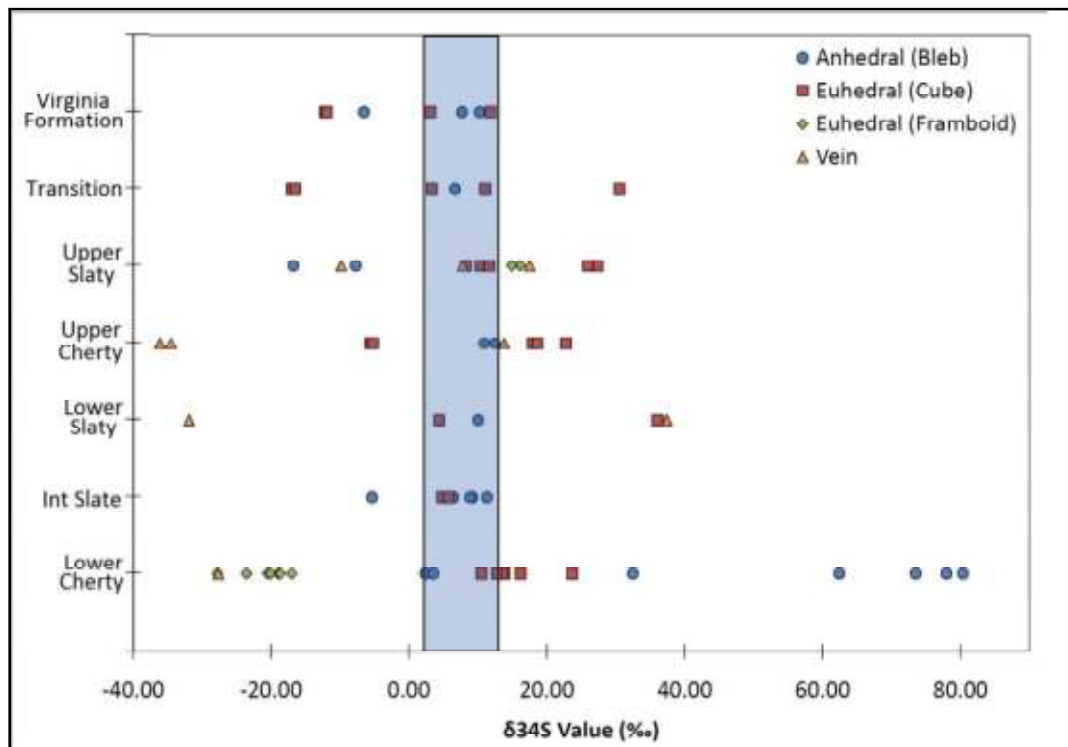


Figure 24: Stratigraphic distribution of  $\delta^{34}\text{S}$  values, in terms of mineral occurrence.

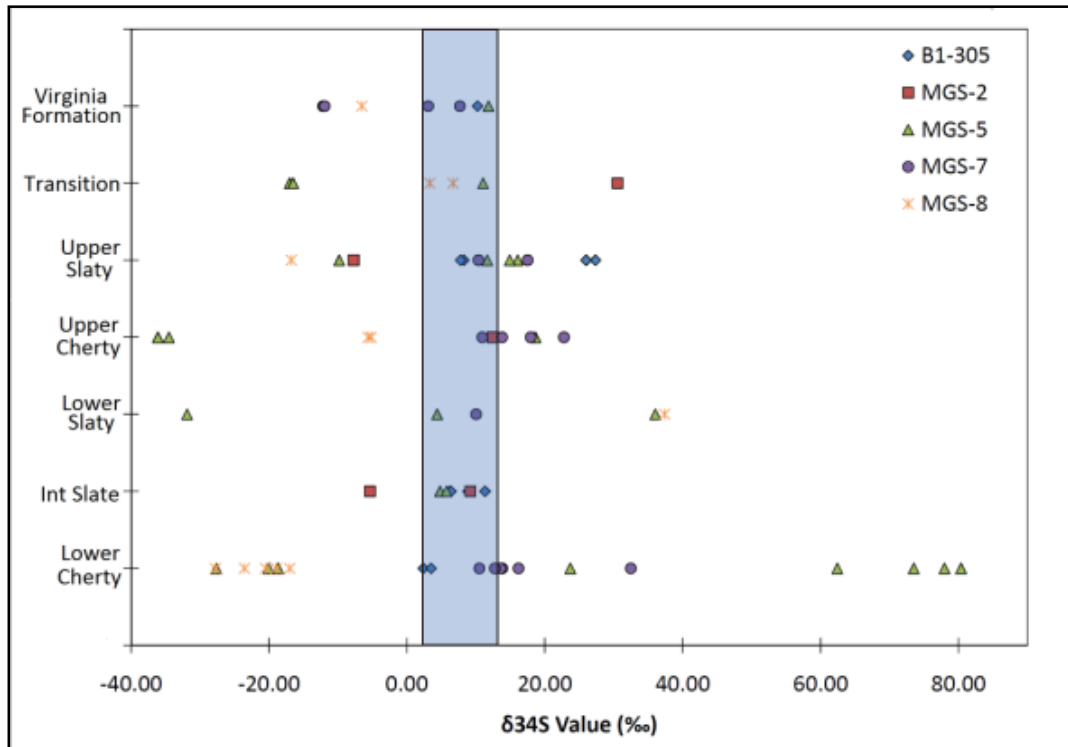


Figure 25: Stratigraphic distribution of  $\delta^{34}\text{S}$  values, in terms of geographic location.

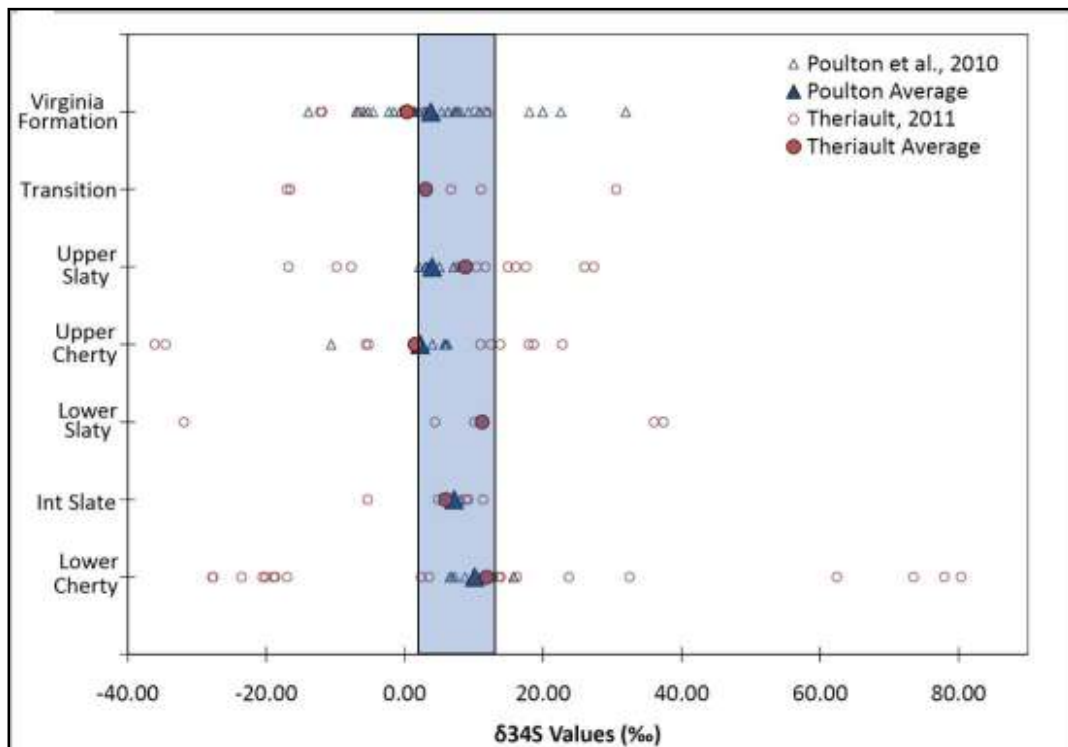


Figure 26: Stratigraphic distribution of  $\delta^{34}\text{S}$  values, comparing values from this study & the Poulton et al. (2010) study.

### 5.2.3 Mineral Occurrence Trends

Carrigan (1990) and Carrigan and Cameron (1991) noted that mineral occurrence is correlative to  $\delta^{34}\text{S}$  values in samples from the Gunflint Iron Formation. Similarly for this study, there appears to be a complex, but distinguishable, relationship between mineral occurrence type and sulfur isotope values in the Biwabik Iron Formation (Figs. 27-29).

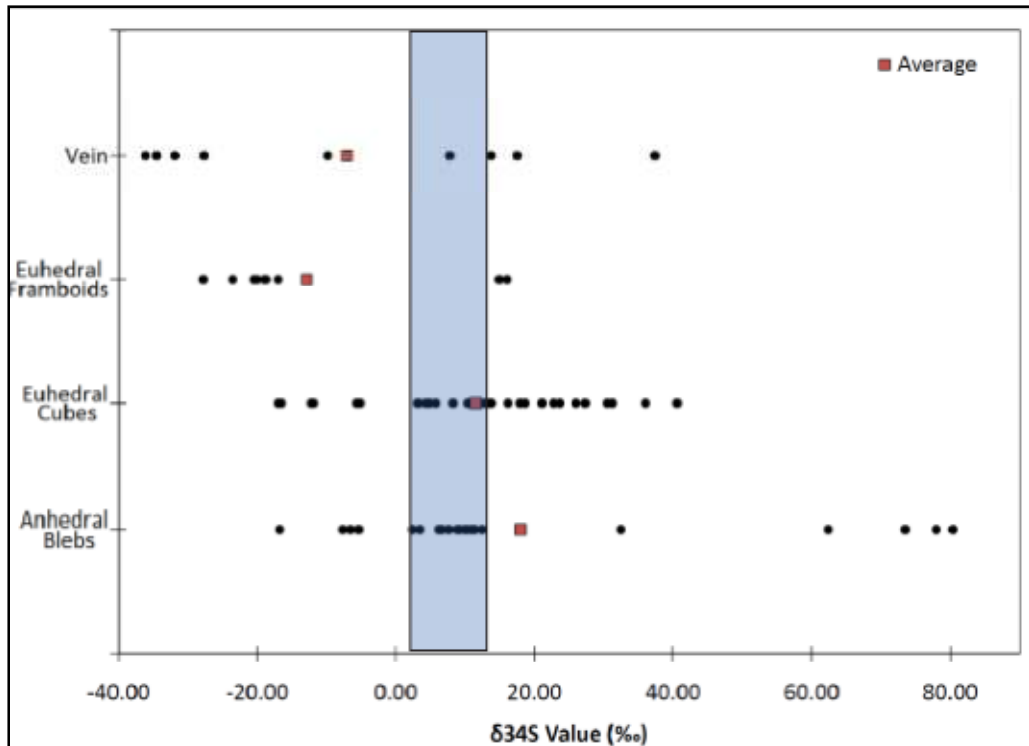


Figure 27: Average and range of  $\delta^{34}\text{S}$  values relative to mineral occurrences.

The anhedral “blebs” have a wide range of  $\delta^{34}\text{S}$  values. Intermediate Slate and Upper Cherty samples with “bleb” occurrences were collected from B1-305, MGS-2, and MGS-7 have  $\delta^{34}\text{S}$  values of 2.39‰ to 12.44‰. Lower Cherty “bleb” samples collected in the middle of the range (MGS-5) contain heavy isotope values, 62.43‰ to 80.73‰, respectively.

Euhedral sulfide minerals appear as both cubes and framboids or spheres. Like the anhedral “blebs”, the cubes have a wide range of values, -17.0‰ to 40.6‰, with an average of 12.5‰ and do not appear to be subsequently related to either sub-unit stratigraphy or sample location. The framboids and/or spheroids, however, range from -27.8‰ to -17.0‰ and 14.9‰ to 16.1‰. The lightest  $\delta^{34}\text{S}$  values were sampled from the Lower Cherty in MGS-5 and MGS-8. The heaviest  $\delta^{34}\text{S}$  values were sampled from the Upper Slaty in MGS-5.

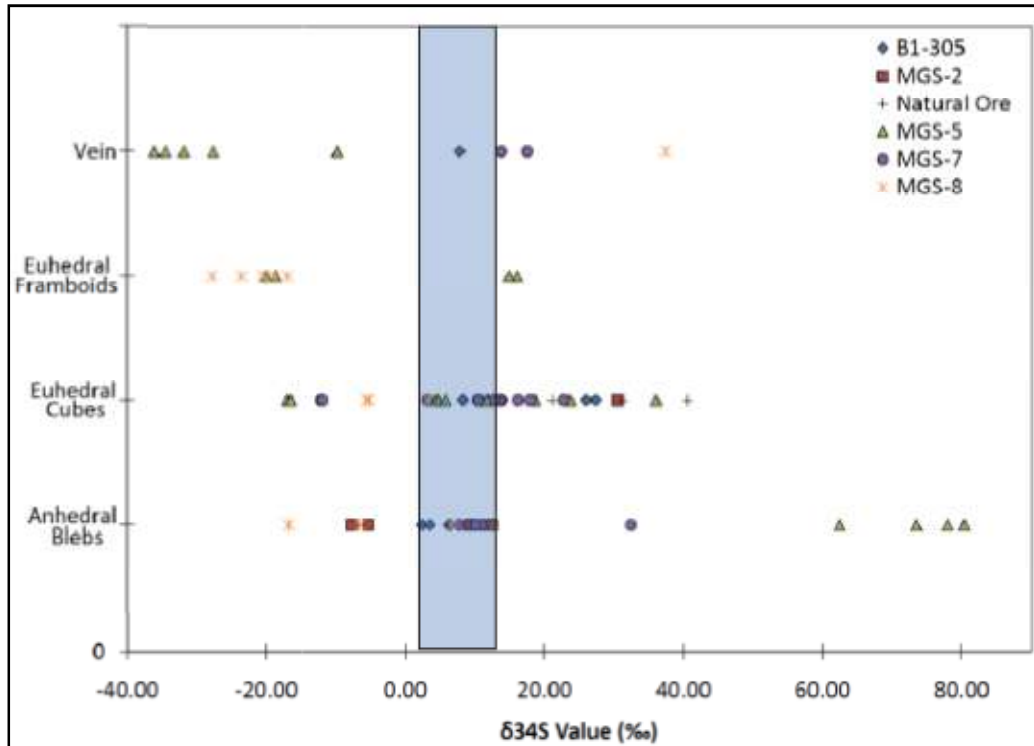


Figure 28: Distribution of the  $\delta^{34}\text{S}$  values associated with the various mineral occurrences present in the Mesabi Range, in terms of geographic location.

Vein sulfides from MGS-5 were characterized by light sulfur isotope values, ranging from -36.1‰ to -9.8‰. The three other singular vein occurrences were in B1-305, MGS-7, and MGS-8 with isotopically heavy values of 7.8‰, 17.5‰, and 37.4‰, respectively.

There does not appear to be a correlation between sub-unit stratigraphy and  $\delta^{34}\text{S}$  values of vein sulfide (Fig. 29).

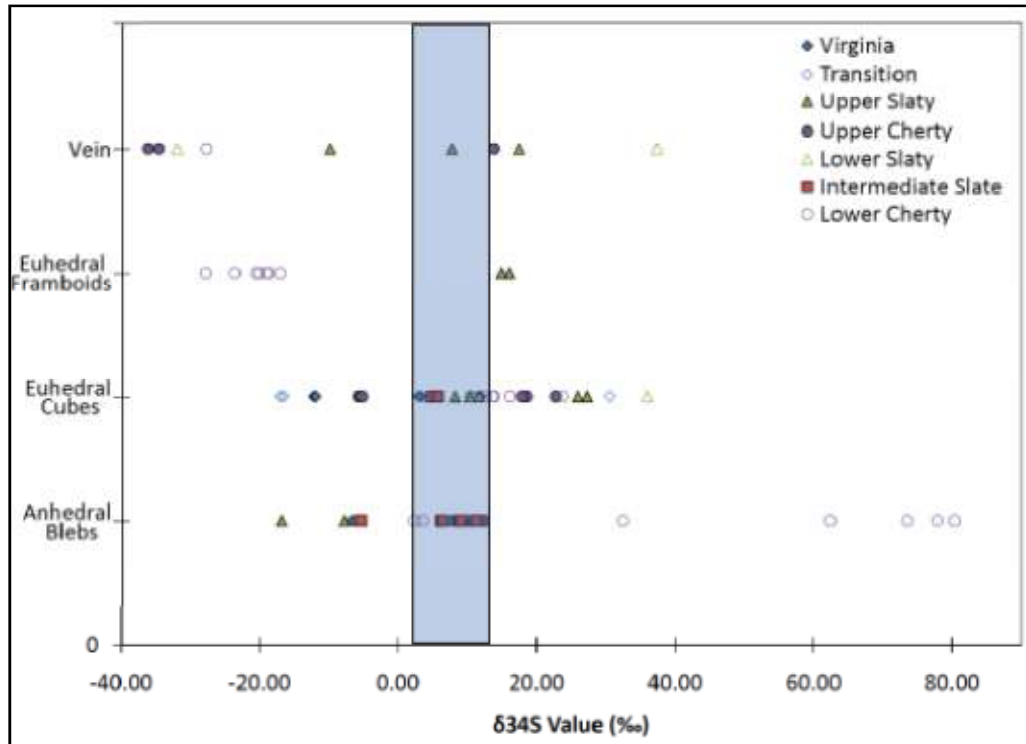


Figure 29: Distribution of the  $\delta^{34}\text{S}$  values associated with the various mineral occurrences present in the Mesabi Range, in terms of stratigraphic sub-unit.

## Chapter 6: Discussion

Macro- and microscopic observations of the sample sulfide minerals, as well as the  $\delta^{34}\text{S}$  values, allow for the opportunity to evaluate sulfide mineral distribution in the Biwabik Iron Formation and their relationship to sulfate  $\delta^{34}\text{S}$  values seen in the St. Louis River Watershed. The isotopic and textural data also permit an assessment of whether a sulfide occurrence is primary (i.e. formed during initial deposition of the iron formation), or a product of secondary, post-depositional processes (Fig. 30). In this study, primary samples are characterized as interstitial, anhedral “blebs” of sulfide whereas secondary sulfides took on a variety of textures: euhedral cubes or framboids, anhedral masses, or within a vein.

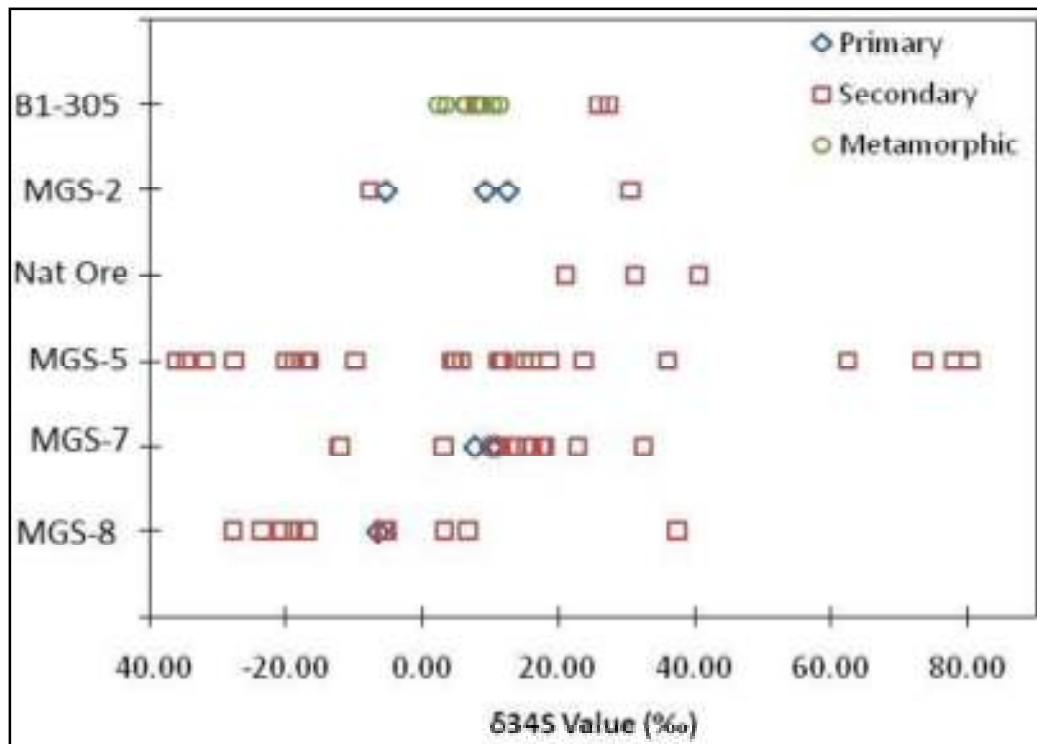


Figure 30: Geographic distribution of primary, secondary, and metamorphic sulfide minerals.

Data collected in this study were also compared to  $\delta^{34}\text{S}$  values of primary sulfides collected in the Poulton et al. (2010) study of the Biwabik Iron Formation. As evident in Figures 22 and 26, the average  $\delta^{34}\text{S}$  values for each geographic location and stratigraphic unit in this study nearly mimics the average  $\delta^{34}\text{S}$  values collected in the Poulton et al. (2010) study. It is important to note that the Poulton et al. (2010) study specifically targeted what they interpreted to be primary sulfides, explaining the narrow range of  $\delta^{34}\text{S}$  values they measured. Alternatively, this study sought out both primary and secondary sulfides, thus a broader range of values is seen.

### 6.1 Identification of Primary and Secondary Sulfides

Primary and secondary sulfide minerals were principally determined based on their textural occurrence. Sulfur isotope values aided in the characterization, but were more useful in assessing trends. As mentioned, previous studies conducted by Carrigan (1990), Carrigan and Cameron (1991), Johnston et al. (2006), and Poulton et al. (2010) defined a range of  $\delta^{34}\text{S}$  values, +2‰ to +13‰, for primary sulfides in the Biwabik and Gunflint Iron Formations. However, a sulfide is not necessarily primary because it falls within the assumed primary range. Rather, the combination of morphology, mineralogy, and sulfur isotope geochemistry is necessary to categorize a sulfide as primary or secondary.

Five main textures were identified in this study and each can be attributed to a primary or secondary precipitation process. Interstitial, anhedral blebs are assumed to be primary textures. Alternatively, large anhedral blebs, or anhedral “masses”, have been classified

as secondary sulfides as they appear to have nucleated from earlier formed interstitial sulfide minerals. Euhedral occurrences, such as cubes and framboids, and those formed within veins and along joint faces are interpreted to be secondary as well.

Several of the secondary sulfides were found in both the oxidized iron formation in the western portion of the Mesabi Range and along lithologic boundaries. Oxidized, or leached, iron formation is characterized as chalky looking, silica poor iron formation containing magnetite, goethite, and limonite, all products of oxidation. These oxidized portions also contain open pore spaces, or vugs, throughout; some of which contain sulfides in the form of framboids. Lithologic boundaries are characterized as an obvious boundary by which fluid may flow through laterally and precipitate out new minerals, such as sulfides. Incorporation of surrounding minerals into the fluid may occur along this pathway, allowing for a hybrid fluid chemistry. These boundaries will hence forth be described as dissolution surfaces. Examples of dissolution surfaces can be seen at the transition between granular and banded iron formation and may appear as thin, dark, strolite-like, layers. An artifact of dissolution surface precipitation is sulfide minerals may appear bedded, or forming within a certain layer. However, it is important to distinguish between bedded sulfides that formed at the time of deposition and sulfides that appear bedded because of preferential secondary precipitation along fluid pathways.

This study also identified six mineralogical variations of sulfides in the Biwabik Iron Formation. Primary sulfides are exclusively associated with pyrite. Pyrrhotite and

chalcopyrite were only found in the metamorphosed samples. Secondary sulfides, related to post-Duluth Complex fluid flow, were composed of pyrite, arsenopyrite, cobaltite, and galena. More specifically, sulfides forming in the veins and as cubes are pyrite whereas some of the anhedral masses contained additional amounts of arsenic and cobalt, forming arsenopyrite and/or cobaltite. The presence of arsenic and cobalt in the anhedral masses may point to a different fluid source than what is associated with the vein and cube sulfides. Only one framboid sample was analyzed for its chemical composition using the SEM, it contained pyrite and a trace amount of arsenic. Galena was only found in a sample located in the transition zone between the Biwabik Iron Formation and the Virginia Formation. See Table 6.1 for summary criteria.

Table 5: Summary Criteria for Primary and Secondary Sulfide Minerals

	Anhedral Bleb	Anhedral Masses	Euhedral Cube	Euhedral Framboid	Veins
<b>B1-305 (east)</b>		Interstitial - Metamorphic	Secondary		Pyrite + Quartz - Secondary
<b>MGS-2</b>	Interstitial - Primary	Dissolution Surfaces - Secondary			
<b>MGS-5</b>		GIF - Secondary		Between GIF & BIF - Secondary	Pyrite + Calcite + Quartz - Secondary
<b>Natural Ore</b>			Aggregates - Secondary		
<b>MGS-7</b>	Interstitial - Primary	GIF - Secondary	Secondary		Pyrite + Calcite + Quartz - Secondary
<b>MGS-8 (west)</b>		Dissolution Surfaces - Secondary		Vugs - Secondary	Pyrite + Calcite + Quartz - Secondary

## 6.2 Primary Sulfide Mineralization

Texture and mineralogy are very important for understanding primary sulfide minerals. For this study, primary sulfides are described as interstitial, anhedral blebs of pyrite with

a range of  $\delta^{34}\text{S}$  values from -5.4‰ to +12.4‰, and an average of +6.2‰. This range generally fits in with the accepted primary ranges cited in previous studies (Carrigan, 1990; Carrigan and Cameron, 1991; Johnston et al., 2006; and Poulton et al., 2010) but outlier samples do exist, attesting to the natural variability of system.

Of all the samples analyzed for their  $\delta^{34}\text{S}$  value, 36% fall within the assumed primary range delineated by previous studies (+2‰ to +13‰). Of those, 50% are anhedral blebs, 46% are cubes, and 4% are in a vein. Anhedral blebs have been determined to be the appropriate texture for primary sulfide minerals but 54% all of the blebs are made up of metamorphic sulfides (pyrrhotite and/or chalcopyrite) and thus are not the product of primary precipitation, but as their morphology suggests they may have nucleated from primary sulfide minerals. Therefore, only five samples characterized as anhedral blebs of interstitial sulfides fall within the primary  $\delta^{34}\text{S}$  range.

Due to the natural variability of  $\delta^{34}\text{S}$  values at the time of precipitation, caused by the flux of available iron and organic material, it is possible for primary sulfide minerals to have values outside the primary range, given they meet the other textural and mineralogical requirements. Also, not all sulfide samples for this study were analyzed for their  $\delta^{34}\text{S}$  value. That being said, of the 92 sulfide samples collected, 31% were categorized as anhedral blebs or masses. Pyrrhotite and chalcopyrite can be found in seven of those samples and are located in the thermal aureole of the Duluth Complex and can be attributed to metamorphism. The remaining anhedral sulfide samples are either

described as interstitial pyrite (24%), anhedral masses (41%), or along dissolution surfaces (16%). Dissolution surfaces and anhedral masses are not considered primary textures. As mentioned, dissolution surfaces suggest preferential fluid flow and precipitation and anhedral masses appear as coarse grained sulfides that may have nucleated on previously precipitated sulfides. In the end, only four additional Biwabik Iron Formation samples meet the requirements and may also be considered primary sulfides, despite their unknown  $\delta^{34}\text{S}$  value. In total, eight of the 92 samples (or 7%) are considered primary sulfide samples because they meet the textural, geochemical, and/or mineralogical requirements.

Primary sulfide samples are located in MGS-2 (upper cherty, intermediate slate, and lower cherty) and MGS-7 (lower slaty and lower cherty) (Fig. 31). An important ancillary question to address is why primary sulfide minerals did not re-equilibrate at any point in the last 1.85 Ga. It is possible that the primary sulfides noted were not in connection with pore spaces, fractures, or dissolution surfaces but rather within units that have low porosity and permeability and thus have been “buffered” from fluid flow through the formation. A good example of sulfide minerals re-equilibrating to form secondary sulfides can be seen in the anhedral masses.

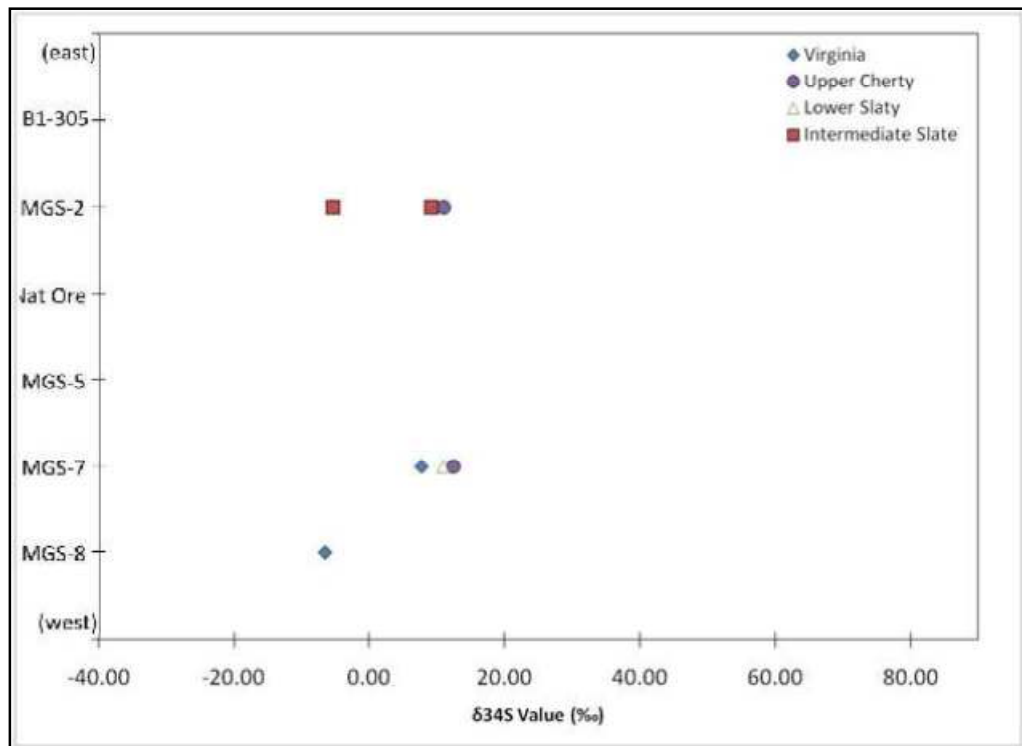


Figure 31: Geographic distribution of primary sulfide minerals in the Biwabik Iron Formation.

### 6.3 Secondary Sulfide Mineralization

Secondary sulfides are located throughout the iron formation (Fig. 32) and mainly appear as anhedral masses, euhedral cubes, euhedral framboids, and within veins (Fig. 33). Sulfide mineral precipitation related to secondary processes can be attributed to a variety of events that have affected the Biwabik Iron Formation since deposition ceased at 1.85 Ga. These events include the thermal metamorphism attending the emplacement of the Duluth Complex and the formation of natural ores by oxidation and desilicification. Only those samples located in the thermal aureole of the Duluth Complex were affected by its emplacement.

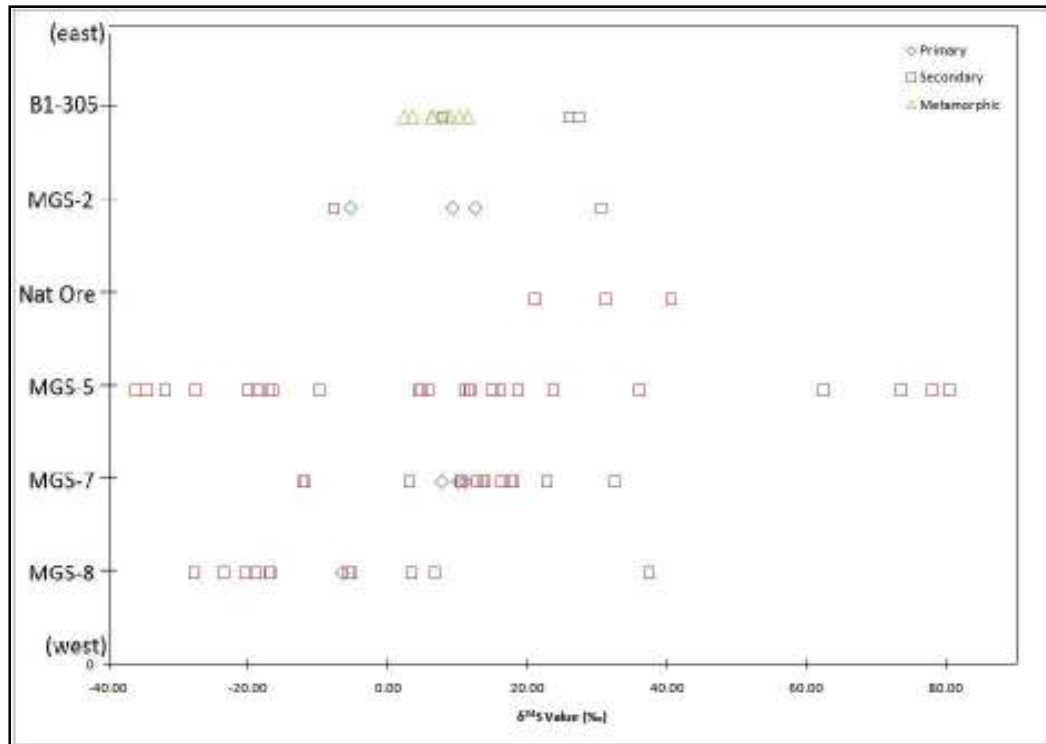


Figure 32: Geographic distribution of secondary sulfides in terms of mineral occurrence.



Figure 33: Different types of sulfide occurrences. A. anhedral mass (MGS-5-21); B. euhedral cubes (MGS-7-17); C. framboidal (MGS-8-16); D. vein (MGS-5-15).

### *6.3.1 Metamorphic Sulfides*

Metamorphic sulfides are only found in the far eastern portion of the Mesabi Range, in B1-305. The Duluth Complex cross cuts the Virginia Formation at the surface and the Biwabik Iron Formation at depth at this location. Sulfides appear as pyrrhotite and chalcopyrite in interstitial anhedral blebs or inclusions within coarse grained metamorphic minerals. The sulfides are interpreted to be primary pyrite that recrystallized into pyrrhotite due to metamorphism (French, 1968). The  $\delta^{34}\text{S}$  values for sulfides range from 2.4‰ to 11.3‰, with an average of +7.0‰, similar to primary values. Because this reaction occurred at a high temperature (Fig. 34) and the degree of fractionation was negligible, that is the  $\delta^{34}\text{S}$  values of the metamorphic sulfides were nearly the same as the original primary sulfides (-5.4‰ to +12.4‰, average +6.2‰), the metamorphism caused by the Duluth Complex can be interpreted as a closed system.

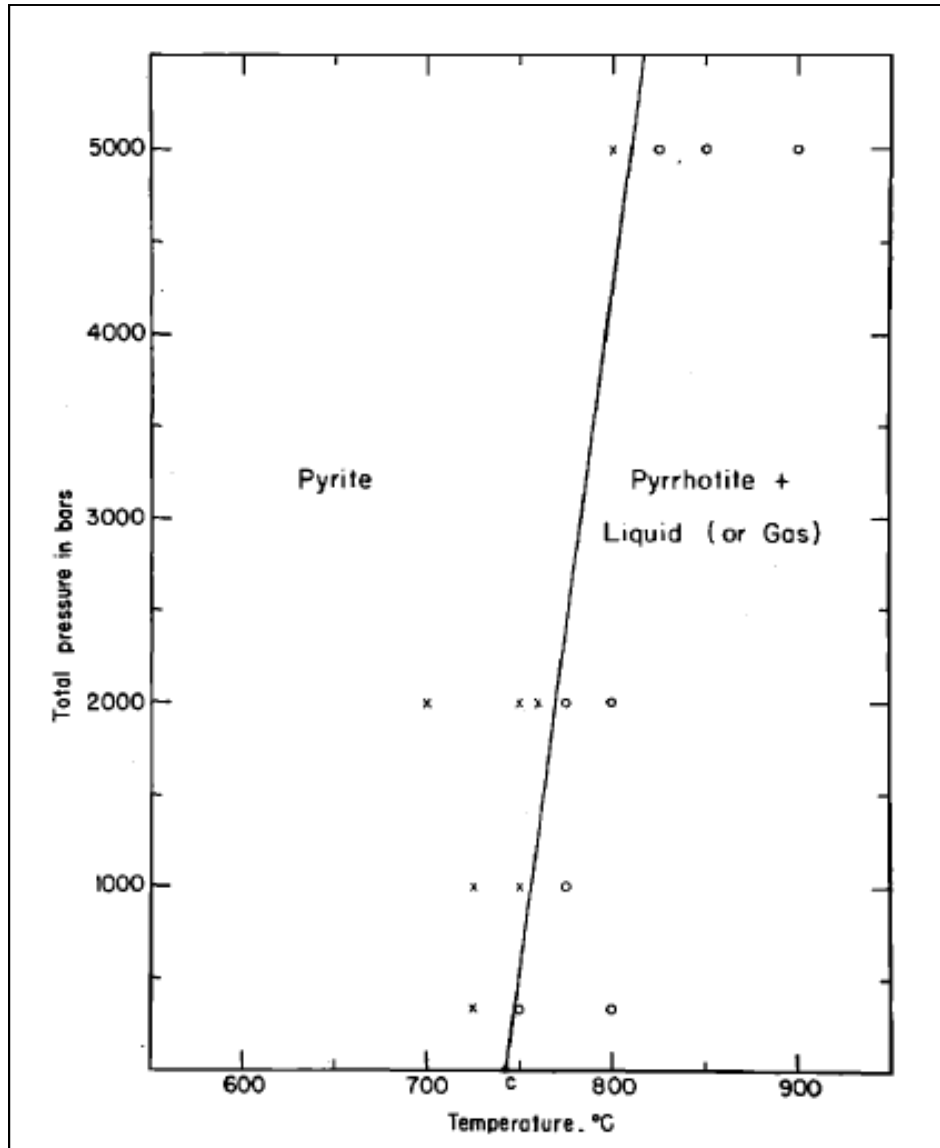


Figure 34: The univariant curve for Pyrite-Pyrrhotite. Point c denotes the termination of this curve, at a temperature of 743°C and 10bars of pressure (or 9.9 atm). As the pressure increases, the temperature necessary for equilibrium between pyrite and pyrrhotite increases as well. The rate increase was calculated to be 14°C/ 1 kbar (Kullerud and Yoder, 1959).

The metamorphic mineral textures also mirror that of primary sulfides. When occurring interstitially, the pyrrhotite and chalcopyrite appear concentrated in layers of fine-grained material that may be relict bedding planes (Fig. 35). If this layering is relict bedding, it

strongly suggests the sulfide was part of the initial deposition of the iron formation. Petrographically, pyrrhotite can also occur as inclusions in the coarser porphyroblasts of orthopyroxene, which is consistent with the sulfides being present prior to the crystallization of pyroxene during metamorphism. It is curious that unlike the silicate phases, sulfide does not coarsen due to metamorphism. Especially given that it goes through a mineral transformation of pyrite to pyrrhotite due to loss of sulfur. It is possible that the metamorphism reduced the available pore space in the eastern portion of the range. This lack of porosity and permeability would retard any fluid flow through the unit that could have re-equilibrated the isotope values with outside sources of sulfur. A study conducted by Crowe (1994), also found that when sulfide minerals were not in contact with one another and were encased in a quartz matrix, they were not susceptible to the overprinting effects of metamorphism and therefore the  $\delta^{34}\text{S}$  value was not re-equilibrated with another source of sulfur.



Figure 35: Core sample B1-305-16 showing layered concentrations of pyrrhotite and magnetite in a metamorphosed section of the Biwabik Iron Formation.

### 6.3.2 Anhedral Sulfides

The textures associated with secondary anhedral sulfides have been described as either forming in masses or along dissolution surfaces. The anhedral masses are coarse-grained sulfides, sometimes appearing to have nucleated from earlier interstitial sulfide (Fig. 33a). Three of the anhedral masses were analyzed using the SEM and were found to contain pyrite with trace amount of arsenic and cobalt and/or cobaltite. One bedded sample was found to contain only pyrite. The presence of trace amounts of As and Co in the masses, but not along the dissolution surfaces, may point to fluids with different mineral chemistry. Interestingly, no anhedral masses were noted in the intermediate slate layer. Sulfides in the intermediate slate were either interstitial primary sulfides or bedded secondary sulfides forming along dissolution surfaces. The bedded sulfides are assumed to be secondary precipitates because of the high degree of concentration and cross cutting relationships.

Isotope analysis of secondary bedded sulfides yielded  $\delta^{34}\text{S}$ -depleted values (-16.8‰ and -7.7‰). These isotope values are both associated with the upper slaty unit and are located on either side of the Mesabi Range (MGS-8 and MGS-2, respectively). Sample MGS-2-2 contains coarse-grained sulfide masses within calcite layers and in MGS-8-4 the sulfide occurs in aggregated masses in oxidized rocks (Fig. 36). The similar isotope values and location of crystal growth along dissolution surfaces suggests that primary sulfides were overgrown or replaced by secondary sulfides derived from a  $\delta^{34}\text{S}$ -depleted fluid, yielding a hybridized  $\delta^{34}\text{S}$  value for the precipitated sulfide.

The  $\delta^{34}\text{S}$  values for the anhedral masses analyzed ranged from 32.5‰ to 80.4‰. All the samples are associated with siliceous granular iron formation in the Lower Cherty unit located in the central portion of the range (MGS-5 and MGS-7). The extremely  $\delta^{34}\text{S}$ -enriched values are associated with the largest sulfide samples collected in this study (Fig. 33a). One may posit that the larger the sulfide mass, the longer and larger the fractionation (in accordance with Rayleigh distillation), assuming a constant supply of sulfate, reactive iron, and organic carbon.



Figure 36: Massive, strata-bound, secondary sulfide masses/aggregates. A. Anhedral sulfide mass located in association with calcite in sample MGS-2-2 B. sulfide aggregation in leached layers in sample MGS-8-4.

### 6.3.3 Euhedral Sulfides

Pyrite cubes can be found throughout the entire formation, in all of the layers, and in the natural ores at the Fayal Mine. However, most of the samples containing cubes are located in the central and western portion of the range (MGS-5, MGS-7, and MGS-8). As mentioned, euhedral cubes have a very wide range of  $\delta^{34}\text{S}$  values (-16.75‰ to +40.57‰); the depleted values associated with the Virginia Formation and the enriched with the natural ore. Their distribution does not appear to be related to geographic location or

associated lithology. Petrographic observations (Appendix A.2) of cubes were made in the following samples: MGS-2-14, MGS-5-18, MGS-5-27, MGS-7-15, MGS-8-1. In some instances, the cubes are cross-cut by veins containing quartz and calcite, suggesting that cube precipitation, in part, occurred prior to the vein formation (Fig. 37).

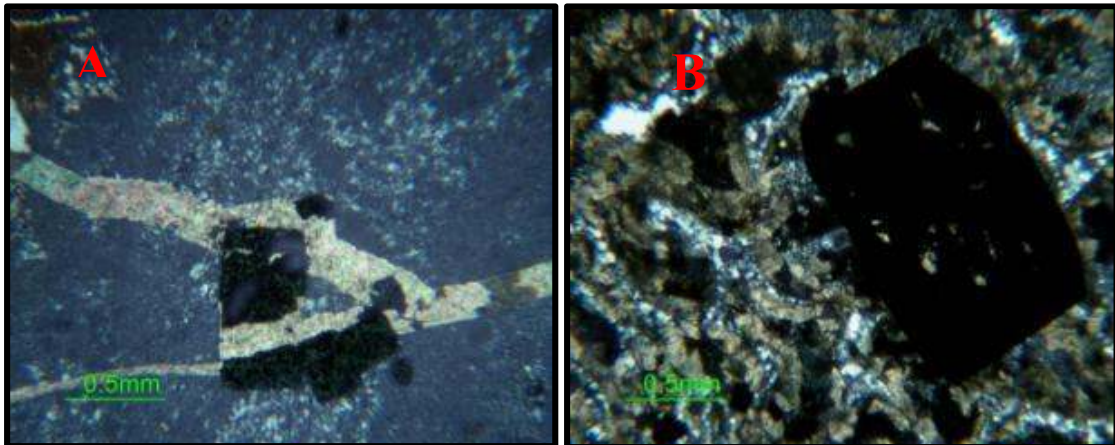


Figure 37: Euhedral cubes of pyrite in the Biwabik Iron Formation. A. pyrite cube cross-cut by calcite vein in sample MGS-5-27, as seen under transmitted and reflected light; B. pyrite cube containing inclusions of granular iron formation in sample MGS-7-19, as seen under transmitted light

Framboids, named for their raspberry-like appearance, are spherical aggregations of microcrystalline euhedral pyrite (Ohfuji and Rickard, 2005; Scott et al., 2009). Scott et al. (2009) concluded from experimental data that a combination of the supersaturation of pyrite and rapid rate of precipitation from a reduced sulfur-rich fluid is one way to form framboids. Furthermore, supersaturation must occur at the site of framboid precipitation, as it is not likely for such fluids to travel considerable distances (Scott et al., 2009). Generally speaking, framboid precipitation can occur where sulfides did not previously exist, as they are not necessary for nucleation. Raisewell (1982) points out that framboidal precipitation involves sourcing iron from the rocks rather than as a dissolved

constituent in the fluid. Thus when the supersaturated, sulfur-rich fluid comes in contact with iron-rich rocks, rapid framboid precipitation occurs in place. This is notable, as most of the framboids sampled in the iron formation are located in the heavily oxidized portions of the range and therefore may have formed during the oxidation of those rocks. Ohfuji and Rickard (2005) additionally posit that the size of individual crystals within the framboids are directly proportionate to the amount of available nutrients.

As noted, samples collected from the far western portion of the range, MGS-8, contained framboids in vugs located in the oxidized, or leached, portions of the lower cherty with  $\delta^{34}\text{S}$  values ranging from -28‰ to -17‰ and an average of -22.45‰ (Fig. 33c). Two samples from MGS-5 (MGS-5-24 and MGS-5-25) contained framboids located between the transition from granular iron formation to banded iron formation (Fig. 38). Duplicate analysis yielded an average  $\delta^{34}\text{S}$  value of -19.4‰ for MGS-5-24. An additional sample (MGS-5-2) contained framboids that appear bedded in the upper cherty unit with an average  $\delta^{34}\text{S}$  value of +15.5‰. The nearly 40‰ divergence in  $\delta^{34}\text{S}$  value along with their obvious physical differences are suggestive of separate precipitation timing for the framboids, characterized by depleted and enriched sulfur isotope values in the fluid. The framboids located in the western end of the formation must be contemporaneous or post-date the removal of silica which significantly oxidized the rocks in that area. In accordance with Rayleigh and our interpretation of primary sulfides, it appears that the  $\delta^{34}\text{S}$ -depleted secondary sulfides were precipitated first and subsequent fractionation of the fluid later precipitated the more  $\delta^{34}\text{S}$ -enriched sulfides. This therefore suggests a

possible lateral west to east secondary fluid flow migration during the formation (oxidation) of the natural ores.

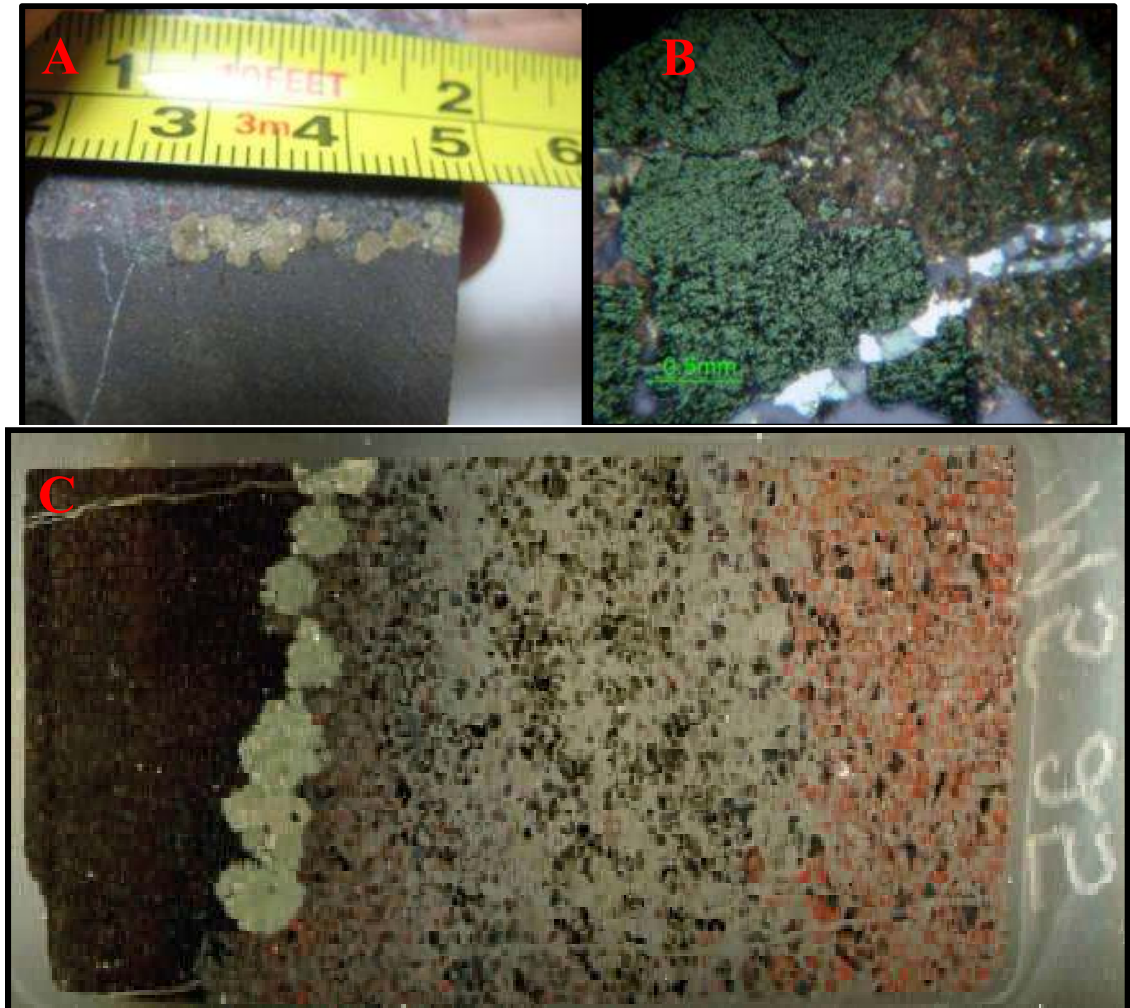


Figure 38: Framboidal pyrite located along dissolution surfaces in sample MGS-5-25 viewed: A. in hand sample; B. in thin section, showing a quartz vein cross-cutting the framboids, as seen under transmitted and reflected light; and C. in a thin section scan.

#### 6.3.4 Vein Sulfides

Veins containing sulfide minerals are located in every stratigraphic unit and at every core location. They are generally characterized as fine grained euhedral to anhedral aggregates of pyrite associated with both quartz and calcite. The isotopic composition of vein sulfide

is remarkably variable, with  $\delta^{34}\text{S}$  values ranging from -36.1‰ to +37.8‰, suggesting various degrees of homogenization between the sulfur in the rocks and the sulfur in the vein fluid to form a hybridized  $\delta^{34}\text{S}$  value for the newly precipitated sulfide. Sulfur isotope values were analyzed from veins in four of the five core locations and in four of the five major units in the Biwabik Iron Formation (no samples were taken for analysis due to lack of availability in MGS-2 or the Intermediate Slate layer).

Samples from MGS-5 are characterized as anhedral sulfides in veins and/or on joint faces with calcite (Fig. 33d). Their  $\delta^{34}\text{S}$  values get progressively enriched, moving down-section, from the upper cherty (-36.1‰) to the lower cherty (-27.6‰). This down section enrichment suggests a secondary horizontal fluid migration pathway, similar to what is seen in the  $\delta^{34}\text{S}$  signature in the framboidal sulfides. An additional vein sulfide sample, MGS-5-4, from the upper slaty has a  $\delta^{34}\text{S}$  value of -9.8‰ and is also associated with calcite on a joint face. The samples from MGS-7 and MGS-8 have  $\delta^{34}\text{S}$  values of +17.5‰ and +37.8‰, respectively. The first is from fine-grained pyrite located on a joint face with calcite and second is fine grained pyrite within a layer of black slate forming along fracture planes without calcite.

Almost all the veins containing sulfide minerals also contain calcite. The presence of calcite suggests that  $\text{CO}_2$  is an important constituent in the secondary sulfide-forming vein fluids. Petrographic evidence also supports this suggestion. Sample MGS-5-13 shows the association of pyrite with calcite+quartz veins (Fig. 39a and 39b). In contrast,

this sample, along with MGS-5-6, shows how quartz-only veins do not contain any sulfides (Fig. 39c and 39d). Interestingly, the B1-305 sample contains pyrite encased in a quartz only-vein and its  $\delta^{34}\text{S}$  value falls within the assumed primary range. Since the vein sulfide value matches that of the interstitial metamorphic sulfides located in the same core, it is possible that fluid remobilized sulfur from the pyrrhotite to form pyrite in the vein.



Figure 39: Secondary sulfide minerals located in veins; A. Calcite vein cross cutting quartz vein, both containing pyrite (MGS-5-13); B. quartz and calcite vein containing pyrite (MGS-5-13); C, D. Quartz only vein with no sulfides present (MGS-5-6, MGS-5-13), all slides seen under transmitted and reflected light microscopy.

### 6.3.5 Other Sulfides

Two samples collected from MGS-7 were characterized as containing unusual needle-like sulfide morphology occurring on a joint face or bedding plane enriched in magnetite. They have a  $\delta^{34}\text{S}$  value of +13.8‰, just slightly above the assumed “primary” sulfide range. In thin section, the “needle” sulfides appear to either cap or precede (original orientation is not known) a layer of granular iron formation. The location of this mineral occurrence suggests that secondary fluid flow along a dissolution surface is the likely cause of precipitation. Mineralogy analysis with the SEM found that the needles are comprised of pyrite with trace amounts of arsenic and cobaltite.



Figure 40: Natural ore containing fine grained, euhedral pyrite aggregates, Fayal Mine.

Finally, the natural ore samples collected from the Fayal Mine are characterized as aggregates of coarse grained, euhedral crystals of pyrite with  $\delta^{34}\text{S}$  values of 20.1‰, 31.2‰, and 40.6‰ (Fig. 40). As discussed in Chapter 2, the Fayal Mine natural ores are

associated with leaching and low-temperature quartz±carbonate mineralization along the Fayal fault (Severson et al., 2010).

#### 6.4 Sources of Sulfur in the Biwabik Iron Formation

Previous studies (Carrigan, 1990; Carrigan and Cameron, 1991; Johnston et al., 2006; Poulton et al., 2010) have interpreted that the  $\delta^{34}\text{S}$  values of the primary sulfide minerals (+2‰ to +13‰; -5.4‰ to +12.4‰ for this study) indicate the sulfur was sourced from bacterial reduction of seawater sulfate in a semi-closed basin. The Animikie Basin ocean chemistry model proposed by Poulton et al. (2010) (shown in Figs. 14-15) also supports this notion. They argue that as the amount of available organic carbon, which is needed to stimulate bacterial reduction, decreases with distance from the assumed strand line, the amount of sulfate reduction, and subsequent sulfide precipitation, decreases as well. Similarly, the flux of Fe (II), sourced from deep ocean hydrothermal vents, also puts limits on sulfide precipitation. The strand line is interpreted to be located in the far eastern portion of the current margin of the iron formation exposure, in the eastern Mesabi Range and the Gunflint Range. As such, they argue that the amount of primary sulfide minerals present and preserved should decrease towards the western portion of the basin (Poulton et al., 2010). This is supported by the lack of primary sulfide minerals observed in this study in the far western Mesabi Range.

Most of the secondary sulfide precipitation was caused by fluid flow through pore spaces, fractures, bedding planes and dissolution surfaces. The wide range of possible  $\delta^{34}\text{S}$  values

associated with secondary sulfides can be tied to the re-equilibration of primary sulfides and/or secondary sulfur in the fluids as well as the degree of fractionation that occurred prior to and during precipitation. Some of the secondary sulfides appear to nucleate from primary sulfide minerals, whereas others precipitated in locations where sulfides did not previously exist. The source of sulfur for the secondary fluid can be generated by dissolution via oxidation and subsequent reduction of primary sulfides from within the Biwabik Iron Formation or can be sourced from meteoric sulfate, volcanic or hydrothermal sulfate, ocean sulfate, or some combination therein.

The sulfur isotope data in this study point toward the low temperature oxidation of primary sulfide minerals, most likely attributed to the meteoric fluid flow during the oxidation of the natural ores. Subsequent fluid migration and sulfate reduction allowed for re-precipitation of secondary sulfides throughout the iron formation; preferential crystallization occurring along fluid flow paths, as mentioned above. Reduction of sulfate, supplied by the oxidized sulfides, via Rayleigh distillation is thought to be the primary mechanism responsible for secondary sulfide isotope values. As mentioned, primary  $\delta^{34}\text{S}$  values fall between -5.4‰ to +12.4‰. Assuming Rayleigh distillation was at play, the secondary  $\delta^{34}\text{S}$  values should be about 30‰ below the primary values, yielding a new  $\delta^{34}\text{S}$  signatures starting at -35‰ and progressively becoming  $\delta^{34}\text{S}$  enriched as reduction continues. The rate and degree of fractionation depends on the amount of available organic material and reactive iron. The considerably large range of  $\delta^{34}\text{S}$  values in the Biwabik Iron Formation supports a slower rate of reduction due to

limited, fluxing organic carbon and/or reactive iron concentrations. In attempt to observe any preferential oxidation pathways through sulfur isotope trends, samples were plotted based on their depth (distance away from the intermediate slate layer) and geographic location. The points were then color coded to match a 10‰ range of sulfur isotope values. Figure 41 shows the geographic and depth distribution of sulfur isotope values in the Biwabik Iron Formation. There does not appear to be any obvious sulfur isotope trends relating to depth or geographic location that may support to presence of an oxidation pathway; that does not, however, suggest that one never existed. Therefore, additional studies are necessary to better constrain the  $\delta^{34}\text{S}$  variability in the Biwabik Iron Formation.

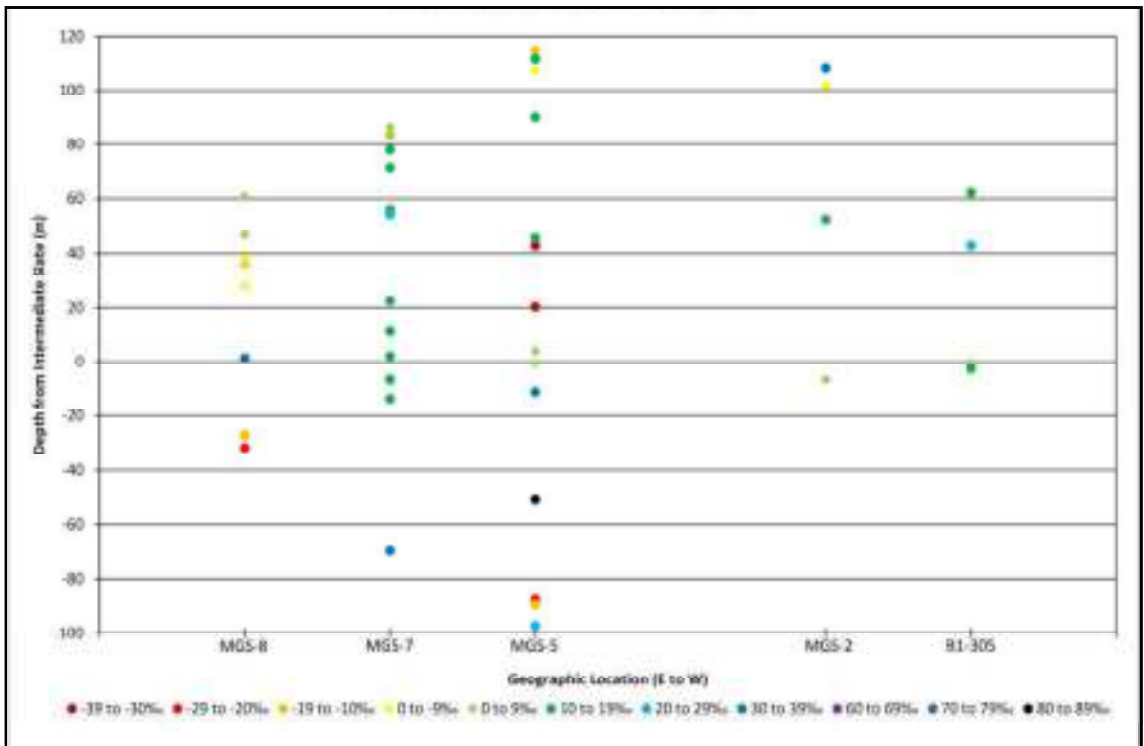


Figure 41: Geographic and Depth Distribution of sulfur isotopes in the Biwabik Iron Formation

## 6.5 Sulfide Mineral Paragenesis in the Biwabik Iron Formation

Three main phases of sulfide precipitation in the Biwabik Iron Formation are supported by both isotopic and textural evidence (Fig. 42). Primary sulfides, as interstitial anhedral blebs of pyrite, were formed during the deposition of the Animikie Group. The emplacement of the Duluth Complex at 1.1 Ga metamorphosed the eastern portion of the Mesabi Range, causing primary sulfides to be recrystallized into pyrrhotite. Little to no fractionation occurred and therefore the range of  $\delta^{34}\text{S}$  values (2.4‰ to 11.3‰) is similar to that of the primary sulfides. The main difference between the metamorphic sulfides and the primary sulfides from which they believed they were formed from is the mineralogy; all other aspects, including morphology, is essentially the same. That being said, one could argue that if secondary sulfides (non-blebs) were present prior to metamorphism as well, then their morphologies should also be visible in the metamorphosed portions of the Biwabik Iron Formation. However, the sulfides present in the eastern Mesabi Range exhibit only primary textures and therefore secondary sulfide mineralization is interpreted to have formed post-Duluth Complex. Secondary, low temperature oxidation via meteoric fluid flow and subsequent sulfate reduction can lead to a large range of  $\delta^{34}\text{S}$  values as the rate at which reduction occurs may vary due to local conditions.

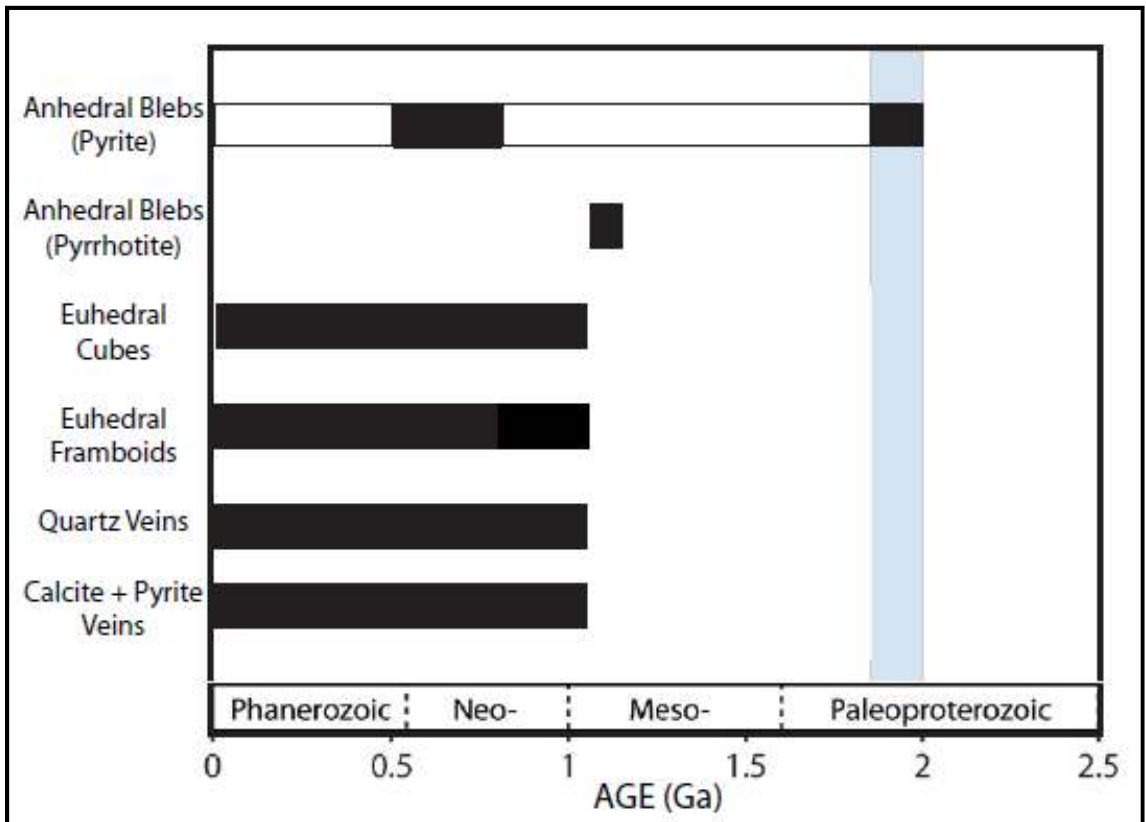


Figure 42: Estimated mineral paragenesis for the sulfide minerals observed in the Biwabik Iron Formation. The blue box indicates the timeframe over which primary precipitation occurred. Pyrrhotite was formed during the emplacement of the Duluth Complex. All subsequent secondary sulfide minerals formed post-Duluth Complex.

Textural evidence also yields observations regarding sulfide paragenesis on a microscopic scale. In sample MGS-5-25, a quartz vein is cross cutting framboids and in MGS-5-27, a calcite vein is cross cutting a cube (Figs. 37a and 38b). This suggests that in some instances, but perhaps not all, veins post-date both framboidal and cube nucleation.

## 6.6 Sources of Sulfur in the St. Louis River Watershed

Sulfate sampling in the St. Louis River Watershed immediately adjacent to mining activity in northeastern Minnesota was conducted by the Minnesota Department of

Natural Resources. Analysis conducted on the water sulfate yielded a range of  $\delta^{34}\text{S}$  values from +4‰ to +9‰. Although  $\delta^{34}\text{S}$  values were conducted on water sulfate, rather than solid sulfide minerals, Berndt and Bavin (2011b) assumed little to no fractionation between the two due to the close proximity between water sampling sites and the rock sources. This assumption therefore allows for direct comparisons between the water sulfate and solid sulfide  $\delta^{34}\text{S}$  values, in attempt to determine the solid source of sulfur to the St. Louis River Watershed. Interestingly, the sulfate range falls comfortably within the primary sulfide range of +2‰ to +13‰. The similarities suggest that sulfides within the Biwabik Iron Formation may be a dominant contributor of sulfur to the St. Louis River Watershed. Because only a small portion of the sampled sulfides in this study contained primary sulfides, it is possible to assume that primary sulfides are not the dominant morphology present in the Biwabik Iron Formation. Additionally, the effect of extreme  $\delta^{34}\text{S}$  values associated with veins, framboids, and massive anhedral sulfides may lead to an average signature that artificially appears primary but is rather, and more appropriately, an average of all the sulfides present in the formation.

## Chapter 7: Conclusion

The main objective of this study was to delineate the areal and stratigraphic distribution of sulfide minerals in the Biwabik Iron Formation and to determine their mineralogy, textural and lithologic occurrence, and sulfur isotope geochemistry. This data could then be evaluated to assess the paragenesis of the various sulfide occurrences, the characteristic isotopic compositions of those occurrences, and the likely genesis of the sulfide-forming events. Furthermore, the  $\delta^{34}\text{S}$  sulfide values for this study were compared to  $\delta^{34}\text{S}$  sulfate values collected for a sulfur cycling study in the St. Louis River Watershed by the Minnesota Department of Natural Resources. This comparison is necessary to estimate the possible sources of sulfur to the St. Louis River Watershed. Therefore, the main conclusions of this study addressed the sulfide-forming processes responsible for and controls on sulfide mineral distribution, and how that distribution correlates to sulfate in the St. Louis River Watershed.

### *Sulfide Mineral Distribution & Formation*

The distribution of the various sulfide occurrences in the Biwabik Iron Formation appear to be somewhat controlled by the internal characteristics of the host lithology. The processes responsible for the formation of the various occurrences can be broadly attributed to three time-frames: primary, metamorphic, and secondary. Primary sulfides are those formed as a product of the environment of original deposition. In the case of the Biwabik Iron Formation, these sulfides are defined as anhedral blebs of interstitial pyrite. Most primary pyrite falls in the  $\delta^{34}\text{S}$  range of +2‰ to +13‰, which others (Carrigan,

1990; Carrigan and Cameron, 1991; Johnston et al., 2006; and Poulton et al., 2010) have interpreted to be consistent with reduction of an ocean sulfate source in a near shore environment of the Paleoproterozoic Animike Sea. Within the Biwabik Iron Formation, the primary sulfide textures appear most often, if not exclusively, in low porosity portions, such as the intermediate slate. Metamorphic sulfides, characterized as interstitial pyrrhotite and chalcopyrite, were exclusively located within the thermal aureole of the Duluth Complex. No outside source of sulfur was integrated into the system at this time and therefore  $\delta^{34}\text{S}$  values of the metamorphic sulfides were merely recrystallized from the primary sulfides. In contrast, secondary sulfides were precipitated from low-temperature, oxidizing meteoric fluid flowing through the iron formation via faults, fractures, pore spaces, and dissolution surfaces. The oxidation, most likely the cause of nature ore formation, remobilized primary sulfide minerals, allowing for subsequent reduction via Rayleigh fractionation, yielded a variety of sulfide textures and a wide range of  $\delta^{34}\text{S}$  as fractionation continued. The textures seen include anhedral masses, cubes, framboids, and within veins. The wide range of  $\delta^{34}\text{S}$  values can be attributed to the homogenization of sulfate in the fluid with primary sulfide in the iron formation and the degree of fractionation, a product of available sulfate, reactive iron, and organic material for fuel.

#### *Correlation to St. Louis River Watershed Sulfate*

When comparing the  $\delta^{34}\text{S}$  values of St. Louis River Watershed sulfate to Biwabik Iron Formation sulfides, it appears, perhaps artificially, that primary and metamorphic

sulfides, anhedral interstitial blebs of pyrite and pyrrhotite, are the main contributors of sulfur as they share the same overall sulfur isotope signature. However, the occurrences associated with secondary, post-depositional fluid flow, average out similarly to the watershed, despite their extreme values. Therefore, although the primary and metamorphic sulfide mineral isotope signatures are more obviously similar to the isotope values seen in the St. Louis River Watershed, it also appears that the secondary sulfides are a plausible contributor to the sulfur budget as well. This seems a more likely conclusion as secondary sulfides are much more wide spread and coarser grained than the primary and metamorphic sulfides in the Biwabik Iron Formation and thus more easily incorporated into the watershed.

#### *Future Implications and Further Studies*

Studies regarding the location and characteristics of sulfide minerals in the Biwabik Iron Formation were limited prior to this study. Although not extensive, the data collected for this study paint a general picture of the distribution of sulfide minerals in the Biwabik, including their geochemistry, host lithology, and morphology. Although no single geographic location, lithology, or morphology contributes more sulfides to the overall sulfur budget of the St. Louis River Watershed, they do all appear to contribute. Therefore it is important, when moving forward and planning for the management of present and future waste rock and tailings basins containing Biwabik Iron Formation, to be aware of the presence of sulfide minerals and their ability to be incorporated into the local ground water and surface water bodies. This may have legal ramifications for

mining companies as well as local, state, and federal government organizations as sulfate concentrations are monitored in nearby watersheds.

As this study principally focused on visible sulfide occurrences and a biased sampling methodology due to financial limitations, it may be helpful if further studies were conducted to determine an unbiased sulfide mineral distribution in the Biwabik Iron Formation. Detailed ion microprobe studies of individual sulfides to check for internal homogeneity and precipitation history would be useful, as well. Additionally, continued research into other possible sources of sulfate to the St. Louis River Watershed, such as sulfide distribution, mineralogy, and geochemistry in the glacial till as well as the Virginia Formation and Duluth Complex, can aid in fully understanding the sulfur budget in the region.

## References

- Addison, W.D., Brumpton, G.R., VAllini, D.A., McNaughton, N.J., Davis, D.W., Kissin, S.A., Fralick, P.W., and Hammond, A.L., 2005, Discovery of distal ejecta from the 1840 Ma Sudbury impact event, *Geology*, v. 33, p. 193-196.
- Beck, J.W., 1988, Implications for early Proterozoic tectonics and the origin of continental flood basalts, based on combined trace element and neodymium/strontium isotopic studies of mafic igneous rocks of the Penokean Lake Superior belt, Minnesota, Wisconsin, and Michigan: Minneapolis, University of Minnesota, Unpublished Ph.D. Dissertation, p. 262.
- Berndt, M. and Bavin, T., 2011a, Sulfate and mercury cycling in five wetlands and a lake receiving sulfate from taconite mines in northeastern Minnesota, Minnesota Department of Natural Resources, p. 78.
- Berndt, M. and Bavin, T., 2011b, A preliminary assessment of sulfate release and cycling processes in the St. Louis River watershed: An Environmental and Natural Trust Fund Progress Report, Minnesota Department of Natural Resources, p. 45
- Bleifuss, R.L., 1964, Mineralogy of oxidized taconites of the western Mesabi and its influence on metallurgical processes, *Society of Mining Engineers Transactions*, v. 229, p. 236-244.
- Bonnichsen, B., 1968, General geology and petrology of the metamorphosed Biwabik Iron Formation, Dunka River area, Minnesota: Minneapolis, University of Minnesota, Unpublished Ph.D. Dissertation, p. 240.
- Bonnichsen, B., 1969, Metamorphic pyroxenes and amphiboles in the Biwabik Iron Formation, Dunka River Area, Minnesota, Mineralogical Society of America Special Paper, n. 2, p. 217-241.
- Canfield, D.E. and Raiswell, R., 1999, The Evolution of the Sulfur Cycle, *American Journal of Science*, v. 299, p. 697-723
- Canfield, D.E., 2004, The evolution of the Earth surface sulfur reservoir, *American Journal of Science*, v. 304, p. 839-861
- Carrigan, W.J., 1990, Stable isotope ratios of carbonate and sulfide minerals from the Gunflint Formation: evidence for the origin of iron-formations [Ph.D. Thesis]: University of Ottawa, p. 199.
- Carrigan, W.J. and Cameron, E.M., 1991, Petrological and stable isotope studies of carbonate and sulfide minerals from the Gunflint Formation, Ontario: evidence for the origin of early Proterozoic iron-formation, *Precambrian Research*, v. 52, p. 347-380

Coplen T. B., Hoppole J. A., Bohlke J. K., Peiser H. S., Reider S. E., Krouse H. R., Rosman K. J. R., Ding T., Vocke R. D., Revesz K. M., Lamberty A., Taylor P. and De Bièvre P., 2002, Compilation of minimum and maximum isotope ratios of selected elements in naturally occurring terrestrial materials and reagents. U.S.G.S. Water – Resources Investigations Report 01-4222, p. 98

Crowe, D.E., 1994, Preservation of original hydrothermal  $\delta^{34}\text{S}$  values in greenschist to upper amphibolites volcanogenic massive sulfide deposits, *Geology*, v. 22, p. 873-876.

Farquhar, J., Wu, N., Canfield, D.E., and Oduro, H., 2010, Connections between sulfur cycle evolution, sulfur isotopes, sediments, and base metal sulfide deposits, *Economic Geology*, v. 105, p. 509-33

Fralick, P., Davis, D., and Kissin, S., 2002, The age of the Gunflint Formation, Ontario, Canada: single zircon U-Pb age determinations from reworked volcanic ash, *Canadian Journal of Earth Sciences*, v. 39, p. 1085-1091

French, B., 1968, Progressive Contact Metamorphism of the Biwabik Iron-formation, Mesabi Range, Minnesota: Minnesota Geological Survey, Bulletin 45, p.103

Goodwin, A.M., 1956, Facies relations in the Gunflint Iron Formation, *Economic Geology*, v. 51, p. 565-595.

Gruner, J.W., 1946, *The mineralogy and geology of the taconites and iron ores of the Mesabi Range, Minnesota*, St. Paul, Minnesota, Office of the Commissioner of the Range Resources and Rehabilitation, p. 127.

Gunderson, J.N. and Schwartz, G.M., 1962, The Geology of the Metamorphosed Biwabik Iron-Formation, Eastern Mesabi District, Minnesota

Gunter, F., 1986, Sulfur, In: Principles of Isotope Geology, p. 523-552

Hemming, S.R., McLenna, S.M., Hanson, G.N., and Krogstad, K.M., 1990, Pb isotope systematics in quartz [abs], *EOS*, v. 71, no.17, p. 654-655.

Hemming, S.R., Hanson, G.N., and McLennan, S.M., 1995, Precambrian crustal blocks in Minnesota: Neodymium isotope evidence from basement and metasedimentary rocks, *U.S. Geological Survey, Bulletin 1904-U*, p. 15.

Hemming, S.R., McLennan, S.M., and Hanson, G.N., 1996, Geochemical source characteristics and diagenetic trends of the Virginia Formation, Mesabi Iron Range, Minnesota [abs], *Institute of Lake Superior Geology, 42<sup>nd</sup> Annual Meeting*, Cable, WI, Proceedings, v.42, p.13.

- Hyslop, E., Valley, J., Johnson, C., and Beard, B., 2008, The effects of metamorphism on O and Fe isotope compositions in the Biwabik Iron Formation, northern Minnesota; *Contributions to Mineralogy and Petrology*; v.155, p.313-328
- Jirsa, M.A., Miller, J.D., and Morey, G.B., 2008, Geology of the Biwabik Iron Formation and Duluth Complex, *Regulatory Toxicology and Pharmacology*, v. 52, p. S5-S10
- Johnston, D.T., Poulton, S.W., Fralick, P.W., Wing, B.A., Canfield, D.E., and Farquhar, J., 2006, Evolution of the oceanic sulfur cycle at the end of the Paleoproterozoic, *Geochimica et Cosmochimica Acta*, v. 70, p. 5723-5739
- Krouse, H.R., 1980, Sulphur Isotopes in our Environment, In: Fritz, P and Frontes, J.C., Handbook of Environmental Isotope Geochemistry
- Kullerud, G., and Yoder, H.S., 1959, Pyrite stability relations in the Fe-S system, *Economic Geology*, v. 54, n.4, p. 533-572.
- La Berge, G.L., 1964, Deveolpment of magnetite in iron-formations of the Lake Superior region, *Economic Geology*, v. 59, n. 7, p. 1313-1342.
- LaBerge, G.L., Robbins, E.I., Han, T.M., 1987, A model for the biological precipitation of Precambrian iron-formations, A: Geological Evidence, IN: Appel, P.W.U. and LaBerge, G.L., eds., Precambrian iron-formations: Athens, Greece, Theophrastus Publications, p. 69-96.
- McSwiggen, P.L. and Morey, G.B., 2008, Overview of the mineralogy of the Biwabik Iron Formation, Mesabi Iron Range, northern Minnesota, *Regulatory Toxicology and Pharmacology*, v. 52, p. S11-S25
- Morey, G.B., 1970, Masabi, Gunflint and Cuyuna Ranges, Minnesota, In: Unesco, 1973, Genesis of Precambrian iron and manganese deposits. Proc. Kiev Symp., 1970, *Earth Sciences*, v.9, p. 193-208
- Morey, G.B., 1972, General Geologic Setting, Mesabi Range, Gunflint Range, Cuyuna District, In: Sims, P.K. and Morey, G.B., Geology of Minnesota: A Centennial Volume, p. 199-239
- Morey, G.B. and Southwick, D. L., 1995, Allostratigraphic Relationships of Early Proterozoic Iron-Formations in the Lake Superior Region, *Economic Geology*, v. 90, p. 1983-1993
- Morey, G.B., 1999, High-grade ore deposits of the Mesabi Range, Minnesota – Product of a continental-scale Proterozoic ground-water flow system, *Economic Geology*, v. 94, p. 133-142.

Ohfuji, H. and Rickard, D., 2005, Experimental synthesis of framboids – a review, *Earth-Science Reviews*, v. 71, p. 147-170.

Ojakangas, R.W., ,1983, Tidal deposits in the early Proterozoic basin of the Lake Superior region – the Palms and the Pokegama Formations: Evidence for subtidal-shelf deposition of Superior-type banded iron-formation, IN: Medaris, L.D., Jr., ed., Early Proterozoic geology of the Great Lakes region: Geological Society of America Memoir 160, p. 49-66.

Ojakangas, R.W., Severson, M.J., Jongewaard, P.K., Arola, J.L., Evers, J.T., Halverson, D.G., Morey, G.B., and Holst, T.B., 2005, Geology and Sedimentology of the Paleoproterozoic Animikie group: the Pokegama Formation, the Biwabik Iron Formation, and Virginia Formation of the Eastern Mesabi Iron Range, and the Thomson Formation near Duluth, Northeastern Minnesota, In: Guidebook Series: Minnesota Geological History, v. 21, p. 208-237

Poulton, S.W., Fralick, P.W., and Canfield, D.E., 2010, Spatial Variability in Oceanic Redox Structure 1.8 Billion Years Ago, *Nature Geoscience*, v.3, p 486-490

Proceedings of the 8th IAEA Consultants Meeting on Future Trends in Stable Isotope Reference Materials and Laboratory Quality Assurance, Vienna, Austria, 2000.

Pufahl, P., Fralick, P., and Scott, J., 2000, Geology of the Paleoproterozoic Gunflint Formation, In: Institute on Lake Superior Geology Proceedings, 46<sup>th</sup> Annual Meeting, Thunder Bay, Ontario, v.46, part 2, p. 103-147

Raiswell, R., 1982, Pyrite Texture, Isotopic Condition, and the Availability of Iron, *American Journal of Science*, v. 282, p.1244-1263

Ripley, E.M., Li, C., Moore, C.H., and Schmitt, A.K., 2010, Micro-scale S isotope studies of the Kharaelakh intrusion, Noril'sk region, Siberia: Constraints on the genesis of coexisting anhydrite and sulfide minerals, *Geochimica et Cosmochimica Acta*, v. 74, p. 634-644

Schulz, K. and Cannon, W., 2007, The Penokean Orogeny in the Lake Superior Region, *Precambrian Research*, v.157, p.4-25

Scott, R.J., Meffre, S., Woodhead, J., Gilbert, S.E., Berry, R.F., and Emsbo, P., 2009, Development of framboidal pyrite during diagenesis, low-grade regional metamorphism, and hydrothermal alteration, *Economic Geology*, v. 104, p. 1143-1168.

Severson, M.J., Heine, J.J., and Meinders Patelke, M., 2010, Plate II: Hung Stratigraphy of the Biwabik Iron Formation showing distribution of internal submembers at the various taconite mines on the Mesabi Range of Minnesota, Report NRR/IR-2009/09

- Severson, M.J., Ojakangas, R.W., Larson, P., and Jongewaard, P.K., 2010, Field Trip 2: geology and stratigraphy of the central Mesabi iron range, *Field Guide to the Geology of Precambrian Iron Formations in the Western Lake Superior Region Minnesota and Michigan*, PRC Guidebook 10-01, p. 15-52.
- Sharp, 2007, Principles of Stable Isotope Geochemistry: Upper Saddle River, NJ, Pearson Prentice Hall, p.344
- Shields-Zhou, G. and Och, L., 2011, The case for a Neoproterozoic Oxygenation Event: Geochemical evidence and biological consequences, *GSA Today*, v. 21, n.3, p.4-11
- Southwick, D.L. and Day, W.C., 1983, Geology and petrology of Proterozoic mafic dikes, north-central Minnesota and western Ontario, *Canadian Journal of Earth Sciences*, v. 20, p. 622-638.
- Studley, S.A., Ripley, E.M., Elswick, E.R., Dorais, M.J., Fong, J., Finkelstein, D., and Pratt, L.M., 2002, Analysis of sulfides in whole rock matrices by elemental analyzer-continuous flow isotope ratio mass spectrometry (short communication), *Chemical Geology*, v. 192, p. 141-148
- Waggoner, 2010, Negaunee Iron Formation, Marquette Range, Michigan, IN: Precambrian Research Center Professional Workshop Series: Geology, Mineralogy, and Genesis of Precambrian Iron Formations Short Course, Duluth, MN.
- Werne, J.P., Lyons, T.W., Hollander, D.J., Schouten, S., Hopmans, E.C., and Sinninghe Damsté, J.S., 2008, *Geochimica et Cosmochimica Acta*, v. 72, p. 3489-3502
- White, D.A., 1954, The stratigraphy and structure of the Mesabi Range, Minnesota, *Minnesota Geological Survey Bulletin* 38, p. 92.
- Williams, C.D., Ripley, E.M., and Li, C., 2010, Variations in Os isotope ratios of pyrrhotite as a result of water-rock and magma-rock interaction: Constraints from Virginia Formation-Duluth Complex contact zones, *Geochimica et Cosmochimica Acta*, v. 74, p. 4772-4792.
- Zanko, L.M., Severson, M.J., Oreskovich, J.A., Heine, J.J., Hauck, S.A., and Ojakangas, R.W., 2003, Oxidized taconite geological resources for a portion of the western Mesabi Iron Range (west half of the Atcturus Mine to the east half of the Canisteo Mine), Itasca County, Minnesota – a GIS-based resource analysis for land-use planning: University of Minnesota Duluth, Natural Resources Research Institute, Technical Report NRRRI/TR-2001/40, p. 85.

## **Appendices**

## Appendix A: Sulfide Sample Observations

Appendix A.1 Macroscopic Observations

Sample Number	Unit Name	Depth (meters)	Macroscopic Hand Sample Description	Classification				
				Anhedral (Blebs)	Euhedral (Cubes)	Framboid / Spheroid	Veins	Others
B1-305-1	Virginia	381.91	Disseminated blebs of sulfide (py & po), not related to specific lith	B				
B1-305-2	Virginia	382.07	Disseminated blebs of sulfide	B				
B1-305-3	Upper Slaty	393.04	Strat controlled cubes (w/in dk unit); possible vf gr blebs disseminated in quartz		C			
B1-305-4a,b	Upper Slaty	401.27	4a&b: cubes present in leached zones		C			
B1-305-4a,b (D)	Upper Slaty	401.27	4a&b: cubes present in leached zones		C			
B1-305-4c	Upper Slaty	401.27	4c: blebs w/in vein of quartz				V	
B1-305-5	Upper Slaty	401.42	Strat controlled sulfide cubes		C			
B1-305-6	Upper Slaty	401.57	Cubes in fracture plane		C			
B1-305-7	Upper Cherty	409.65	-					
B1-305-8	Upper Cherty	409.80	-					
B1-305-9	Lower Slaty	419.86	-					
B1-305-10	Lower Slaty	420.01	-					
B1-305-11	Lower Slaty	420.32	-					
B1-305-12	Lower Slaty	434.95	disseminated po	B				
B1-305-13	Lower Slaty	437.39	Strat controlled blebs of sulfide	B				
B1-305-14	Int Slate	444.40	Disseminated sulfide throughout (vfr); larger dissem blebs; at least 2 types sulfide?	B				
B1-305-15	Int Slate	445.31	Disseminated sulfide throughout (vfr); larger dissem blebs; at least 2 types sulfide?	B				
B1-305-16	Int Slate	446.23	Po blebs in magnetite strat (vfr)	B				
B1-305-17	Int Slate	446.53	Po blebs in magnetite strat (vfr); po whips (blebs) in mag strat/bands	B				
B1-305-18	Lower Cherty	447.60	sulfide blebs within mag layers	B				
B1-305-18 (D)	Lower Cherty	447.60	sulfide blebs within mag layers	B				
B1-305-19	Lower Cherty	447.75	Pos blebs of sulfide not enough for isotopes	B				

Sample Number	Unit Name	Depth (meters)	Macroscopic Hand Sample Description	Classification				
				Anhedral (Blebs)	Euhedral (Cubes)	Framboid /Spheriod	Veins	Others
MGs-2-A	Virginia	481.58	pos vein sulf; disseminated blebs throughout as well	B			V	
MGs-2-B	Transition	489.81	disseminated subeuhedral cubes or sulf in specific banding/lith (xcutting existing lith including a quartz vein); blebs in another band (not x-cutting); some blebs in base black layer		C			
MGs-2-1	Upper Slaty	496.06	Pyrite blebs near/within quartz (possibly in veins, too); some fine grained blebs w/in (few)	B			V	
MGs-2-2	Upper Slaty	496.21	2- blebs, v fgr disseminated throughout w/ quartz (more than circled); 2a - v fine grained, stratigraphically controlled, near quartz and black bits	B				
MGs-2-3	Upper Slaty	496.82	3a - on surface? (pos f grained w/in matrix); 3b - cubes & blebs (pyrrhotite), v f grained, pos not enough for sampling; 3 - blebs, f gr throughout; smaller chips have cubes & blebs	B	C			
MGs-2-4	Upper Slaty	503.83	-					
MGs-2-5	Upper Cherty	522.88	f gr disseminated sulfides + vuggy blebs (secondary replacement??)	B				
MGs-2-6	Upper Cherty	527.91	-					
MGs-2-7	Upper Cherty	529.13	sulfides (dark gold) circled; some f gr in quartz (few) pos not enough	B				
MGs-2-8	Upper Cherty	536.30	-					
MGs-2-9	Upper Cherty	537.97	Stratigraphically controlled blebs (pos v fgr)	B				
MGs-2-10	Upper Cherty	545.29	Sulfide blebs, possible fine grained stratigraphically controlled (?)	B				
MGs-2-11	Lower Slaty	573.02	-					
MGs-2-12	Lower Slaty	576.22	-					
MGs-2-13	Lower Slaty /Int Slaty	599.69	Disseminated, strat controlled blebs (pos in clasts); pos fgr sulf in layers	B				
MGs-2-14	Lower Slaty /Int Slaty	600.15	Blebs throughout, not strat controlled, only in cherty areas	B				
MGs-2-15	Lower Slaty /Int Slaty	602.28	Blebs in specific clasts/or strat (quartz/chert &/or plag), possible fine grained strat controlled	B				

MGS-2-16	Lower Slaty /Int Slate	604.72	Disseminated blebs within cherty/quartz strat	B			
MGS-2-16 (D)	Lower Slaty /Int Slate	604.72	Disseminated blebs within cherty/quartz strat	B			
MGS-2-17	Lower Slaty /Int Slate	612.65	Round blebs, disseminated throughout; f & c gr blebs dissem throughout chert	B			
MGS-2-18	Lower Slaty /Int Slate	614.17	vf grained disseminated in quartz veins/strat(?) (bottom); not w/in veins but on edges (cubes?)			V	
MGS-2-19	Lower Slaty /Int Slate	617.52	Vfgr strat controlled blebs (only component of strat)	B			
MGS-2-20	Lower Slaty /Int Slate	617.68	subhedral cubes on surface		C		
MGS-2-21	Lower Cherty	617.98	disseminated f grained sulfide	B			
MGS-2-22	Lower Cherty	620.27	Blebs w/ quartz, pos only on surface, strat controlled	B			
MGS-2-23	Lower Cherty	620.57	Cubes (f gr) in slaty (black chert) strat		C		
MGS-2-24	Lower Cherty	623.01	-				
MGS-2-25	Lower Cherty	654.41	Possibly disseminated, one bleb – not enough to analyze	B			

Sample Number	Unit Name	Depth (meters)	Macroscopic Hand Sample Description	Classification				
				Anhedral (Blebs)	Euhedral (Cubes)	Framboid /Spheroid	Veins	Others
MGS-5-A	Transition	154.69	conglomeration of cubes (tiny) in clast/inclusion (pos connected to qrtz vein); doesn't appear to have sulf elsewhere		C			
MGS-5-A (D)	Transition	154.69	conglomeration of cubes (tiny) in clast/inclusion (pos connected to qrtz vein); doesn't appear to have sulf elsewhere		C			
MGS-5-B	Transition	158.04	larger cube conglomeration, semi-related to a specific layer; pos disseminated sulf throughout slate unit		C			
MGS-5-1	Transition	158.19	Strat controlled subhedral cubes; layers wrap around large cube cluster- mostly w/in chert; flat, fgr sulf on joint/surf w/ calcite		C			
MGS-5-2	Upper Slaty	158.34	Strat controlled sulf framboids/spheres, few cubes; in dark unit, weakly magnetic			F		
MGS-5-2 (D)	Upper Slaty	158.34	Strat controlled sulf framboids/spheres, few cubes; in dark unit, weakly magnetic			F		
MGS-5-3	Upper Slaty	162.15	Blebs on joint surface with calcite (fgr); related to calcite filled veins with some sulf				V	
MGS-5-4	Upper Slaty	162.46	F gr on joint surface with calcite				V	
MGS-5-5	Upper Slaty	179.68	Remnants of sulfide cube with quartz – can't tell if disseminate or secondary; trace bleb sulfides on joint (chert)		C			
MGS-5-6	Upper Slaty	189.74	Dissem blebs of sulf in quartz vein; one bleb w/in chert-like vague vein; poss dissem blebs throughout	B			V	
MGS-5-7	Upper Slaty	202.08	Framboids/spheres on joint; doesn't follow lithology				V	
MGS-5-8	Upper Slaty	210.01	Dissem cubes in cherty matrix; pos strat controlled blebs/spheres as well	B	C			
MGS-5-9	Upper Cherty	223.88	One dissem cube in quartz/cherty zone		C			
MGS-5-10	Upper Cherty	224.18	Single dissem cube in quartz/cherty zone (same as mgs-5-9)		C			
MGS-5-11	Upper Cherty	226.92	V fgr subhedral sulf in veins with calcite (calcite mostly gone)				V	
MGS-5-11 (D)	Upper Cherty	226.92	V fgr subhedral sulf in veins with calcite (calcite mostly gone)				V	

MG5-5-12	Lower Slaty	249.33	framoids/spheres of sulf on joints with calcite (1/2 mm wide plane)				V
MG5-5-13	Lower Slaty	255.12	Sulf on edges of veins filled with calcite (and quartz?); grew from edges of fractures in; some all sulf, all calcite, all quartz, or combination				V
MG5-5-14	Lower Slaty	262.89	Strat controlled sulf cubes; pos veins		C		
MG5-5-15	Lower Slaty	265.79	Strat controlled cubes (euhedral to subhedral); pos related to clasts (chert) – surrounding clasts		C		
MG5-5-16	Lower Slaty /Int Slate	270.36	Dissem sulf cubes in specific strat unit		C		
MG5-5-16 (D)	Lower Slaty /Int Slate	270.36	Dissem sulf cubes in specific strat unit		C		
MG5-5-17	Lower Slaty	274.47	Large dissem sulf cubes (in dark layer); cross cut by large calcite vein		C		
MG5-5-18	Lower Slaty	278.89	F gr dissem blebs (few cubes) strat controlled	B	C		
MG5-5-19	Lower Slaty	280.87	Cubes & f gr blebs capping cherty layer w/ dissem f gr cubes of sulf w/in chert		C		
MG5-5-20	Lower Slaty	288.49	Vfgr blebs (large), layer/clast w/ few cubes around; some sulf veins w/ quartz; between chert & carbonates - cubes with quartz; large blebs	B	C		
MG5-5-21	Lower Cherty	320.04	large (massive) sulfide blebs, sulfides also surrounds clasts (radiates out into dissem)	B			
MG5-5-21 (D)	Lower Cherty	320.04	large (massive) sulfide blebs, sulfides also surrounds clasts (radiates out into dissem)	B			
MG5-5-22	Lower Cherty	320.95	F gr dissem blebs in strat (f gr dark bands) + large (massive) blebs on surf	B			
MG5-5-22 (D)	Lower Cherty	320.95	F gr dissem blebs in strat (f gr dark bands) + large (massive) blebs on surf	B			
MG5-5-23	Lower Cherty	357.53	Sulfide on joint (v f gr cubes/framboids)				V
MG5-5-24	Lower Cherty	359.36	Sulfide blebs btwn two strat (lith – granular chert & fe carb yellow)			F	
MG5-5-24 (D)	Lower Cherty	359.36	Sulfide blebs btwn two strat (lith – granular chert & fe carb yellow)			F	
MG5-5-25	Lower Cherty	361.34	Dissem blebs pos throughout cherty unit; larger blebs separate red cherty w/ f gr unit; f gr dissem sulfide blebs in maroon unit; *grtz vein cut thru sulfide	B			

MGS-5-26	Lower Cherty	366.98	Large sulfide cubes throughout; pos fgr disseminated sulfide between quartz/chert grains						
MGS-5-27	Lower Cherty	367.28	Cubes disseminated throughout quartz/chert				C		

Sample Number	Unit Name	Depth (meters)	Macroscopic Hand Sample Description	Classification				
				Anhedra (Blebs)	Euhedral (Cubes)	Framboid /Spheroid	Veins	Others
MGS-7-A	Virginia	235.61	disseminated subeuhedral cubes within specific strat (massive bedded, pos xcut by qrtz vein); sulfide bleb inclusion in fgr "shale" lith (layered unit); pos fgr sulfide throughout		C			
MGS-7-B	Virginia	238.35	fgr cube inclusions/clasts in massive bedded unit; pos xcut by qrtz vein; fgr sulfide throughout (esp in layered parts)		C			
MGS-7-B (D)	Virginia	238.35	fgr cube inclusions/clasts in massive bedded unit; pos xcut by qrtz vein; fgr sulfide throughout (esp in layered parts)		C			
MGS-7-C	Virginia	238.81	fgr zones, tiny cubes and clasts/inclusions; all over whisp/flow-like banding; pos 2 types of sulfide	B				
MGS-7-1	Virginia	238.96	Massive; pyrite + pyrrhotite; blebs + (pos vein infill) – strat controlled	B			(V)	
MGS-7-2	Upper Slaty	242.93	On surface with quartz; few strat controlled blebs; vein infill (rx clasts imbricated)	B			V	
MGS-7-3	Upper Slaty	244.14	Fine grained surface coating on joint (?); perhaps a layer?				V	
MGS-7-4	Upper Slaty	245.52	-					
MGS-7-5	Upper Slaty	245.97	Fine grained on surface; coating with quartz; in veins with quartz, too				V	
MGS-7-6	Upper Slaty	250.55	Disseminated blebs and cubes (stratigraphically controlled)		C			
MGS-7-7	Upper Cherty	262.89	Vug like infill (weathered out replacement (?)), disseminated throughout; on core edge - POS NONE??	B				
MGS-7-8	Upper Cherty	266.09	Disseminated, fine grained strat controlled; fibers/needles on joint surface					needles
MGS-7-9	Upper Cherty	266.17	Few disseminated cubes; fibers/needles on joint surface					needles
MGS-7-10	Upper Cherty	267.61	maybe vug like infill (weathered out replacement); disseminated throughout; large cube on top		C			
MGS-7-11	Upper Cherty	299.62	Possible disseminated in quartz, fine grained in shale, 2 larger cubes		C			
MGS-7-12	Upper Cherty	311.20	Disseminated blebs; strat controlled within black shale	B				
MGS-7-13	Lower Slaty	320.04	Disseminated blebs/cubes within clasts	B				
MGS-7-13b	Lower Slaty	319.89	Cubes in pink area (like granite or fe stained quartz)		C			

MGS-7-14	Lower Cherty	328.88	Disseminated cubes in pink area					
MGS-7-14 (D)	Lower Cherty	328.88	Disseminated cubes in pink area				C	
MGS-7-15	Lower Cherty	329.03	Cubes on surface (joints); some disseminated cubes; veins (15b); disseminated cubes (15b)				C	V
MGS-7-16	Lower Cherty	335.74	Cubes and blebs on surface (ends) - cubes disseminated w/in				C	
MGS-7-17	Lower Cherty	335.74	Cubes within black (boudin like) strat; cubes in pink areas; blebs on ends				C	
MGS-7-17 (D)	Lower Cherty	335.74	Cubes within black (boudin like) strat; cubes in pink areas; blebs on ends				C	
MGS-7-18	Lower Cherty	338.48	Trace disseminated fine grained pyrite cubes in shale (pos within clasts or spec layers w/in)				C	
MGS-7-19	Lower Cherty	380.85	Disseminated cubes; shale with clasts + pyrite (fine grained)				C	
MGS-7-20	Lower Cherty	383.90	Two disseminated blebs				B	
MGS-7-21	Lower Cherty	392.13	Massive blebs				B	
MGS-7-22	Lower Cherty	413.00	Disseminated blebs in chert (red)				B	

Sample Number	Unit Name	Depth (meters)	Macroscopic Hand Sample Description	Classification				
				Anhedral (Blebs)	Euhedral (Cubes)	Framboid /Spheroid	Veins	Others
MGS-8-A	Transition	445.62	sizable cube w/in quartz (vein?); pos fgr dissem in black "shale" unit		C			
MGS-8-B	Transition	459.64	blebs w/ inclusions w/in; pos actually groups of cubes; fgr dissem in vuggy areas	B				
MGS-8-1	Transition	468.17	Pyrite on surface (secondary)				V	
MGS-8-2	Transition	468.48	Disseminated blebs throughout	B				
MGS-8-3	Transition	469.39	Fine stringers of pyrite (disseminated); possible disseminated throughout shale, some blebs	B				
MGS-8-4	Upper Slaty	469.85	Disseminated, some strat control	B				
MGS-8-5	Upper Slaty	471.53	Pyrite cubes disseminated; more on 5b		C			
MGS-8-6	Upper Cherty	478.23	Highly altered – brecciated (?) vug infill of pyrite		C			
MGS-8-6 (D)	Upper Cherty	478.23	Highly altered – brecciated (?) vug infill of pyrite		C			
MGS-8-7	Upper Cherty	488.59	-					
MGS-8-8	Upper Cherty	503.22	-					
MGS-8-9	Lower Slaty	504.60	-					
MGS-8-10	Lower Slaty	504.90	Fine grained disseminated, visible blebs				V	
MGS-8-11	Lower Slaty /Int Slaty	506.58	Possible disseminated, strat controlled	B				
MGS-8-12	Lower Cherty	518.46	Highly altered/leached; sulfide framboids in vugs		C			
MGS-8-13	Lower Cherty	518.62	Highly altered/leached; sulfide framboid and cubs in vugs and fracture planes		C			
MGS-8-14	Lower Cherty	533.10	sulfide spheres in vugs, highly altered				F	
MGS-8-14 (D)	Lower Cherty	533.10	sulfide spheres in vugs, highly altered				F	
MGS-8-15	Lower Cherty	533.17	sulfide spheres in vugs; Highly altered		C			
MGS-8-16	Lower Cherty	533.25	large sulfide framboid in vug				F	
MGS-8-17	Lower Cherty	535.84	Framboids/spheres and cubs on end; highly altered (weathered, etc)		C			
MGS-8-18	Lower Cherty	537.82	Highly altered (weathered, etc); framboids/spheres - vug infill				F	

MGS-8-18	Lower Cherty	537.82	Highly altered (weathered, etc); framboids/spheres - vug infill				F		
MGS-8-19	Lower Cherty	541.17	Highly altered, weathered; less leached; framboids/spheres on top (perhaps throughout)			C			
Sample Number	Unit Name	Depth (meters)	Macroscopic Hand Sample Description	Classification					
				Anhedral (Blebs)	Euhedral (Cubes)	Framboid /Spheroid	Veins	Others	
NatOre I			conglomeration of cubes		C				
NatOre (II)			conglomeration of cubes		C				
NatOre (II) (D)			conglomeration of cubes		C				



Date: 5/27

Sample Name: M2-17

Location	_____
BIF Unit	_____
Lithology	_____

Thin Section Map



Notes

figs blebs associated almost exclusively w/ grains in Gf. on hour edges - not in matrix <sup>lead</sup>  
 Centers missing / dark - cores  
 look almost framboidal/spheroidal

<sup>cores</sup>  
 formed during deposition towards the end - perhaps came in w/ matrix fluid & attached to grains.

Sulfides

--	--	--	--

T5-004 bl/ba/spheroes PR R  
 T5-005 " PL R  
 T5-006 " XP RAT

Date: 5/27  
SEM 6/14

Sample Name: M2-18

Location	_____
BIF Unit	_____
Lithology	_____

Thin Section Map



Notes

→ lots! *fracta bound, some infiltration into transition layer massive - associated w/ dark layers (mag? illman?) - sulfide = green*

→ *fig #/or cubes exclusively hosted in non-matrix*

SEM → *pos inclusions of silicates in sulf*

Sulfides

--	--	--	--

TS-007	Stateboard	PL R	TS-011	"	PL T
TS-008	"	PL R+T			
TS-009	"	XN R			
TS-010	"	XN R+T			

Date: 5/27  
SEM 6/4

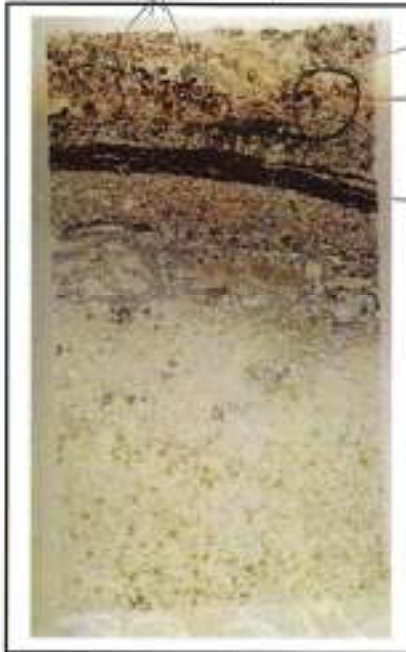
Sample Name: M2-22

Location \_\_\_\_\_

BIF Unit \_\_\_\_\_

Lithology \_\_\_\_\_

Thin Section Map



Notes

SEM

\* sulf - associated w/ vein relic calc

→ NONE IN HERE

mag: makes up matrix

matrix associated w/ dark rimming relic grains

mag = white/gray

not sulf.

sulf w/ calcite

Sulfides

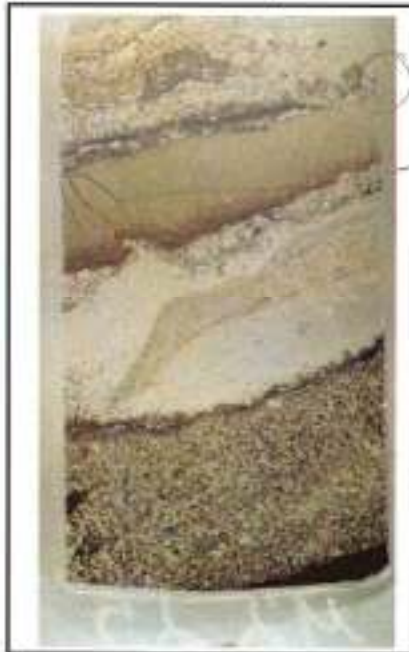
SEM arsenopyrite (white) + pyrite  
Cobaltite & chalcite??

TS-012 Pyrite mag in vein PL + TSD16 " XP R  
 TS-015 " PL T+R TS-017 " XP R+T  
 TS-014 Pyrite calc vein? PL R  
 TS-015 " PL T+R

Sample Name: M2-25

Location	_____
BIF Unit	_____
Lithology	_____

Thin Section Map



Notes

sulf  
 mg + py outside of  
 mag free  
 mag rich

Sulfides

--	--

TS 018 Pyr Mag N vein PL T  
 TS 020 " " PL R  
 TS 019 " " XN R

Sample Name: M5-6

Location	_____
BIF Unit	_____
Lithology	_____

Thin Section Map



Notes

mag matrix  
 ?  
 no visible sulfides ?  
 pos asbestos in vein  
 → a mag inclusion  
 vein = PLT

Sulfides

--

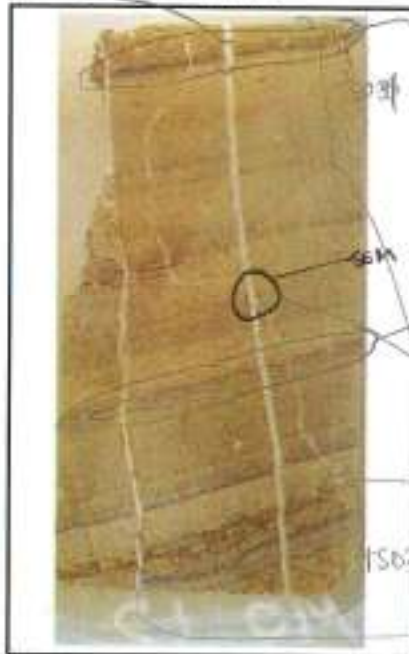
TS-022 Qtz with + mag PL R+T  
 TS-023 " X+ R+T  
 TS-024 " PL T

Date: 5/28  
SEM 6/14

Sample Name: M5-13

Location \_\_\_\_\_  
BIF Unit \_\_\_\_\_  
Lithology \_\_\_\_\_

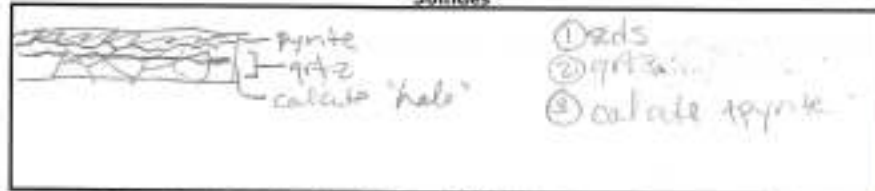
TS #025  
Thin Section Map



Notes

Sulf (pyrite) on edges of veins suggesting sulfide in first pulse of fluid & entrained Fe or its was first to crystallize  
w/ quartz in veins  
also sulf bearing layers  
calcite x-axis over quartz  
- calcite  
- quartz only with  $\rightarrow$  no Pt  
- quartz calcite

Sulfides



TS-025 quartz  
calcite  
Pt

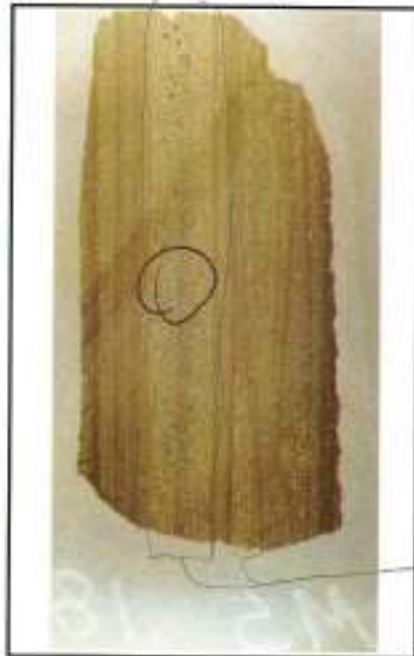
TS\_025 Quartz + Calcite + Py vein XP R TS\_029 Calcite + quartz XP R  
TS\_026 TS\_027 " XP Pt TS\_030 " XP Pt  
TS\_028 Calcite + Py XP R TS\_028 #1 TS\_031 Quartz XP R

Date: 2/28  
SEM 6/14

Sample Name: M5-18

Location	_____
BIF Unit	_____
Lithology	_____

Thin Section Map



Notes

pos pyrite throughout  
(or mag?)

↑ pitied/inclusions  
w/ green fibers  
slightly wavy

coarser gr pyrite → cubes & blebs

pos w/ calcite?

ground

Sulfides

--

TS\_023 Pyrite FL RIT  
 TS\_024 " XP RIT  
 TS\_025 Pyrite BIF → BIF PL RIT

Date: 5/28  
SEM

Sample Name: M5-20

Location \_\_\_\_\_

BIF Unit \_\_\_\_\_

Lithology \_\_\_\_\_

Thin Section Map



Notes

almost all are vfg/mud sulf, density - strat controlled, but present in all of the bottom portion.

all quartz, fgr - replacement of gdf

coarsest sulf located in boundary between the two

→ magnetite? Magnetite green yellow

SEM: LTB circles of Pyrite

Sulfides

\_\_\_\_\_

TS\_036 Py+quartz PL T  
 TS\_037 " XP 7+K  
 TS\_038 Py, cov/hyp + green/yellow PL R  
 TS\_050 PL R+K

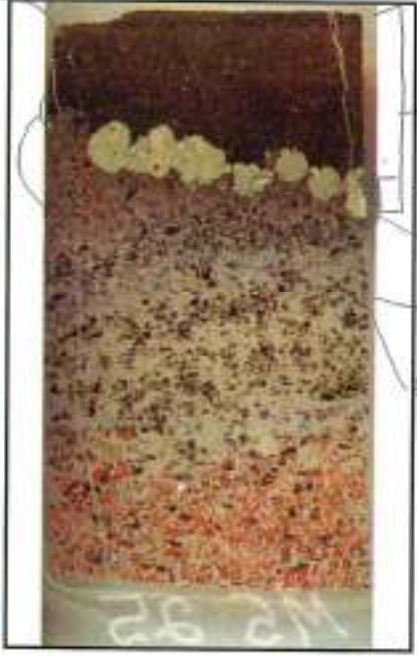
Sample Name: M5-25

Location \_\_\_\_\_

BIF Unit \_\_\_\_\_

Lithology \_\_\_\_\_

Thin Section Map



Notes

in large (fram??) before

- calcite + bt inclusions?

Sulf through out  
cube-like, small

- Secondary

qtz vein x-cuts py  
fringes + no sulf in it

qtz vein (+ calcite?)  
x-cuts fr sulf

Calcite newest - overprint?

Sulfides

\_\_\_\_\_

- TS-040 Py frim + py-fring PL T
- TS-041 Py frim + qtz vein + py fr
- TS-042 " sulf PL TIF

Sample Name: M5-27

Location \_\_\_\_\_  
 BIF Unit \_\_\_\_\_  
 Lithology \_\_\_\_\_

Thin Section Map



Notes

euhedral-cube  
 aggregates  
 calcite  
 replaced or replacing  
 get (anis) → *diffuse*  
 X out by calcite vein  
 sulf only w/ fgr grtz  
 chert  
 not w/ calcite - limestone  
 Laminar-esp

Sulfides

\_\_\_\_\_

TS\_043 Pyrite + sil by calcite vein XP RIT  
 TS\_044 Pyrite - replace grains PL RIT  
 TS\_045 Pyrite + reflect RP RIT GIF

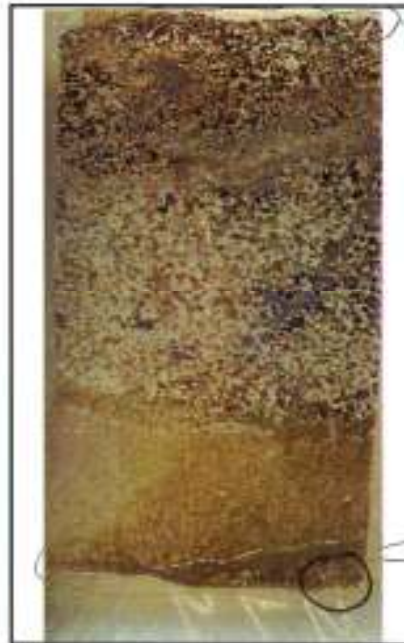
Sample Name: M7-9

Location \_\_\_\_\_

BIF Unit \_\_\_\_\_

Lithology \_\_\_\_\_

Thin Section Map



Notes

NEEDLES

Soft sed claf or pressure  
stylolites  
rimmed edge of sulf

interstitial mag?  
+ ~~small~~ granules + ~~replace~~  
qtz groundmass

Sulf - looks like  
relict cubes

forms @ most of top of BIF

disseminated fgr  
Sulf w coarse at  
edges of sulf  
strip

Sulfides

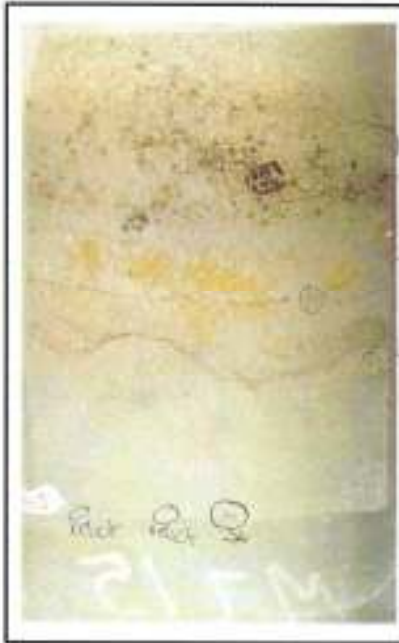
\_\_\_\_\_

TS\_040 Py descom, # needles? PL T  
 TS\_047 PL T+P  
 TS\_048 Py in equilibrium with ship XP T+P

Sample Name: M7-25

Location	_____
BIF Unit	_____
Lithology	_____

Thin Section Map



Notes

Not in GIF (<sup>chert</sup> qtz & gron in qtz matrix)

Few aeg. NO discorn

Styolite does NOT cross a pyrite cube

↓ calcite

qtz + calcite, more discorn

discorn = 'stylite' sulf

discorn sulf (cube)

Sulfides

--	--	--	--	--	--

TS 049 71 discorn sulf (cube) PL T TS 052 <sup>chert</sup> calcite in styolite PL T  
 TS 050 " PL 712 TS 053 " PL 71R  
 TS 051 " RP 71R TS 054 " XP 71R

Sample Name: M7-18

Location	_____
BIF Unit	_____
Lithology	_____

VP Thin Section Map



Notes

- mag reappears ~~at~~  
 - above  
 - disseminated sulf. in BIF  
 - stylolite - pressure soft sed. dy  
 - mag replacement of  
 GfF

Sulfides

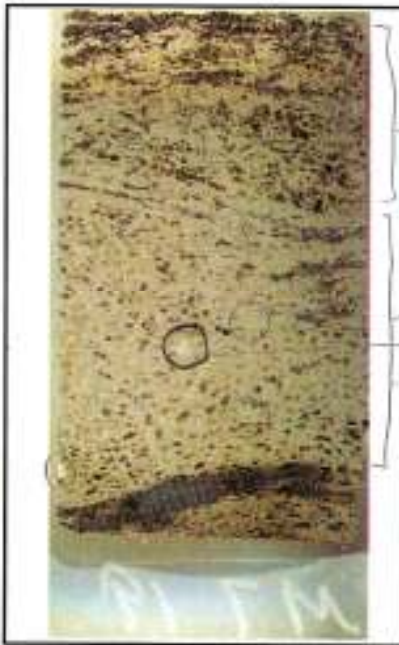
--

TS. 855 by above PL TRF

Sample Name: M7-19

Location	_____
BIF Unit	_____
Lithology	_____

Thin Section Map



Notes

mag becomes subhedral & larger

less mag

inclusions of carb

GIF

mag = formed in inclusions

Self x-cut all (last)

Sulfides

--	--	--	--

TS_059a	Pyrite inclusions	XP R	TS_05B	Pyrite, inclusions	XP T
TS_059	"	XP R/T	TS_057	"	XP T/R

Sample Name: M7-20

Location	_____
BIF Unit	_____
Lithology	_____

Thin Section Map



Notes

no mag or sulf  
- mag on edges & interstitial  
  ↳ replacing or being replaced  
  ↳ pos sulf □  
  
no sulf

Sulfides

--

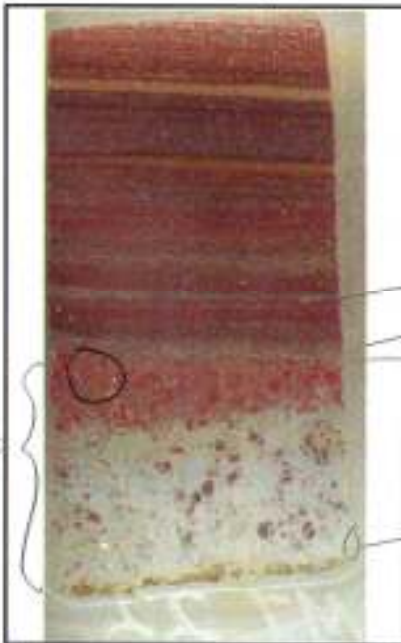
Sample Name: M7-22

Location \_\_\_\_\_

BIF Unit \_\_\_\_\_

Lithology \_\_\_\_\_

Thin Section Map



Notes

interbedded  
GIF & BIF

vein stops at st/alk  
one sulf in st/

calc abe (part)

dissem sulf = calcite

Sulfides

Fig 1  
mass sulf  
GIF (white)

mass sulf  
GIF (white)

12-060 N. Lake MIF Pa. R  
15-060 " " PL. RRI

Date: 5/29

Sample Name: M8-1

Location	_____
BIF Unit	_____
Lithology	_____

## Thin Section Map



## Notes

fine grained, dissem  
sulf throughout  
cubes

pos related to  
granules

radial qtz extinction  
few calcite cubes  
present

## Sulfides



TS_062	actinolite	PL R	TS_065	actinolite	PL RIT
TS_063	"	PL RIT	TS_066	"	XP RIT
TS_064	"	XP RIT	TS_067	"	PL RIT

Sample Name: M8-13

Location	_____
BIF Unit	_____
Lithology	_____

Thin Section Map



Notes

no visible sulf  
but they are  
from in vugs  
  
made up of goethite  
hematite  
+qtz +mag?

Sulfides

--

Date: 5/30

Sample Name: B1-2

Location	_____
BIF Unit	_____
Lithology	_____

Thin Section Map



Notes

Sulf are interstitial  
 w/ bit of qtz & hb/ol?  
 &  
~~plag~~ plag - twinn  
 pos retrograde  
 related

Sulfides

<i>chalcopyrite</i>		
---------------------	--	--

TS_068	Polychrom	PL T
TS_069	"	PL TIR
TS_070	"	XP T
TS_071	"	XP TIR

TS_072	SD 2	XP T
TS_073	"	XP TIR

Sample Name: B1-5

Location	_____
BIF Unit	_____
Lithology	_____

Thin Section Map



Notes

po  
 pos associated  
 w/ a vein

lots of missing  
 xHS in strat

check rock

Sulfides

--	--

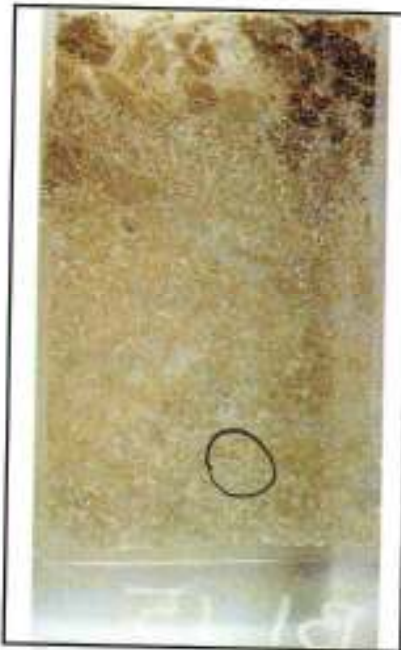
TS-074 Po+Mag PL R  
 TS-074 " PL R+T  
 TS-094 " XP R+T

Date: 5/20

Sample Name: B1-15

Location	_____
BIF Unit	_____
Lithology	_____

Thin Section Map



Notes

very white/lt yellow  
 interstitial to small  
 & inclusions to  
 bigger xls (pyx)

ms  
 pyx  
 ps  
 play

Sulfides

--	--

TS-077	pat stnd	PL T
TS-078	"	PL T&K
TS-079	"	XP T
TS-080	"	XP T&R

TS-085	pat inclusions	PL K
TS-086	"	PL PIT
TS-087	"	XP T
TS-088	"	XP TIR

Sample Name: B1-16

Location	_____
BIF Unit	_____
Lithology	_____

Thin Section Map



Notes

appear vein like  
 → assume seed  
 stratigraphy of  
 growth  $\text{B}_{\text{in}}\text{-meta}$

Seen only of  
 small xtls

Mixed of mag  
 def shear directions  
 in mineral n/in  $\downarrow$   
 xtls

Sulfides

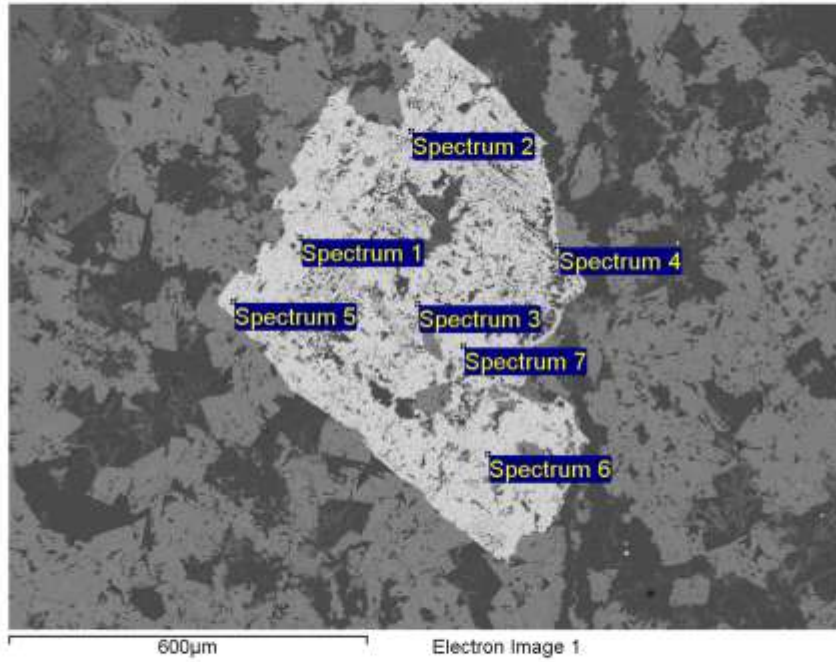
--	--	--	--

TS.081 Po 1 Mag PL R  
 TS.082 " " XP FIT ] unbalanced |  
 TS.083 Po PL R  
 TS.084 " XP FIT

## Appendix A.3: SEM-EDS Results

Steph Theriault 061411 - 214

8/14/2013 10:54:51 AM



Processing option : All elements analysed

Spectrum	In stats.	Si	P	S	Fe	Total
Spectrum 1	Yes	0.14	0.33	60.69	48.52	109.68
Spectrum 2	Yes	0.17	0.35	60.70	48.79	110.01
Spectrum 3	Yes	0.19	0.23	60.38	48.38	109.18
Spectrum 4	Yes	0.34	0.31	60.93	47.98	109.56
Spectrum 5	Yes	0.16	0.30	61.11	48.48	110.05
Spectrum 6	Yes	0.14	0.32	59.81	48.07	108.34
Spectrum 7	Yes	0.56	0.31	60.22	47.25	108.34
Mean		0.24	0.31	60.55	48.21	109.31
Std. deviation		0.15	0.04	0.45	0.50	
Max.		0.56	0.35	61.11	48.79	
Min.		0.14	0.23	59.81	47.25	

All results in weight%

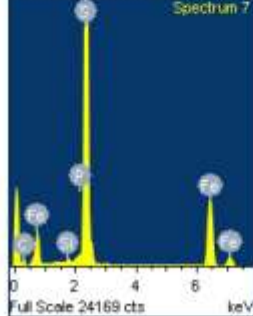
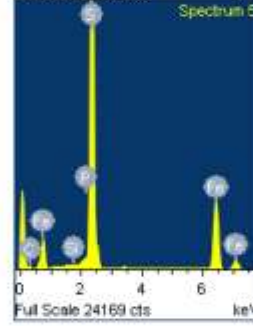
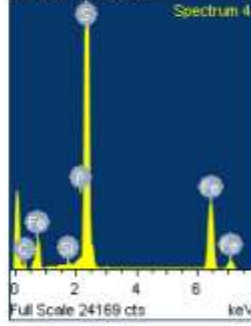
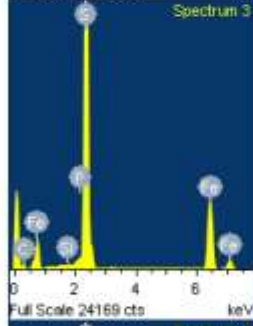
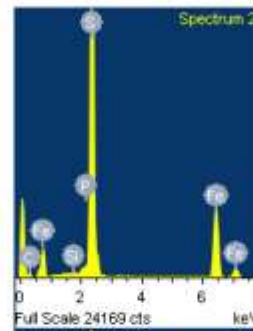
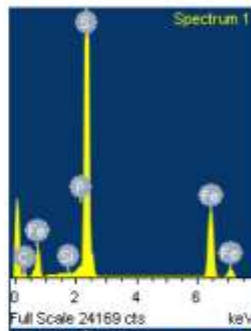
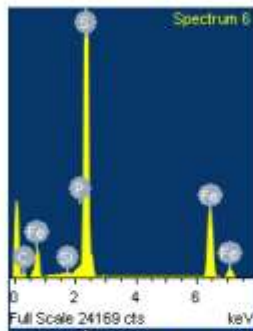


Project: Steph Theriault 061411

Sample: 214

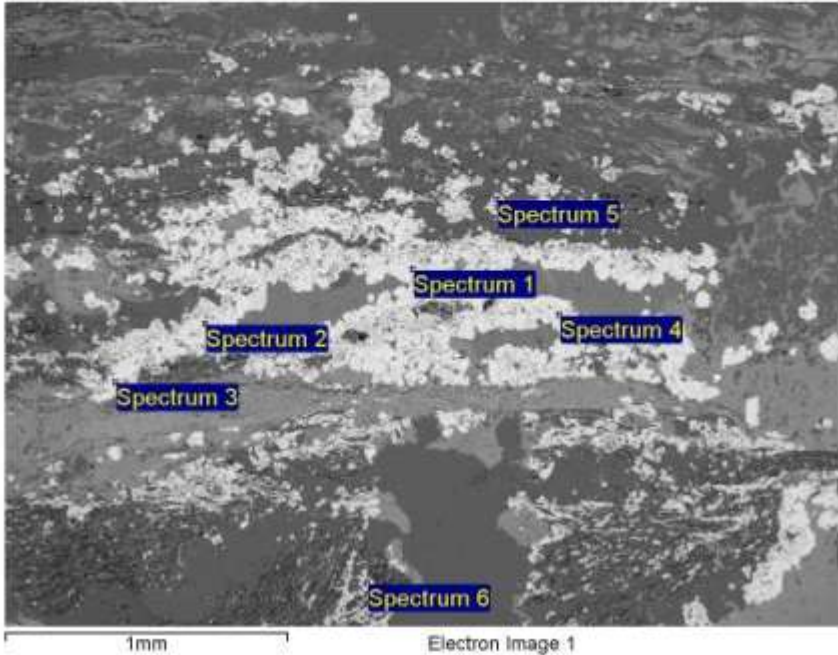
Owner: Inca User

Type: Default



Comment:





Processing option : All elements analysed

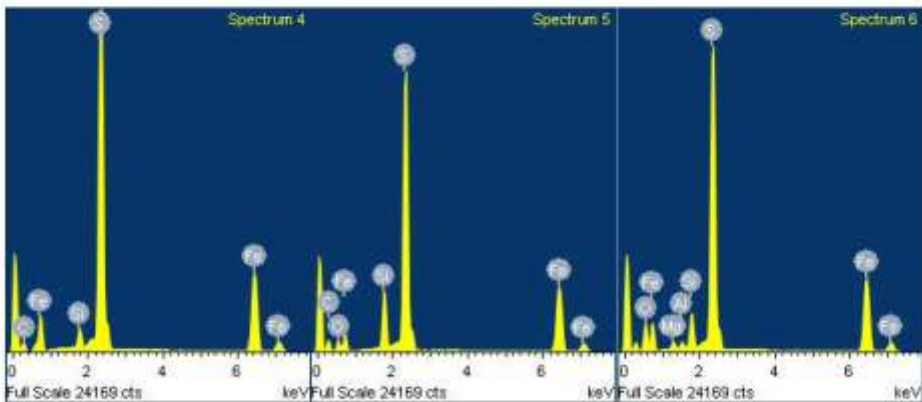
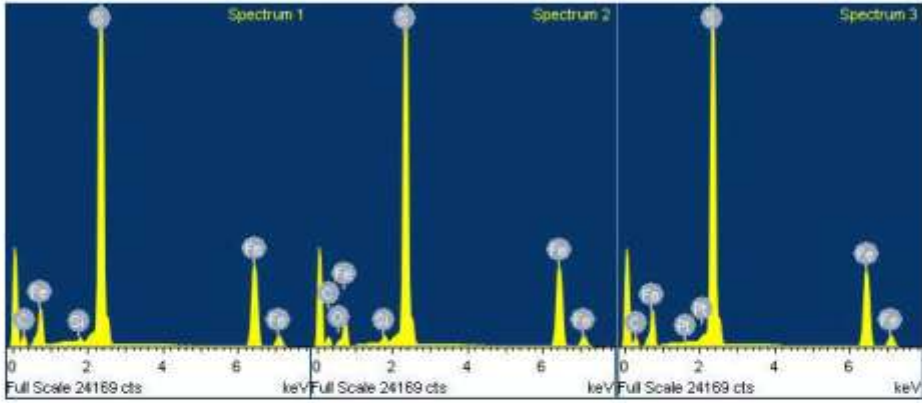
Spectrum	In stats.	D	Mg	Al	Si	S	Fe	Pt	Total
Spectrum 1	Yes				0.57	61.24	48.16		109.98
Spectrum 2	Yes	3.23			1.07	57.20	47.78		109.28
Spectrum 3	Yes					56.95	44.89	3.47	105.31
Spectrum 4	Yes				2.68	57.49	46.49		106.65
Spectrum 5	Yes	8.77			8.25	45.22	38.68		100.93
Spectrum 6	Yes	22.09	1.31	0.77	5.10	49.03	43.74		122.03
Max.		22.09	1.31	0.77	8.25	61.24	48.16	3.47	
Min.		3.23	1.31	0.77	0.57	45.22	38.68	3.47	

All results in weight%



Project: Steph Theriault 061411  
Owner: Inca User

Sample: 218  
Type: Default



Comment:



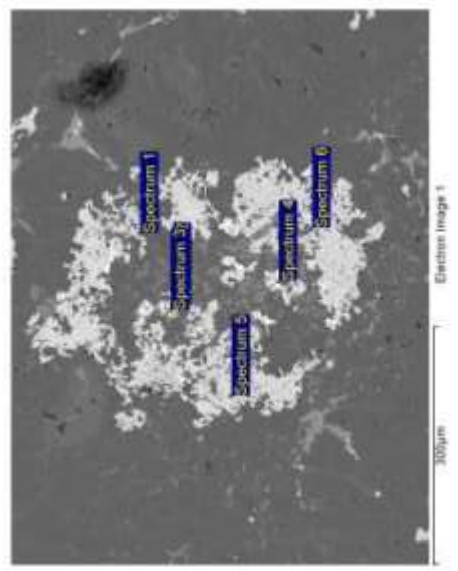
**Steph Theriault 061411 - 222**

Project: Steph Theriault 061411  
 Owner: Inca User  
 Sample: 222  
 Type: Default

Processing option: All elements analysed

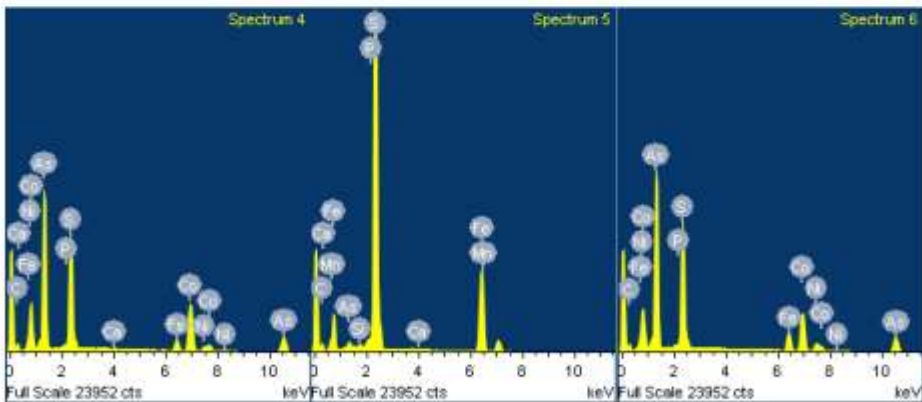
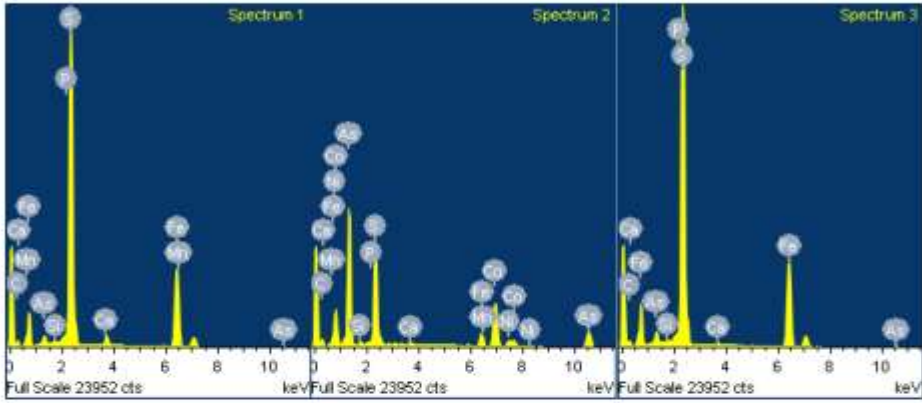
Spectrum	In stats	Si	P	S	Ca	Mn	Fe	Co	Ni	As	Total
Spectrum 1	Yes	0.16	0.30	54.20	2.32	0.49	46.06			2.75	106.28
Spectrum 2	Yes	0.57	0.00	20.82	0.24	0.22	6.34	28.63	4.36	44.14	105.32
Spectrum 3	Yes	0.21	0.29	64.50	0.24		50.23			3.86	119.33
Spectrum 4	Yes		0.17	23.23	0.20		5.38	31.21	3.42	50.04	113.66
Spectrum 5	Yes	0.20	0.34	61.50	0.28	0.33	48.75			1.96	113.36
Spectrum 6	Yes		0.22	25.37			9.31	24.34	6.36	54.42	120.01
Max.		0.57	0.34	64.50	2.32	0.49	50.23	31.21	6.36	54.42	
Min.		0.16	0.00	20.82	0.20	0.22	5.38	24.34	3.42	1.96	

All results in weights%



Project: Steph Theriault 061411  
Owner: Inca User

Sample: 222  
Type: Default



Comment:

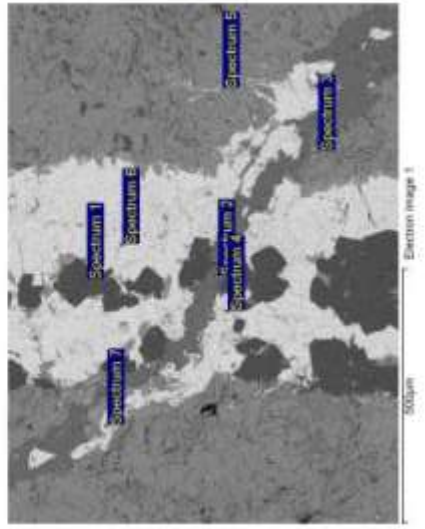


Project: Steph Theriault 061411  
 Owner: Inca User  
 Sample: 513  
 Type: Default

Processing option : All elements analysed

Spectrum	In Start	O	Mg	Al	Si	P	S	Ca	Mn	Fe	Total
Spectrum 1	Yes	54.13	0.13	53.56							107.82
Spectrum 2	Yes	35.81	0.96					36.44	2.53	1.99	77.73
Spectrum 3	Yes					0.38	58.70			46.55	105.63
Spectrum 4	Yes	5.05			3.73	0.22	41.08			41.88	91.96
Spectrum 5	Yes				0.17	0.30	58.25			47.01	105.73
Spectrum 6	Yes				0.62	0.33	58.72			46.87	106.54
Spectrum 7	Yes				0.18	0.23	57.16			47.09	104.67
Max.		54.13	0.96	0.13	53.56	0.38	58.72	36.44	2.53	47.09	
Min.		5.05	0.96	0.13	0.17	0.22	41.08	36.44	2.53	1.99	

All results in weights

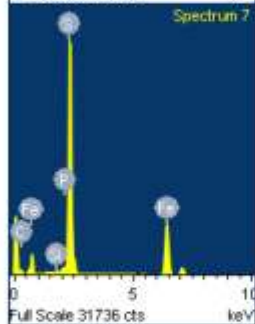
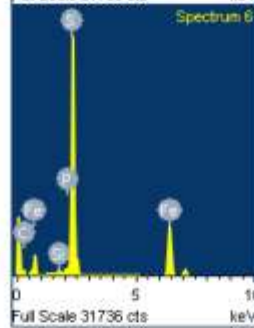
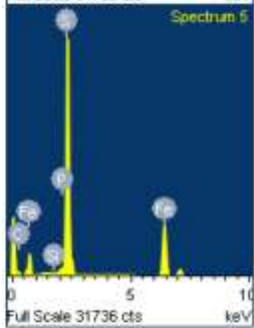
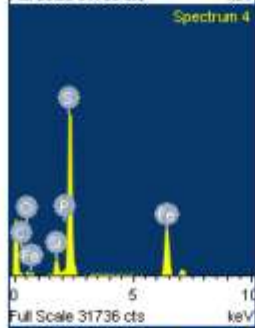
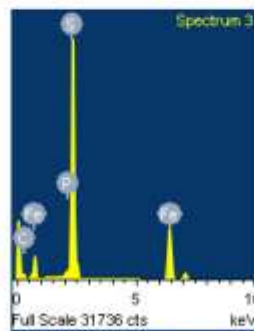
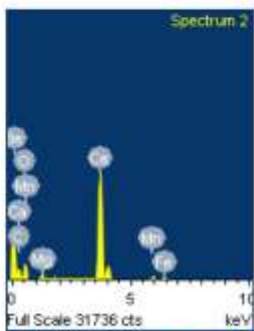
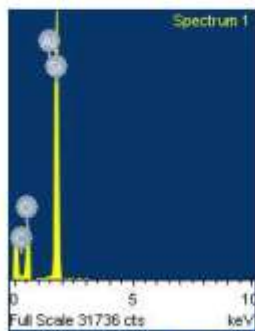


Project: Steph Theriault 061411

Sample: 513

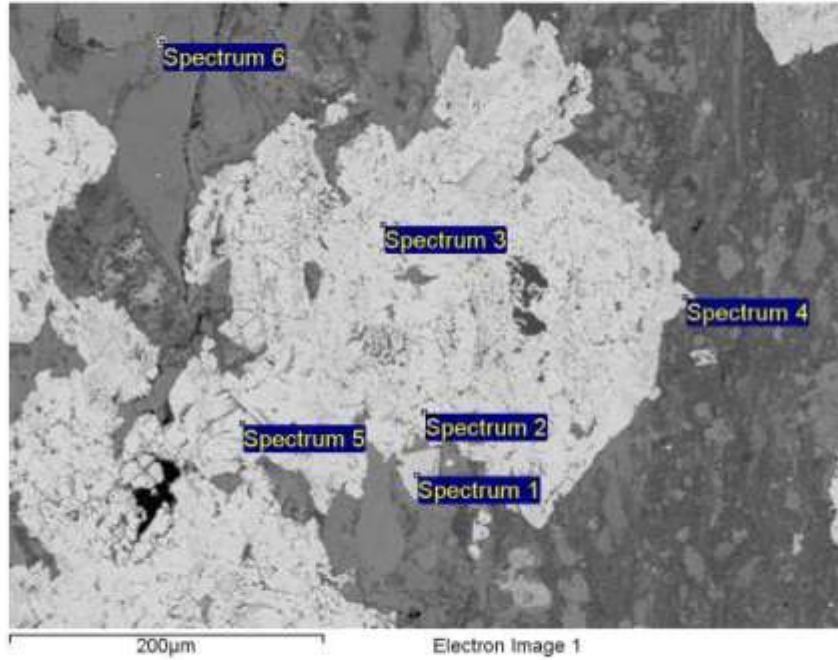
Owner: Inca User

Type: Default



Comment:





Processing option : All elements analysed

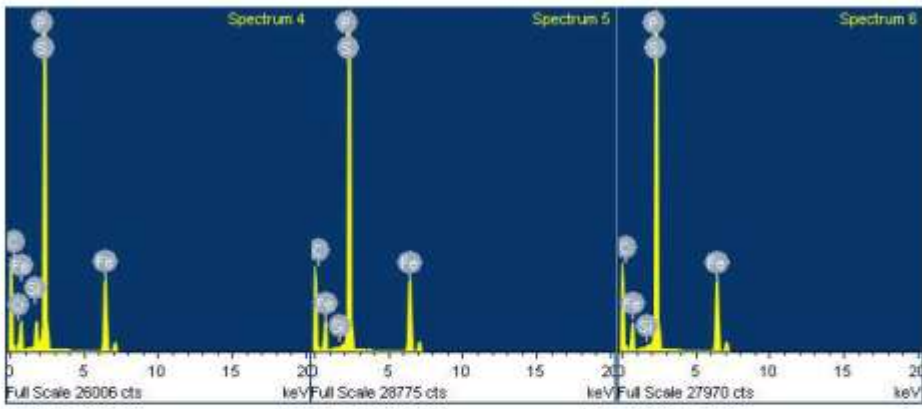
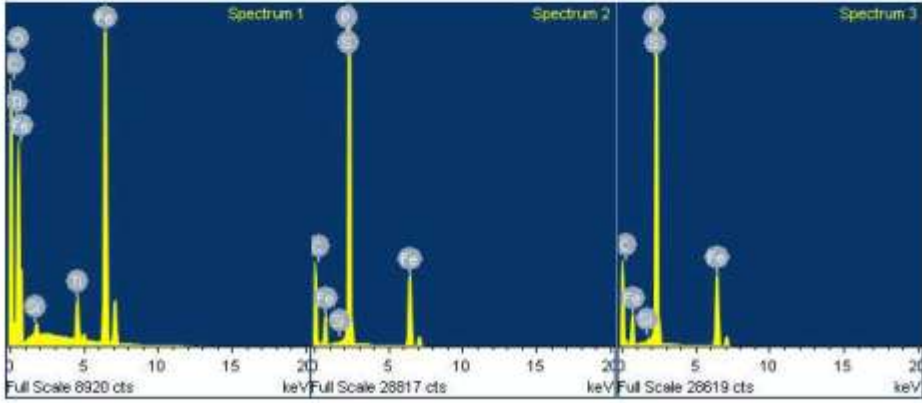
Spectrum	In stats	O	Si	P	S	Ti	Fe	Total
Spectrum 1	Yes	25.76	0.68			3.87	62.19	92.50
Spectrum 2	Yes		0.25	0.31	54.31		43.93	98.80
Spectrum 3	Yes		0.57	0.31	54.06		43.80	98.74
Spectrum 4	Yes	6.56	3.66	0.30	50.32		41.07	101.91
Spectrum 5	Yes		0.33	0.31	54.23		43.99	98.85
Spectrum 6	Yes		0.42	0.27	52.87		43.12	96.68
Max.		25.76	3.66	0.31	54.31	3.87	62.19	
Min.		6.56	0.25	0.27	50.32	3.87	41.07	

All results in weight%



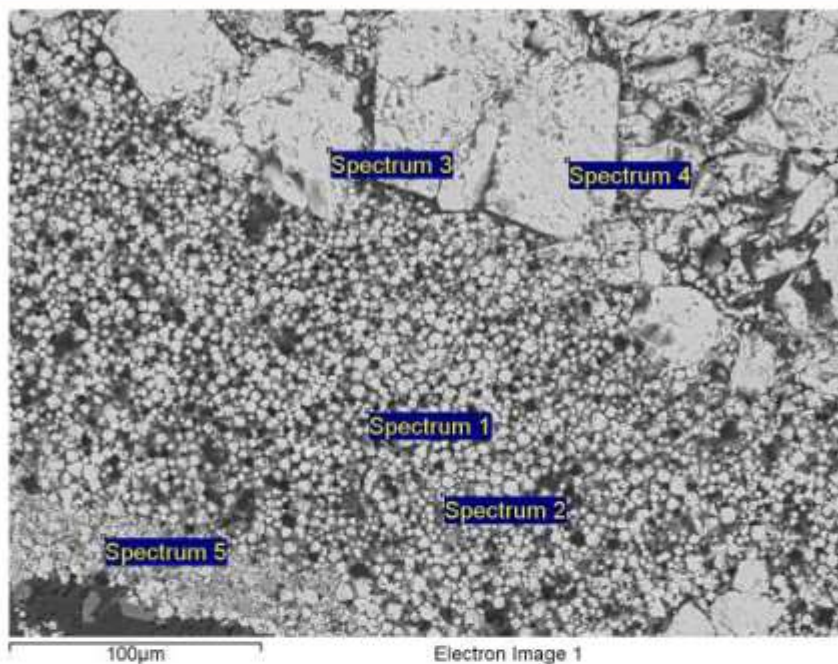
Project: Steph Theriault 061411  
Owner: Inca User

Sample: 518  
Type: Default



Comment:





Processing option : All elements analysed

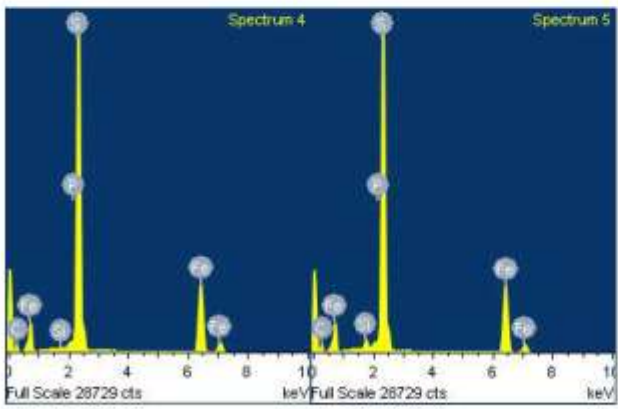
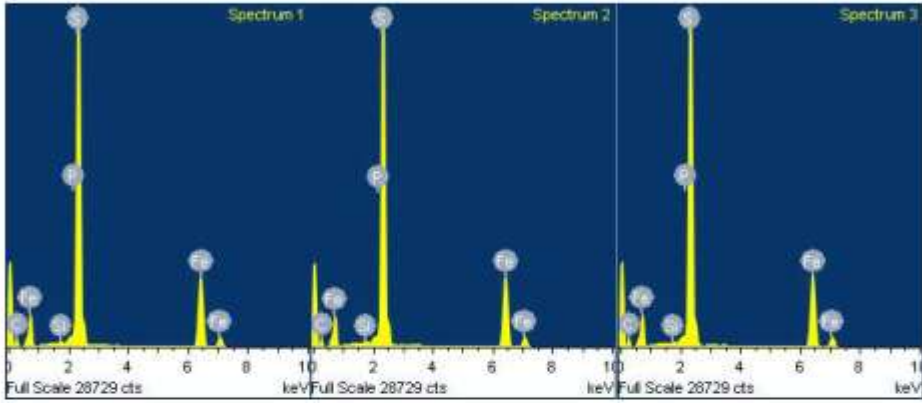
Spectrum	In stats	Si	P	S	Fe	Total
Spectrum 1	Yes	0.32	0.26	54.05	42.97	97.60
Spectrum 2	Yes	0.28	0.32	53.82	42.84	97.26
Spectrum 3	Yes	0.21	0.27	54.11	43.09	97.67
Spectrum 4	Yes	0.14	0.31	53.09	42.63	96.16
Spectrum 5	Yes	1.32	0.24	52.00	40.94	94.50
Mean		0.45	0.28	53.41	42.49	96.64
Std. deviation		0.49	0.03	0.89	0.88	
Max.		1.32	0.32	54.11	43.09	
Min.		0.14	0.24	52.00	40.94	

All results in weight%



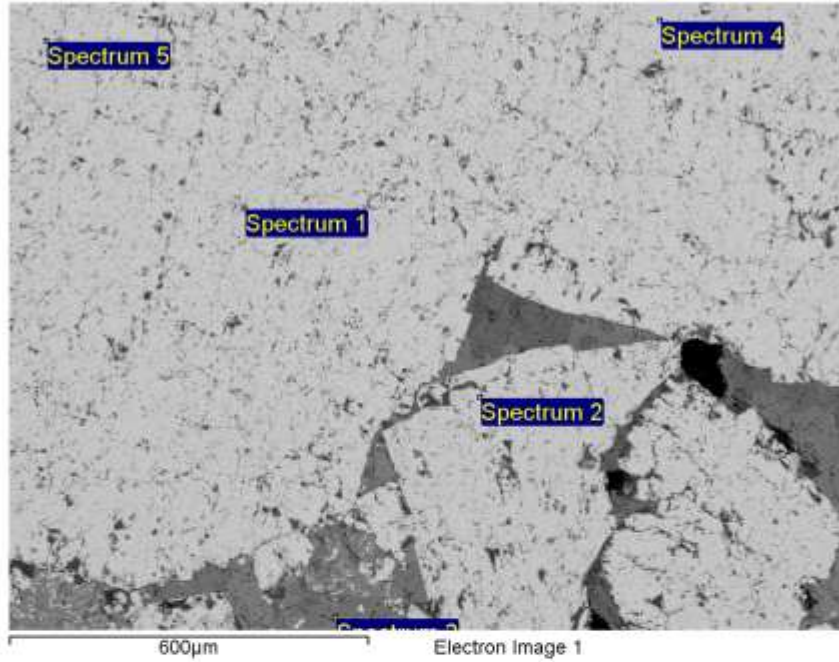
Project: Steph Theriault 061411  
Owner: Inca User

Sample: 520  
Type: Default



Comment:





Processing option : All elements analysed

Spectrum	In stats.	O	Si	P	S	Fe	As	Total
Spectrum 1	Yes			0.30	52.92	42.27	0.91	96.40
Spectrum 2	Yes			0.28	51.82	42.02	0.93	95.06
Spectrum 3	Yes	22.94	0.38			63.73		87.05
Spectrum 4	Yes			0.30	52.70	43.29	0.79	97.07
Spectrum 5	Yes		0.56	0.23	52.31	42.78	0.87	96.75
Max.		22.94	0.56	0.30	52.92	63.73	0.93	
Min.		22.94	0.38	0.23	51.82	42.02	0.79	

All results in weight%

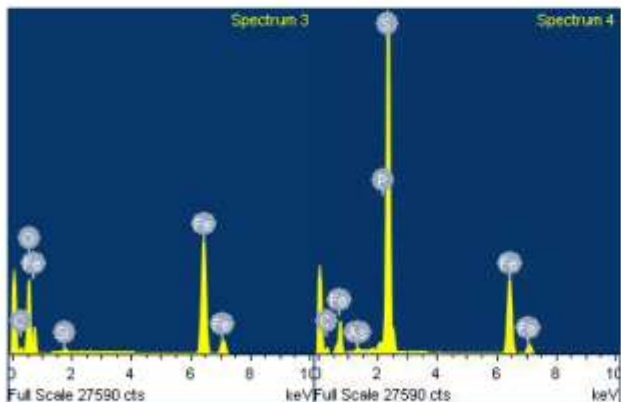
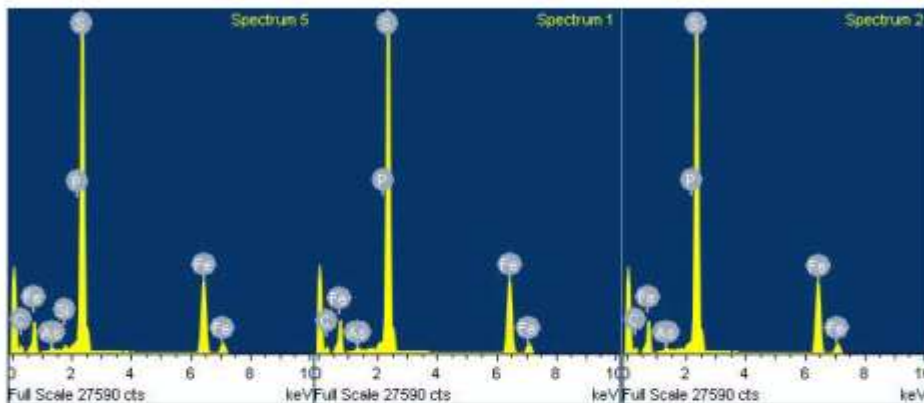


Project: Steph Theriault 061411

Sample: 525

Owner: Inca User

Type: Default



Comment:



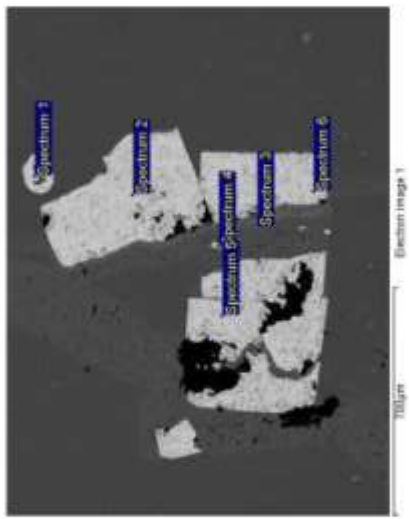
**Steph Theriault 061411 - 527** 4/14/2011 2:30:14 PM

Project: Steph Theriault 061411 Sample: 527  
 Owner: Inca User Type: Default

Processing option : All elements analysed

Spectrum	In stats.	O	Mg	Si	P	S	Cl	Ca	Mn	Fe	Al	Total
Spectrum 1	Yes		0.48	0.29	52.92					42.27	1.41	97.36
Spectrum 2	Yes		0.20	0.32	54.35					43.15		98.02
Spectrum 3	Yes	37.45	9.42			0.31	19.37	1.20		4.64		72.39
Spectrum 4	Yes		0.15	0.27	48.32		0.29			40.79		89.83
Spectrum 5	Yes		0.24	0.26	51.53					41.50		93.53
Spectrum 6	Yes		0.19	0.24	52.49					41.79		94.71
Max.		37.45	9.42	0.48	0.32	54.35	0.31	19.37	1.20	43.15	1.41	
Min.		37.45	9.42	0.15	0.24	48.32	0.31	0.29	1.20	4.64	1.41	

All results in weight%

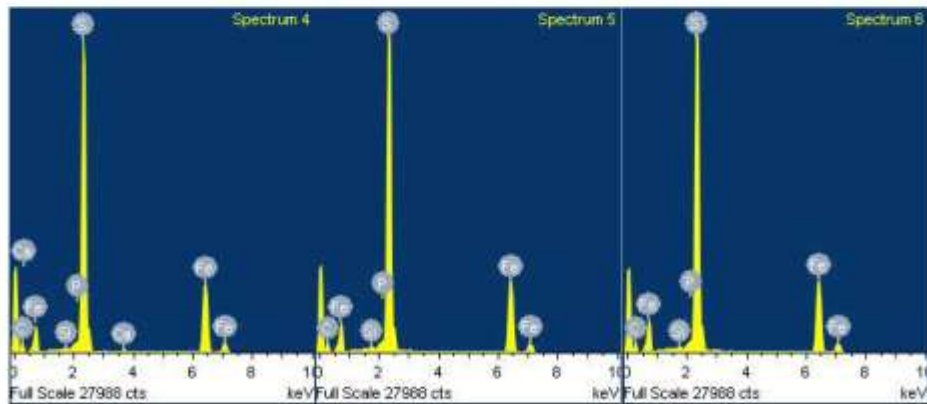
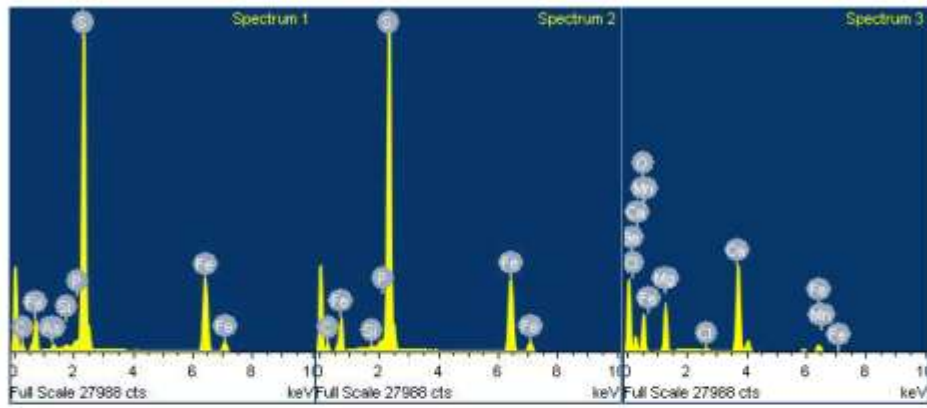


Project: Steph Theriault 061411

Sample: 527

Owner: Inca User

Type: Default



Comment:



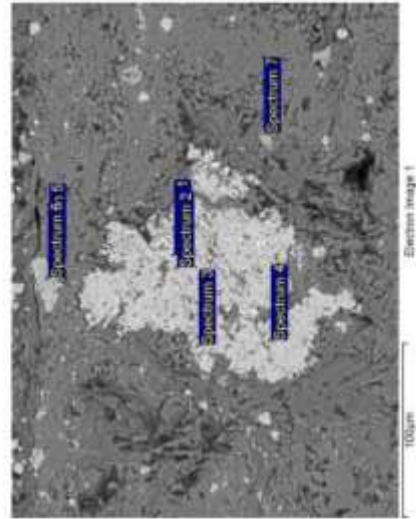
**Steph Theriault 061411 - 709** 6/14/2013 2:46:34 PM

Project: Steph Theriault 061411  
 Owner: Inca User  
 Sample: 709  
 Type: Default

Processing option : All elements analysed

Spectrum	In stat.	O	Mg	Al	Si	P	S	Ca	Ti	Mn	Fe	Cu	M	As	Total
Spectrum 1	Yes				0.24	0.15	34.13				16.77	17.70	2.69	27.71	98.39
Spectrum 2	Yes				0.14	0.29	51.68				41.05			1.75	95.51
Spectrum 3	Yes				0.32	0.15	26.30				11.04	21.63	2.60	38.27	100.31
Spectrum 4	Yes				0.17		50.71				41.95			1.65	94.47
Spectrum 5	Yes	26.36	0.34	0.12	1.32			0.20			60.70				89.03
Spectrum 6	Yes	32.49	0.30	0.30	0.17			19.18			44.22				96.37
Spectrum 7	Yes	27.63	3.09	0.10				0.34		0.54	38.04				69.73
Max.		32.49	3.09	0.30	1.32	0.29	51.68	0.34	19.18	0.54	60.70	21.63	2.69	38.27	
Min.		26.36	0.34	0.12	0.10	0.15	26.30	0.34	0.20	0.54	11.04	17.70	2.60	1.65	

All results in weights

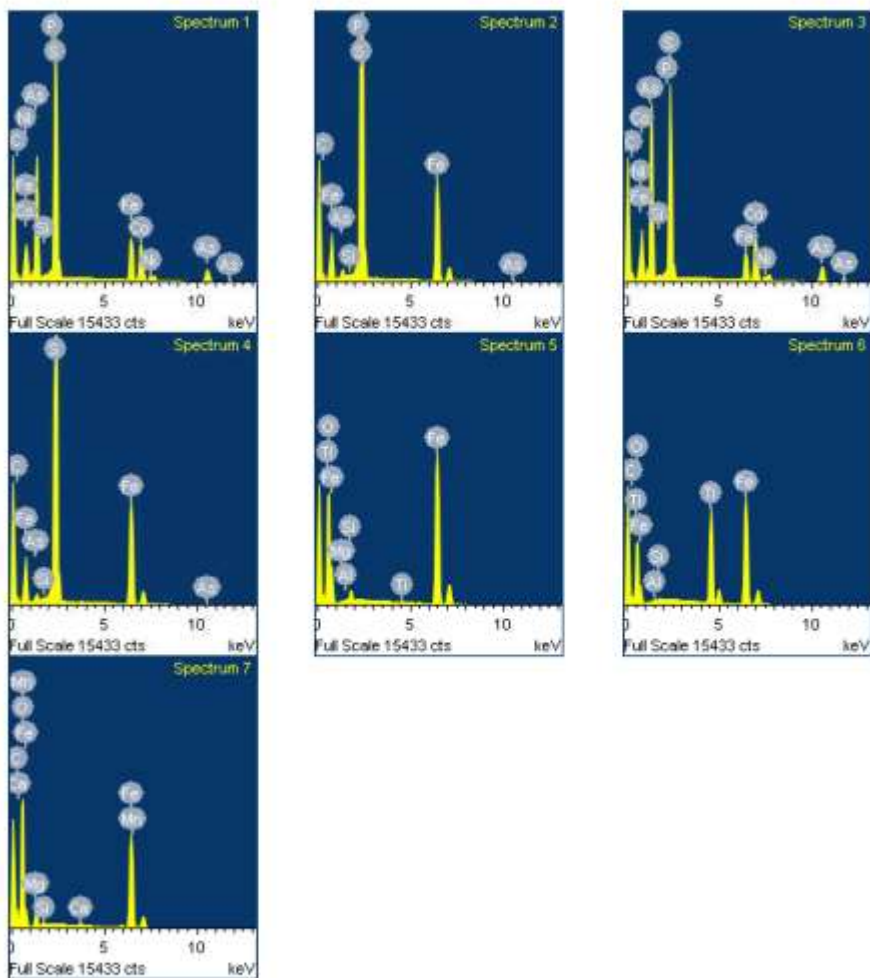


Project: Steph Theriault 061411

Sample: 709

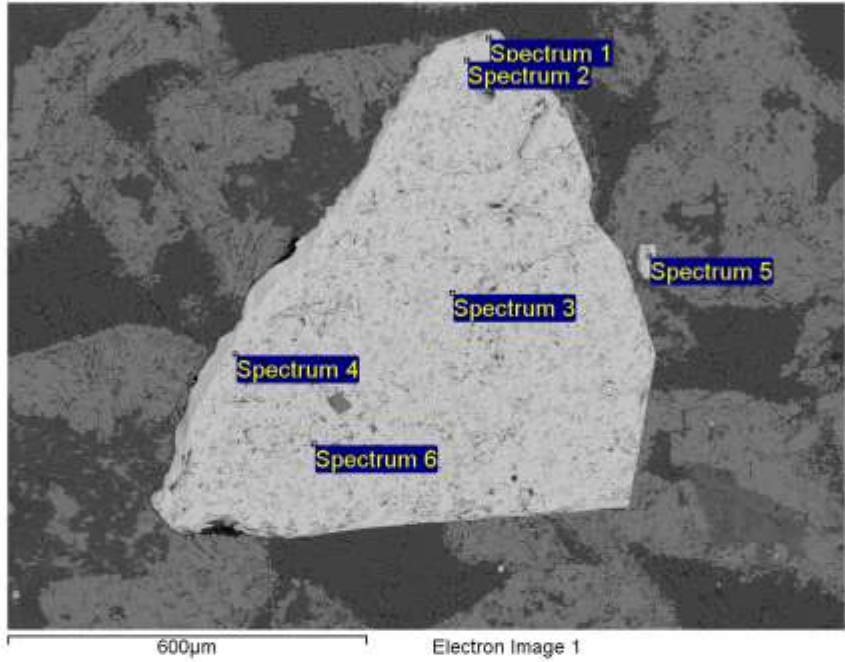
Owner: Inca User

Type: Default



Comment:





Processing option : All elements analysed

Spectrum	In stats.	Si	P	S	Fe	As	Total
Spectrum 1	Yes	0.46	0.37	58.85	43.57		103.24
Spectrum 2	Yes	0.12	0.31	54.57	43.31	0.55	98.85
Spectrum 3	Yes		0.24	54.34	43.24		97.82
Spectrum 4	Yes		0.23	52.80	42.40	0.48	95.93
Spectrum 5	Yes	0.17	0.21	53.74	43.28		97.41
Spectrum 6	Yes	0.22	0.24	52.39	42.30		95.14
Max.		0.46	0.37	58.85	43.57	0.55	
Min.		0.12	0.21	52.39	42.30	0.48	

All results in weight%

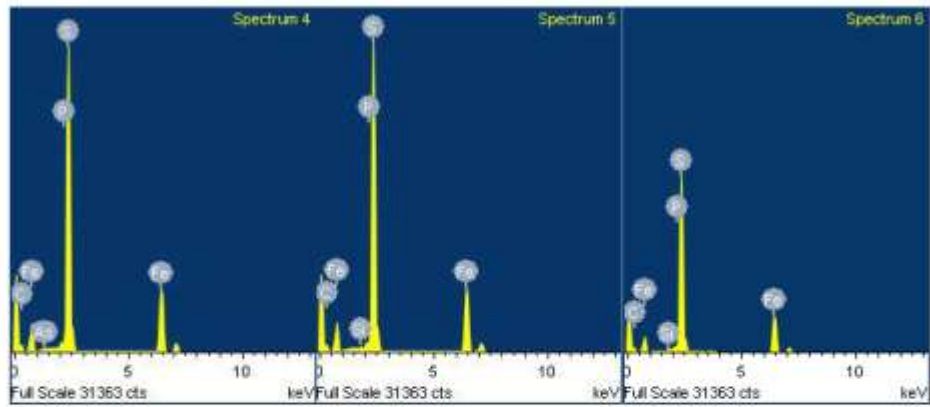
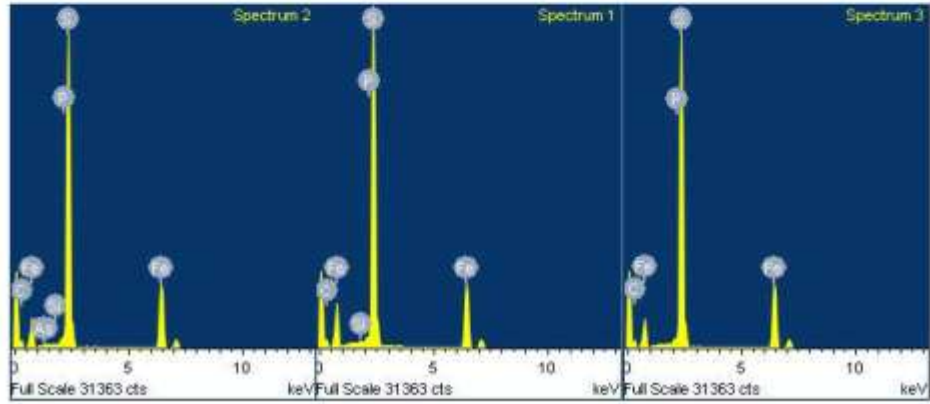


Project: Steph Theriault 061411

Sample: 719

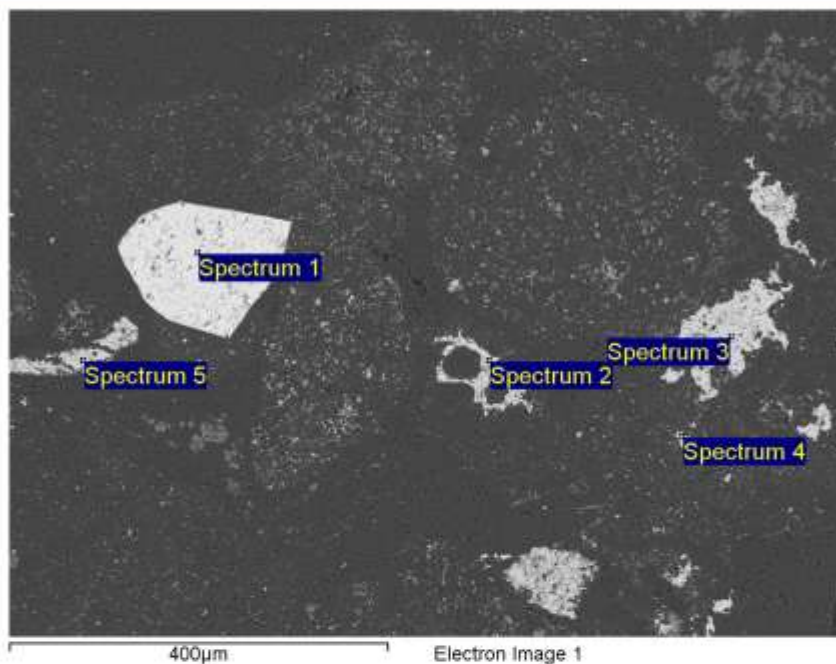
Owner: Inca User

Type: Default



Comment:





Processing option : All elements analysed

Spectrum	In stats.	O	Al	Si	P	S	Fe	Co	As	Total
Spectrum 1	Yes				0.32	56.98	45.37	1.08	1.76	105.51
Spectrum 2	Yes	24.43		0.93			66.64			92.00
Spectrum 3	Yes	27.37		0.36			68.39			96.12
Spectrum 4	Yes	26.01	0.38	0.59			67.19			94.16
Spectrum 5	Yes	29.32	0.48	1.31			67.35			98.47
Max.		29.32	0.48	1.31	0.32	56.98	68.39	1.08	1.76	
Min.		24.43	0.38	0.36	0.32	56.98	45.37	1.08	1.76	

All results in weight%

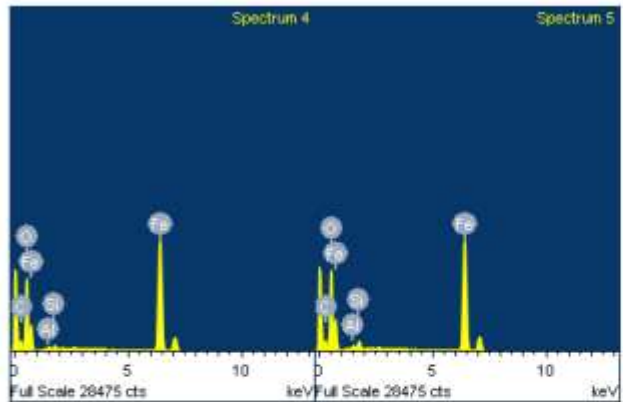
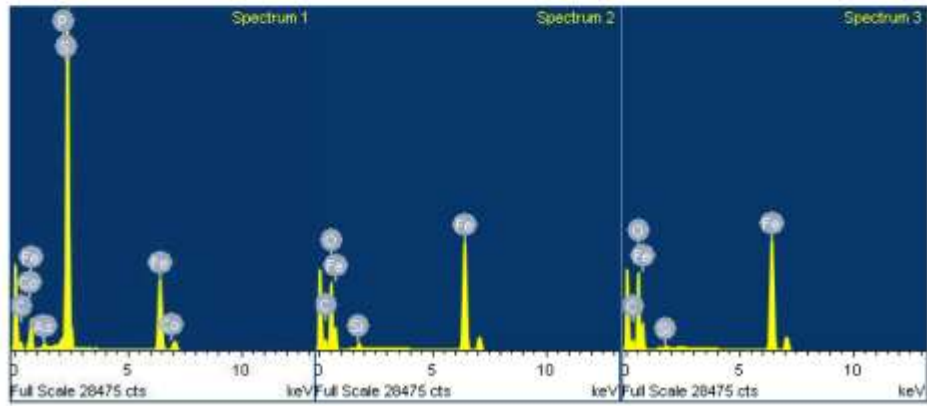


Project: Steph Theriault 061411

Sample: 722

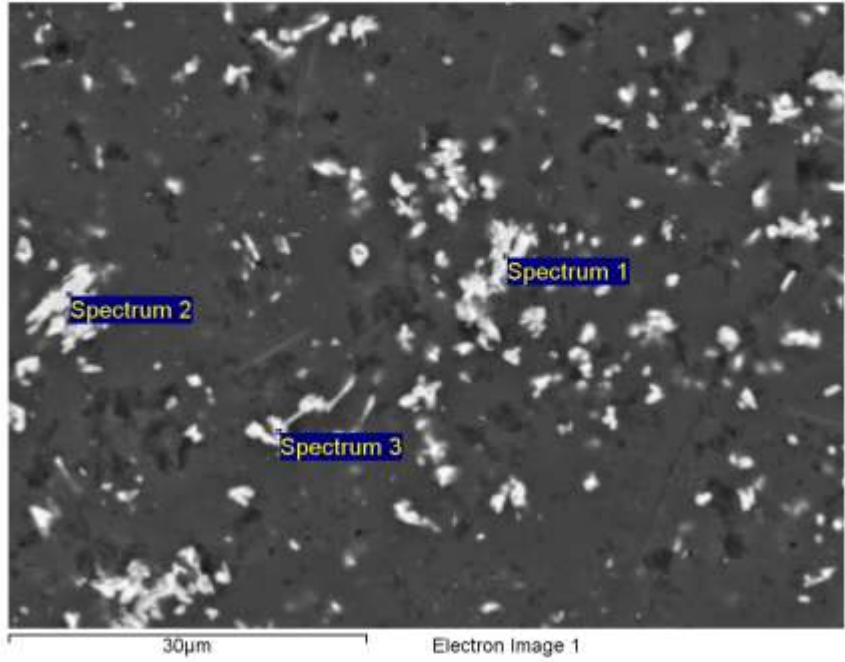
Owner: Inca User

Type: Default



Comment:





Processing option : All elements analysed

Spectrum	In stats.	O	Al	Si	Fe	Total
Spectrum 1	Yes	29.23	0.25	2.69	65.42	97.59
Spectrum 2	Yes	28.69	0.50	2.69	65.22	97.11
Spectrum 3	Yes	36.37	0.37	13.60	56.99	107.33
Mean		31.43	0.37	6.33	62.54	100.68
Std. deviation		4.29	0.13	6.30	4.81	
Max.		36.37	0.50	13.60	65.42	
Min.		28.69	0.25	2.69	56.99	

All results in weight%

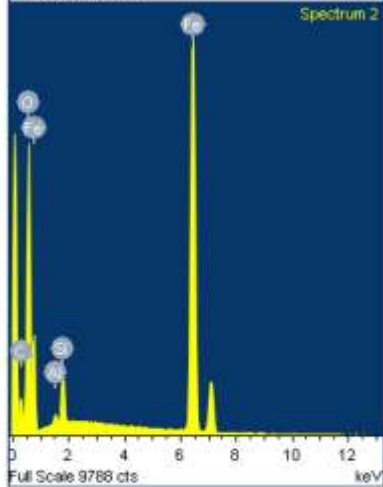
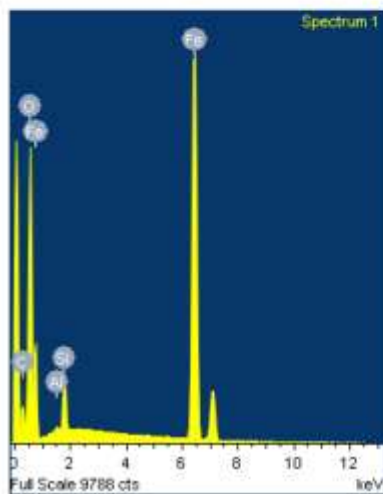
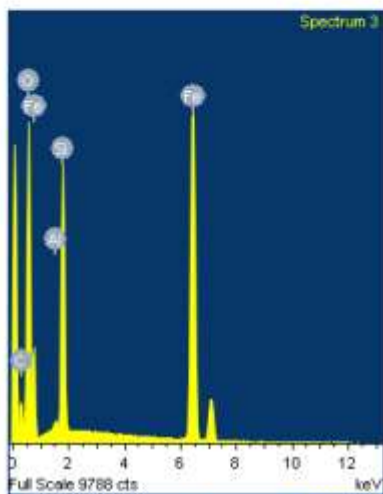


Project: Steph Theriault 061411

Sample: 722

Owner: Inca User

Type: Default



Comment:

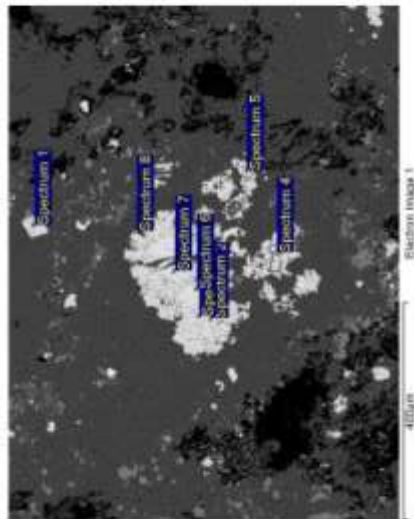


Project: Steph Theriault 061411  
 Owner: Inca User  
 Sample: 81  
 Type: Default

Processing option : All elements analysed

Spectrum	In stats.	O	Si	P	S	Fu	Ni	Cu	As	Sr	Pb	Total
Spectrum 1	Yes	0.23	0.25	57.55	46.36							104.19
Spectrum 2	Yes	15.84	4.50	9.52	3.35	0.63				2.76	62.52	99.11
Spectrum 3	Yes	0.28	0.32	55.47	45.09		1.23					102.89
Spectrum 4	Yes	1.15	0.17	52.60	41.17	1.19			2.01			98.30
Spectrum 5	Yes	0.24	0.24	55.70	44.77		0.60					101.56
Spectrum 6	Yes	4.80	1.20	22.75	12.47				2.37	58.46		102.06
Spectrum 7	Yes	0.32	0.28	53.85	42.74	0.60			2.50			100.29
Spectrum 8	Yes	0.86	0.32	56.70	44.31		1.91					104.11
Max.		15.84	4.50	0.32	57.55	46.36	1.19	0.63	2.50	2.76		62.52
Min.		4.80	0.23	0.17	9.52	3.35	0.60	0.63	0.60	2.37		58.46

All results in weights.

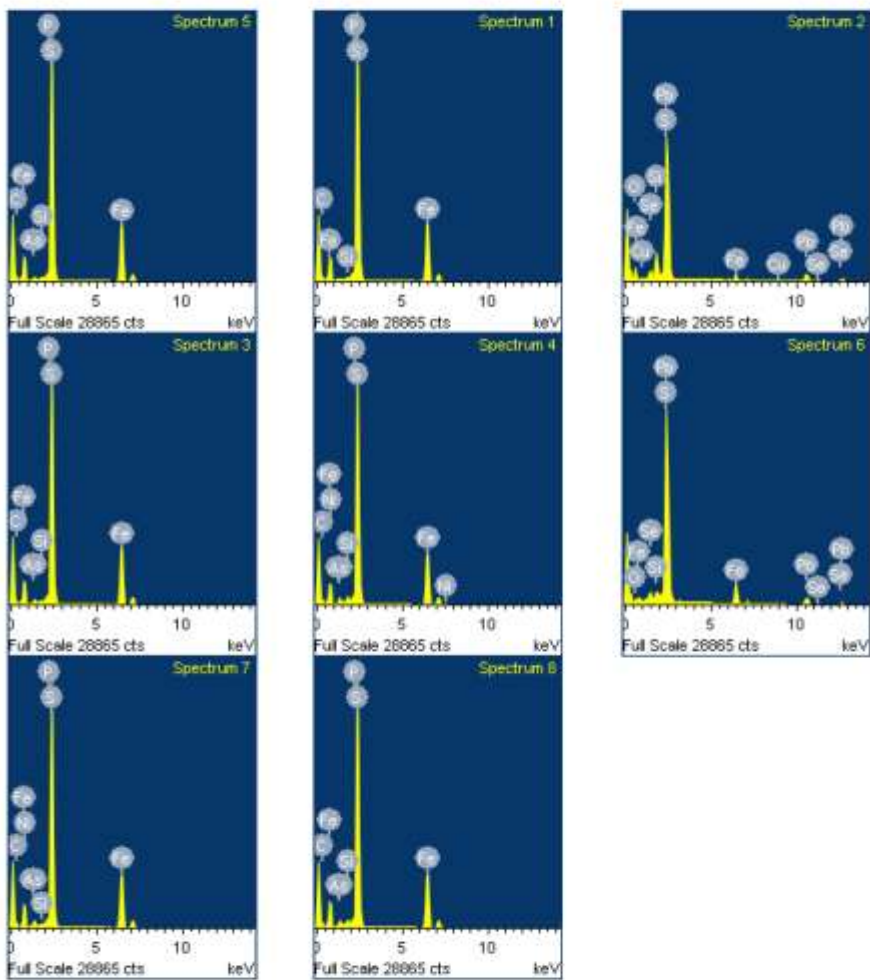


Project: Steph Theriault 061411

Sample: 81

Owner: Inca User

Type: Default



Comment:

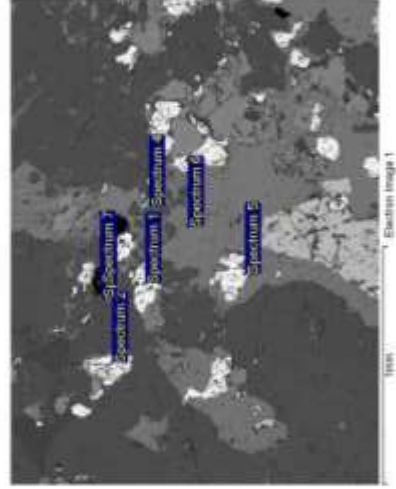


Project: Steph Theriault 061411 Sample: 305-2  
 Owner: Inca User Type: Default

Processing option : All elements analysed

Spectrum	In stat.	O	Mg	Al	Si	P	S	K	Ti	Fe	Cu	Total
Spectrum 1	Yes			0.24	0.21	36.30				29.66	32.41	98.63
Spectrum 2	Yes			0.38	0.19	37.89				30.12	32.68	101.08
Spectrum 3	Yes	7.49		2.72	0.16	39.25				50.18		99.00
Spectrum 4	Yes			0.59	0.15	37.06				26.41	32.36	99.57
Spectrum 5	Yes			0.20	0.17	37.05				20.91	32.75	100.06
Spectrum 6	Yes	38.76	4.96	7.71	17.80		7.60	2.22	18.76			97.81
Spectrum 7	Yes	0.98	0.23	0.28	1.99				0.88			4.36
Max.		38.76	4.96	7.71	17.80	0.21	38.25	7.60	2.22	50.18		32.75
Min.		0.98	0.23	0.28	0.18	0.15	36.30	7.60	2.22	0.88		32.36

All results in weights

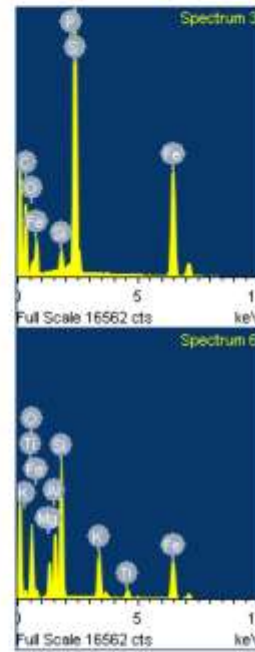
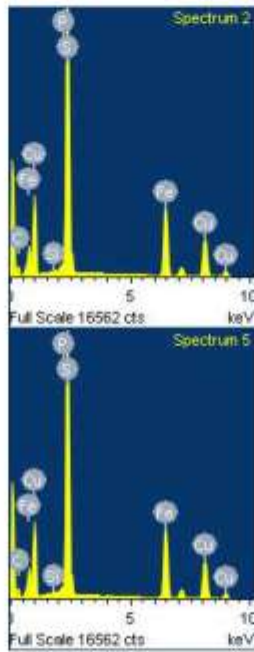
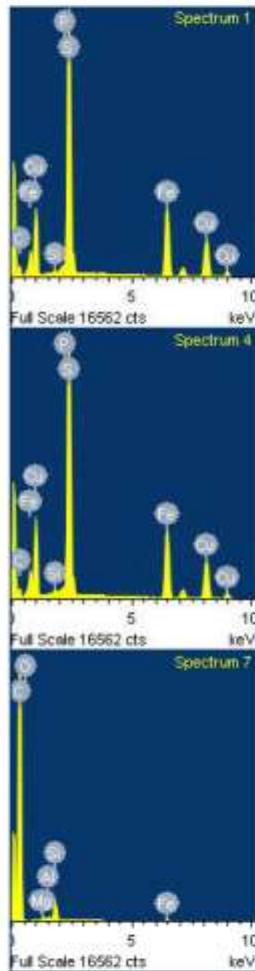


Project: Steph Theriault 061411

Sample: 305-2

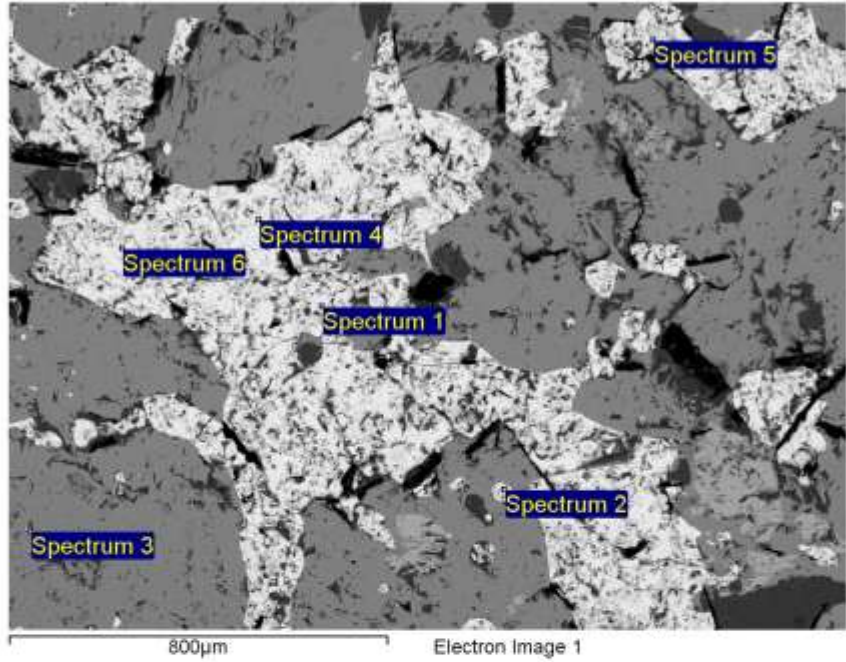
Owner: Inca User

Type: Default



Comment:





Processing option : All elements analysed

Spectrum	In stats.	O	Mg	Si	P	S	Fe	Total
Spectrum 1	Yes			0.18	0.00	40.12	60.78	101.08
Spectrum 2	Yes			0.21	0.19	40.76	59.05	100.21
Spectrum 3	Yes	6.76	0.49	2.73	0.15	33.18	53.24	96.55
Spectrum 4	Yes			0.19	0.17	41.48	59.83	101.68
Spectrum 5	Yes			0.38	0.22	40.49	59.65	100.72
Spectrum 6	Yes			0.18	0.16	41.00	59.99	101.33
Max.		6.76	0.49	2.73	0.22	41.48	60.78	
Min.		6.76	0.49	0.18	0.00	33.18	53.24	

All results in weight%

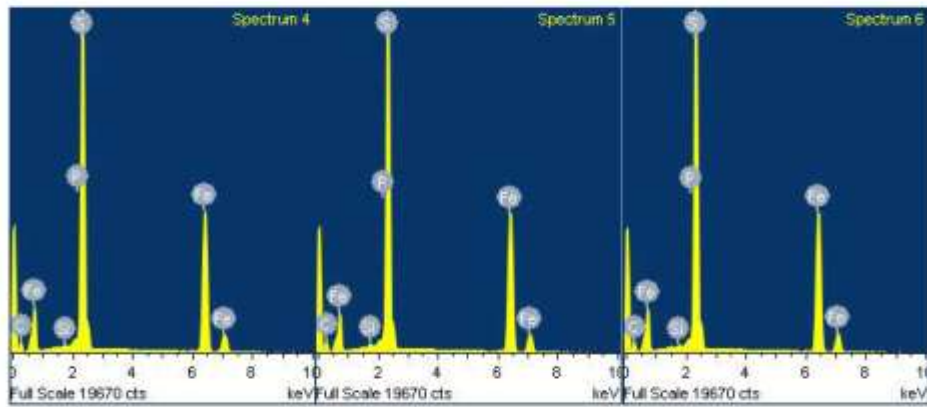
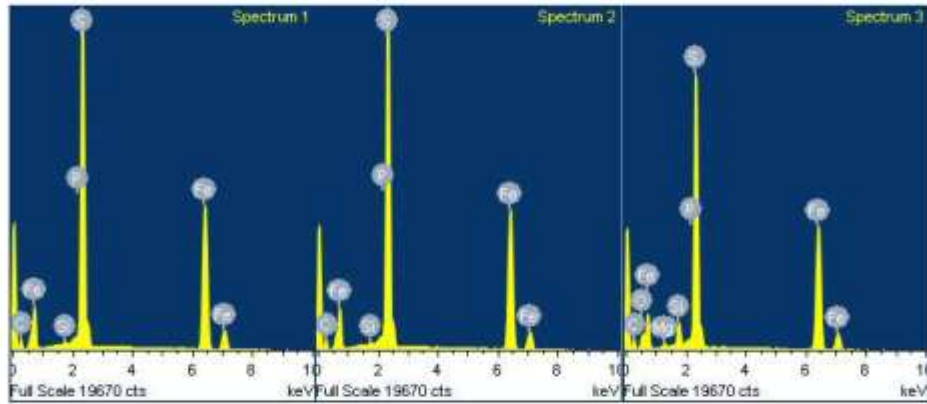


Project: Steph Theriault 061411

Sample: 305-15

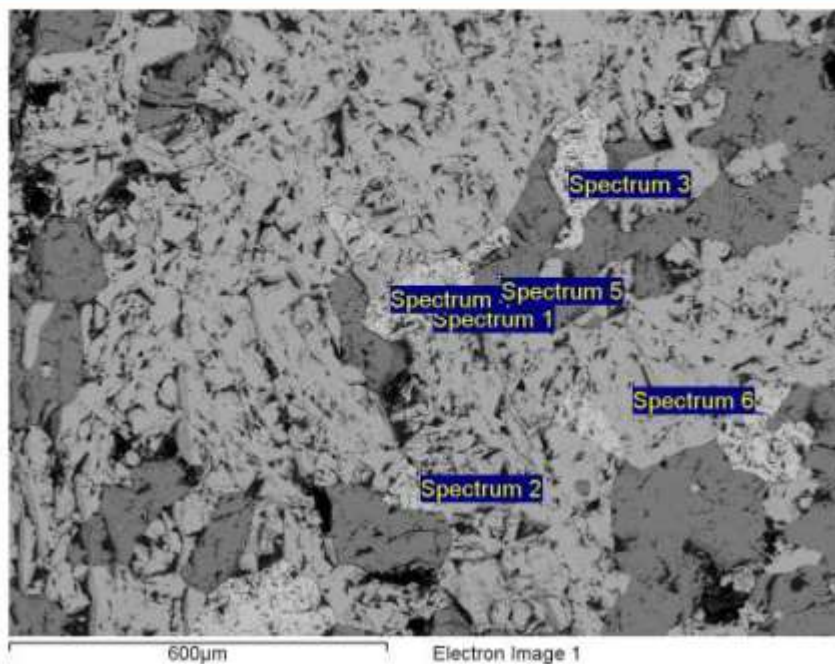
Owner: Inca User

Type: Default



Comment:





Processing option : All elements analysed

Spectrum	In stats.	O	Mg	Al	Si	P	S	Mn	Fe	Total
Spectrum 1	Yes					0.26	40.19		57.67	98.12
Spectrum 2	Yes					0.23	39.45		57.26	96.95
Spectrum 3	Yes					0.27	39.58		57.85	97.70
Spectrum 4	Yes	23.81		0.45					66.95	91.21
Spectrum 5	Yes	31.03	6.43		15.61			5.87	36.55	95.49
Spectrum 6	Yes	22.92		0.51				0.27	66.35	90.04
Max.		31.03	6.43	0.51	15.61	0.27	40.19	5.87	66.95	
Min.		22.92	6.43	0.45	15.61	0.23	39.45	0.27	36.55	

All results in weight%

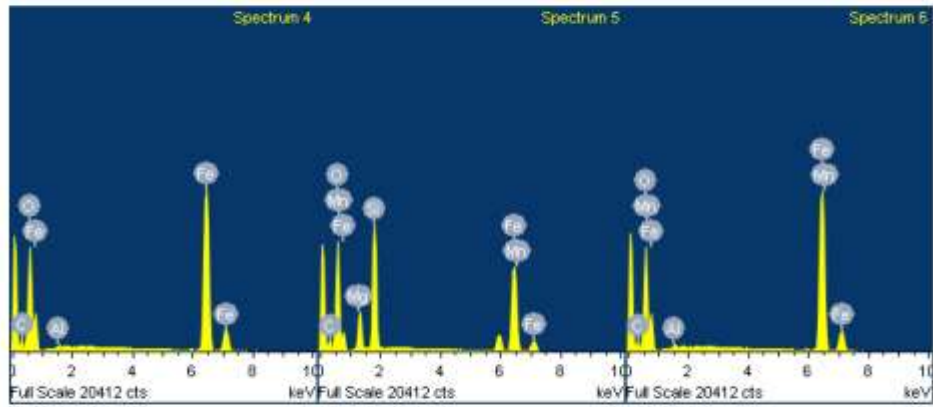
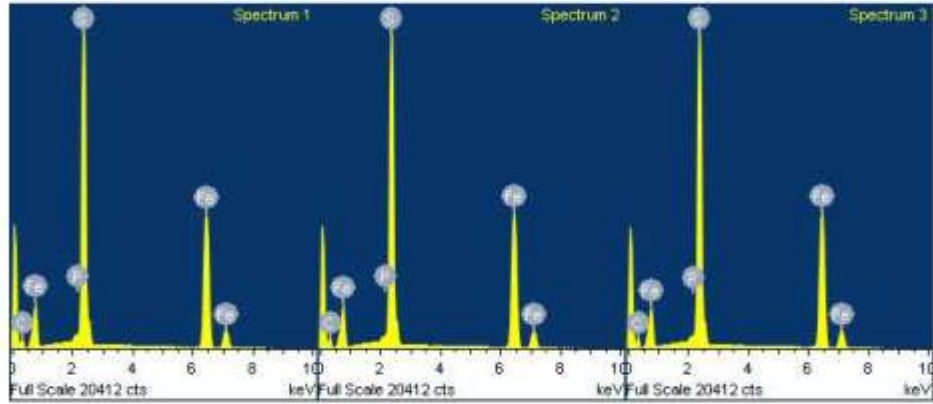


Project: Steph Theriault 061411

Sample: 305-16

Owner: Inca User

Type: Default



Comment:



## Appendix B: Sulfur Isotope Analysis

Appendix B.1 Raw and Corrected Sulfur Isotope Data

Sample Number	Raw $\delta^{34}\text{S}$ (‰)	Corrected $\delta^{34}\text{S}$ (‰)
MGS-2-B	30.21	30.55
MGS-2-2	-7.36	-7.71
MGS-2-10	12.63	12.44
MGS-2-16	9.31	9.20
MGS-2-16 (D)	-5.04	-5.35
MGS-5-A	-16.68	-17.00
MGS-5-A (D)	-14.93	-16.50
MGS-5-B	11.13	11.05
MGS-5-1	12.03	11.84
MGS-5-2	16.17	16.07
MGS-5-2 (D)	14.94	14.91
MGS-5-4	-9.43	-9.81
MGS-5-5	11.90	11.66
MGS-5-10	18.81	18.65
MGS-5-11	-35.70	-36.11
MGS-5-11 (D)	-33.77	-34.52
MGS-5-12	-31.48	-31.87
MGS-5-15	4.61	4.38
MGS-5-16	5.26	4.81
MGS-5-16 (D)	6.47	5.75
MGS-5-19	36.12	36.04
MGS-5-21	79.44	80.37
MGS-5-21 (D)	73.89	73.52
MGS-5-22	77.85	77.96
MGS-5-22 (D)	61.76	62.43
MGS-5-23	-27.01	-27.65
MGS-5-24	-18.85	-20.05
MGS-5-24 (D)	-18.17	-18.69
MGS-5-26	23.58	23.71
MGS-7-A	3.33	3.10
MGS-7-B	-11.86	-12.16
MGS-7-B (D)	-11.51	-11.93
MGS-7-C	7.90	7.69
MGS-7-3	17.68	17.51
MGS-7-6	10.59	10.39
MGS-7-8	14.49	13.81
MGS-7-10	22.68	22.78

Sample Number	Raw $\delta^{34}\text{S}$ (‰)	Corrected $\delta^{34}\text{S}$ (‰)
MGS-7-11	18.00	17.96
MGS-7-12	11.01	10.93
MGS-7-13	10.33	10.05
MGS-7-14	14.00	13.83
MGS-7-14 (D)	13.74	13.56
MGS-7-16	10.78	10.51
MGS-7-17	16.37	16.20
MGS-7-17 (D)	12.81	12.76
MGS-7-21	32.59	32.49
MGS-8-A	3.52	3.33
MGS-8-B	6.90	6.68
MGS-8-2	-5.17	-6.53
MGS-8-4	-15.92	-16.76
MGS-8-6	-5.34	-5.61
MGS-8-6 (D)	-4.88	-5.20
MGS-8-10	37.08	37.38
MGS-8-14	-18.59	-18.92
MGS-8-14 (D)	-16.50	-16.99
MGS-8-16	-27.13	-27.78
MGS-8-18	-22.24	-23.56
MGS-8-18	-19.96	-20.49
B1-305-1	10.35	10.25
B1-305-4a,b	27.46	27.34
B1-305-4a,b (D)	25.85	25.99
B1-305-4c	8.01	7.80
B1-305-6	8.39	8.27
B1-305-14	6.41	6.19
B1-305-15	6.62	6.41
B1-305-16	8.96	8.85
B1-305-17	11.53	11.34
B1-305-18	2.91	2.39
B1-305-18 (D)	3.72	3.53
NatOre I	40.22	40.57
NatOre II	21.06	21.11
NatOre II (D)	31.80	31.21

## Appendix B.2 Sulfur Isotope Analysis Standards

